UNIVERSITÀ DEGLI STUDI DI NAPOLI
"FEDERICO II"

Dipartimento di Scienze Fisiche

Dottorato di Ricerca in Fisica Fondamentale ed Applicata
XVII ciclo

OPTICAL INVESTIGATION
OF
MOLECULAR ROTATIONAL DYNAMICS

Carlo Manzo

SUBMITTED IN PARTIAL FULFILLMENT OF THE REQUIREMENTS
FOR THE DEGREE OF DOCTOR OF PHILOSOPHY AT
UNIVERSITÀ DEGLI STUDI DI NAPOLI "FEDERICO II"

Dated: November 30, 2004

Coordinator:

Prof. Arturo Tagliacozzo

Author:

Carlo Manzo

to my parents

Table of Contents

Acknowledgements

I would like to thank all the people who helped and supported me during my studies leading to this dissertation.

First of all, I would like to give my special thanks and all my love to my mum, my dad and my brother. With their love they are always the point of reference of my life.

I wish to express my highest gratitude to my advisor, Prof. Lorenzo Marrucci, without whom this work would have been impossible to accomplish, and to Dr. Domenico Paparo for providing invaluable assistance during my studies. I greatly appreciate their support throughout these years. They constantly encouraged me and they also taught me several things aside from physics.

My appreciation goes to Guido Celentano for his assistance during the PhD program, going beyond the bureaucratic task.

Last but not least, I wish to really thank Rocco, Giuseppe, Valerio, Claudio, Luciano and Ernesto for their friendship and for changing my life "to worse". Special thanks also go to Procolo and Dario who shared with me the "PhD experience", and to Andrea and Raffaele, somehow always by my side.

I should also thank many other people. Since they will never see this dissertation, I will do in person...

Napoli,
November 30, 2004

Carlo Manzo

Introduction

This dissertation presents the results of experimental studies carried out on the rotational dynamics of photosensitive molecules and droplets dissolved in liquid solutions.

Molecules in solution, as well as particle suspended in a fluid, move in a chaotic way (Brownian motion) owing to the random collisions with the surrounding medium. While for macroscopic objects the motion is influenced only by the particles geometry and size, by fluid viscosity and by temperature, on a molecular scale, such a motion is influenced also by molecular specific interactions and correlations. The latter factors in many cases are not yet completely clarified; for these reasons the molecular Brownian motion continues to be a topical field of research in molecular physics.

We focused our attention on particular anisotropic molecules, belonging to the class of the anthraquinone-derivatives dye. These materials attracted our interest because of their ability to increase the nonlinear optical response of liquid crystals (LC). This nonlinearity enhancement, also known as Jánossy effect, has been explained by assuming a photoinduced change of the strength of the interactions between the dye and the liquid crystal molecules. The role played by the dye-LC interactions has been confirmed by the observation of a further enhancement of the effect for deuterium-substituted dye. We investigated the effect of the deuterium substitution on the

rotational Brownian motion of the dye molecules by the time-resolved fluorescence depolarization technique. The molecules were dissolved in both organic liquids and nematic liquid crystals. As we will see, our results confirmed the important role of specific intermolecular interactions in the molecular Brownian motion.

We also studied the effect of the excess photon excitation energy on the rotational diffusion of dye molecules. When exciting absorbing molecule with a photon having energy in excess with respect to the minimum for optical absorption, this extra-energy is suddenly changed into vibrational energy and exchanged by means of collisions with the surrounding molecules. This induces a significant local heating (up to several hundreds of Kelvins) that is dissipated in a time of the order of the thermal relaxation time (few picoseconds for molecular scale). In several works it has been supposed that such heating can produce effects on the molecules orientation, such as its partial or full randomization. By means of time-resolved fluorescence we measured the degree of orientational order of a dye solution in a liquid solvent immediately after the thermal relaxation, varying the excitation photon energy. We also measured the dependence on the excitation energy of the excited state lifetime and of the rotational time and, by means of steady-state fluorescence technique, the same dependence for the fluorescence quantum yield. These measurements have been carried out also in order to understand if one of these parameters has an influence in determining the unexpected wavelength dependence observed in the Jánossy effect. As we will see, the results of these experiments will enable us to give an upper limit to the aforementioned orientational randomization, and to gain a better understanding of the photophysics of these dyes. This understanding is also useful to interpret the wavelength dependence of the Jánossy effect.

The dye-enhanced nonlinearity, i.e. the Jánossy effect, can be ascribed to a corresponding enhancement of the molecular torque exerted by light in the dye-LC system. In the molecular model proposed to explain the effect, the angular momentum exchange associated with the additional torque occurs, via dye molecules, with the internal translational degrees of freedom of the LC molecules. Being this an internal exchange of angular momentum, the Jánossy effect should not lead to any enhancement of the net angular momentum exchanged by the dye-LC system as a whole. This fact, however, has never been directly checked and for this reason, the proposed molecular model is still debated. In order to verify directly the nature of the angular momentum exchange in the Jánossy effect, we built an optical tweezers setup in a particular configuration. This setup makes use of the light of two superimposed laser beams to trap and induce rotation on micrometric dye-doped liquid crystal droplets. Only one of the two beams, having wavelength lying in the absorption spectrum of the dye, can induce the excitation responsible of the Jánossy effect. Since the rotational motion of the whole droplets depends only on the net angular momentum exchanged with external sources, from the comparison of the rotation induced by the two different beams we can verify if there is a dye-induced enhancement of the overall angular momentum exchange or not.

This dissertation is organized as follows. In Part 1 we provide theory elements useful to understanding both the subject of our investigation and the experimental framework. Chapter 1 describes the motion of a particle in a fluid. The first section reviews the rotational friction forces acting on an object due to its motion in a fluid. The following sections deal with the diffusion theory and Brownian motion. The last section describes dispersive forces and torques induced by the light on an anisotropic

object. Chapter 2 describes some basic features of dye molecules. In the first section we focus our attention on their diffusion motion in liquid solvent. In the second section a description of their energetic spectrum is given in connection with their photophysics. In the last section we derive an expression describing the polarization of the emitted fluorescence following the excitation induced by a linear polarized light pulse. Chapter 3 reviews the basic features of nematic liquid crystals. The liquid crystalline phases, the order parameter, and the liquid crystal alignments are defined; sections 2 and 3 provide qualitative descriptions of the nonlinear optical responses of liquid crystals and of the dye-induced enhancement of the optical nonlinearity. The last section deals with the molecular model proposed by Jánossy. The model seems to explain the origin of the dyeinduced torque but does not give a clear explanation of some observed features, such as the wavelength dependence of the nonlinearity.

In Part 2 the experimental techniques are described. The characteristics of the dyes and the liquid crystals that were used in the experiments, along with their molecular structures, are provided in Chapter 4. In Chapter 5 the details of time-resolved and steady-state fluorescence techniques are given, along with descriptions of setups, instruments, and calibration and test measurements. Chapter 6 describes in brief the basics of the optical tweezers technique. In section 1 we describe our "double-wavelength" apparatus, allowing to trap and put in rotation, by means of two superimposed laser beam, micro-sized objects. Sections 2 describes theorically the orientational and rotational manipulation of birefringent particles.

In Part 3 we report and discuss our experimental results. In Chapter 7 are presented the results of a time-resolved fluorescence study of the rotational dynamics of normal and deuterium-substituted dye molecules in organic solvents. The large

deuterium-induced effect, leading to an increase of the rotational time of the dye molecules in polar solvent and vanishing in nonpolar host suggest that the specific interactions play a significant role in our materials. The experimental data are then compared with the prediction of the classical Stokes-Einstein-Debye model. Our studies on the effect of the excess excitation energy on the relaxation dynamics of dye molecules in liquid solution, utilizing time-resolved and steady-state fluorescence techniques, are presented in Chapter 8. From our data we can rule out the validity of some models proposed in the past in order to describe the molecular random reorientation ensuing light excitation. These measurements also provide a possible explanation of the wavelength dependence observed in the dye-enhanced optical nonlinearity of liquid crystals. Finally, in Chapter 9 we report measurements of the rotation frequency of dye-doped liquid crystal droplets in water. The rotation is induced by circularly polarized light with wavelengths lying in and out the absorption spectrum of the dye. Since no significant variations in the droplet rotational speed are observed, this result directly shows that the angular momentum associated with the dye-induced optical torque is not associated with an enhancement of the total angular momentum exchanged by the dye-LC system with the external environment.

Part I

Theory Elements

Chapter 1

Small Particles in a Liquid Environment: Brownian Motion

1.1 Translational and Rotational Friction of a Small Particle in a Fluid

An object moving through a fluid is affected by the friction of that fluid acting on the object surface. If we consider a sphere with radius R moving with velocity $\mathbf{v}$ in an unbounded fluid with viscosity η the friction force is given by the Stokes law:

$$\mathbf{F} = -\varsigma \mathbf{v}, \tag{1.1}$$

where

$$\varsigma = 6\pi\eta R \tag{1.2}$$

is the friction coefficient for the sphere.

Fluid friction differs from dry-surface friction because the strength of the force depends on how fast the object is moving through the fluid. If we consider a sphere rotating with angular velocity $\boldsymbol{\omega}$ in the fluid we obtain the analogous of Eq. 1.1 for

the rotational case, that is

$$\boldsymbol{\tau} = -\varsigma\boldsymbol{\omega}, \tag{1.3}$$

where $\boldsymbol{\tau}$ is the total torque acting on the sphere and the rotational friction coefficient ς is given by

$$\varsigma = 8\pi\eta R^3 = 6\eta V. \tag{1.4}$$

This equation has been also generalized for other particle shapes as, for example, ellipsoidal or cilindric [1, 2]; in general the effect of the shape on the diffusion constant is taken into account by multiplying the particles volume for a shape factor f. In certain applications, another correction factor C is also considered; the latter can be considered as an empirical "coupling parameter", as it takes into account the boundary conditions used in solving the hydrodynamic equations [3] to determine the friction coefficient. The standard solution presupposes a so-called "stick" boundary condition, leading to $C = 1$, wherein the fluid layer immediately adjacent to the object is assumed to move with the same velocity of the rotating object. This assumption is always valid for large object. However, a so-called "slip" boundary condition, assuming zero tangential velocity of the fluid layer adjacent to the particle, becomes useful in certain applications; for a spherical particle this implies no friction on rotation ($C = 0$). For a nonspherical particles, the value of C predicted by hydrodynamic calculations is a function of the particle shape and ranges from zero to unity.

The general expression for ς in the rotational case is therefore

$$\varsigma = 6\eta V f C. \tag{1.5}$$

1.2 Brownian Motion in One Dimension

The Brownian motion is the random walk motion of small particles suspended in a fluid due to collisions with molecules obeying a Maxwellian velocity distribution. The phenomenon was first observed by Jan Ingenhousz in 1785, but was subsequently rediscovered by Brown in 1828. Einstein used kinetic theory to derive the diffusion constant for such motion in terms of fundamental parameters of the particles and liquid, and this equation was subsequently used by Perrin to determine Avogadro's number. Eistein's theory is a phenomenological approach regarding Brownian motion as a stochastic process and leading to a phenomenological equation based on known macroscopic laws. A way to derive this equation is by the generalization of the diffusion equation; in such a way we obtain the so-called Smoluchowski equation which has a clear relevance to the thermodynamics of irreversible processes.

The diffusion process is phenomenologically decribed by Fick's law, which says that if the concentration of particles is not uniform, this non-uniformity generates a current $j(x,t)$ proportional to the spatial gradient of the distribution function $f(x,t)$[1]:

$$j(x,t) = -D\frac{\partial f}{\partial x} \tag{1.6}$$

where D is called the diffusion constant. If there is an external potential $U(x)$, this potential will exert a force on the particles and it will give rise to a non-vanishing average velocity. In the condition of weak force the velocity v is linear in the force so that

$$v = -\frac{1}{\varsigma}\frac{\partial U}{\partial x}. \tag{1.7}$$

[1]If we consider non-interacting particles we can identify the concentration $c(x,t)$ with the distribution function $f(x,t)$.

The constant ς is called the friction constant. The average velocity of the particles gives an additional flux $v \cdot f$ so that the total flux is

$$j = -D\frac{\partial f}{\partial x} - \frac{f}{\varsigma}\frac{\partial U}{\partial x}. \tag{1.8}$$

From Eq. 1.8 it is possible to derive the Einstein relation for the diffusion constant. At the equilibrium $j = 0$ the distribution function is given by the well known Boltzmann distribution $f_{eq}(x) \propto \exp\left(-U(x)/kT\right)$; it follows that

$$D = \frac{kT}{\varsigma}. \tag{1.9}$$

By means of Eqs .1.8 and 1.9, together with the continuity equation

$$\frac{\partial f}{\partial t} = -\frac{\partial j}{\partial x} \tag{1.10}$$

we obtain the Smoluchowski equation for the diffusion

$$\frac{\partial f}{\partial t} = -\frac{\partial j}{\partial x} = \frac{\partial}{\partial x}\frac{1}{\varsigma}\left(kT\frac{\partial f}{\partial x} + f\frac{\partial U}{\partial x}\right). \tag{1.11}$$

Since the total current j can be rewritten as

$$j = -\frac{f}{\varsigma}\frac{\partial}{\partial x}\left(kT\ln f + U\right) \tag{1.12}$$

we can give a thermodynamic interpretation to the Smoluchowski equation. The quantity $kT\ln f + U$ is in fact the chemical potential for noninteracting particles with concentration f. Thus the current is proportional to the spatial gradient of the chemical potential. This is a natural generalization of Fick's law, because when the external field is nonzero, what must be constant in the equilibrium state is not the concentration but the chemical potential.

1.3 Rotational Brownian Motion of Rodlike Particles

Consider a particle with a strongly elongated shape. Dealing with their diffusion motion we can treat it as a rigid rod and define an unit vector $\mathbf{s}$ parallel to their long axis direction in order to describe its orientation.

For rodlike particles we can distinguish two kind of Brownian motion: translational and rotational. The translational Brownian motion is the random motion of the position vector of the center of mass; the rotational Brownian motion is instead the random motion of the long axis versor $\mathbf{s}$. Such a motion can be visualized as a random walk on the unit sphere of possible orientations. For short times, the random motion of $\mathbf{s}(t)$ can be regarded as Brownian motion on a two-dimensional flat surface. By the expression of the mean square displacement of $\mathbf{s}(t)$ in time it is possible to define the rotational diffusion constant D

$$\langle (\mathbf{s}(t) - \mathbf{s}(0))^2 \rangle = 4Dt. \tag{1.13}$$

Eq. 1.13 holds only if $Dt \ll 1$. The most general case has been discussed by Kirkwood and coworkers [4]. To our purposes is therefore sufficient the elementary method given hereafter [5].

Let us start considering a small rod placed in a quiescent viscous fluid. If an external field exerts a torque $\boldsymbol{\tau}$ on the rod, the rod will rotate with an angular velocity $\boldsymbol{\omega}$. For thin rod we can neglect the rotation around its long axis $\mathbf{s}$ and assume that both $\boldsymbol{\tau}$ and $\boldsymbol{\omega}$ are perpendicular to $\mathbf{s}$; for small $\boldsymbol{\tau}$ we can also assume linearity between $\boldsymbol{\tau}$ and $\boldsymbol{\omega}$ (as in Eq. 1.3):

$$\boldsymbol{\omega} = -\frac{1}{\varsigma}\boldsymbol{\tau}. \tag{1.14}$$

By symmetry the vectors are moreover considered parallel. The coefficient ς is the rotational friction constant.

Consider now an external field $U(\mathbf{s})$; suppose that this field induce a small rotation $\delta\boldsymbol{\psi}$ which changes $\mathbf{s}$ to $\mathbf{s} + \delta\boldsymbol{\psi} \times \mathbf{s}$; equating the work done $-\boldsymbol{\tau} \cdot \delta\boldsymbol{\psi}$ by the system to the change in the potential, i.e.

$$-\boldsymbol{\tau} \cdot \delta\boldsymbol{\psi} = U(\mathbf{s} + \delta\boldsymbol{\psi} \times \mathbf{s}) - U(\mathbf{s}) = (\delta\boldsymbol{\psi} \times \mathbf{s}) \cdot \frac{\partial}{\partial \mathbf{s}} U = \delta\boldsymbol{\psi} \cdot \left(\mathbf{s} \times \frac{\partial}{\partial \mathbf{s}} U \right), \quad (1.15)$$

we obtain for the torque $\boldsymbol{\tau}$ the expression

$$\boldsymbol{\tau} = -\mathbf{s} \times \frac{\partial}{\partial \mathbf{s}} U = -\mathcal{R} U, \quad (1.16)$$

where the differential operator $\mathcal{R}$, called rotational operator, plays the role of the gradient in the translational diffusion.

Therefore the angular velocity of a small rod immersed in a fluid subject to an external potential $U(\mathbf{s})$ is given as

$$\boldsymbol{\omega} = -\frac{1}{\varsigma} \mathcal{R} U. \quad (1.17)$$

To include the effect the Brownian motion we add to the potential U the "Brownian potential" $kT \ln f$, where $f(\mathbf{s}, t)$ is the function distribution of $\mathbf{s}$. The angular velocity is now given by

$$\boldsymbol{\omega} = -\frac{1}{\varsigma} \mathcal{R}(kT \ln f + U). \quad (1.18)$$

Since $\mathbf{s}$ changes with velocity $\boldsymbol{\omega} \times \mathbf{s}$ we can write the continuity equation

$$\frac{\partial f}{\partial t} = -\frac{\partial}{\partial \mathbf{s}} \cdot (\boldsymbol{\omega} \times \mathbf{s}) f = -\left(\mathbf{s} \times \frac{\partial}{\partial \mathbf{s}} \right) \boldsymbol{\omega} f = -\mathcal{R} (\boldsymbol{\omega} f). \quad (1.19)$$

From Eqs. 1.18 and 1.19 we have the Smoluchowski equation for the rotational diffusion

$$\frac{\partial f}{\partial t} = D\mathcal{R} \cdot \left(\mathcal{R} f + \frac{f}{kT} \mathcal{R} U \right), \quad (1.20)$$

where D is defined by the rotational Einstein's relation

$$D = \frac{kT}{\varsigma}. \tag{1.21}$$

If we neglect the effect of external fields ($U = 0$) the Eq. 1.20 reduces to

$$\frac{\partial f}{\partial t} = D\mathcal{R}^2 f = -\hat{\Lambda} f. \tag{1.22}$$

In the following we will show that constant D introduced in Eq. 1.20 agrees with the rotational diffusion constant defined in Eq. 1.13.

1.4 Sperical Harmonics Approach to Rotational Brownian Motion

We assume that the system has cylindrical symmetry around our axis z, so that we can retain only the dependence of the distribution function on the azimuthal angle θ. The operator $\hat{\Lambda}$ defined in Eq. 1.22 is nothing but the angular part of the ordinary ∇ operator in spherical coordinates times the constant D and, owing to the symmetry, its explicit expression is given by

$$\hat{\Lambda} = -\frac{D}{\sin\theta}\frac{\partial}{\partial\theta}\sin\theta\frac{\partial}{\partial\theta}. \tag{1.23}$$

It can be shown that the Legendre polynomials form a complete set of eigenfunctions of $\hat{\Lambda}$ with eigenvalue given by

$$\hat{\Lambda} P_l(\cos\theta) = Dl(l+1)P_l(\cos\theta). \tag{1.24}$$

A solution of Eq. 1.22 can be then written as

$$f(\theta, t) = \frac{1}{4\pi}\sum_l (2l+1)Q^{(l)}(t)P_l(\cos\theta), \tag{1.25}$$

where

$$Q^{(l)}(t) = \langle P_l(\cos\theta)\rangle_{f(\theta,t)} = \int f(\theta,t) P_l(\cos\theta) d\Omega. \tag{1.26}$$

are the Legendre moments of the distribution f. Therefore the infinite set of moments $Q^{(l)}$ provides an equivalent description of the system dynamics by means of the set of equations

$$\dot{Q}^{(l)}(t) = -l(l+1)DQ^{(l)}(t) \tag{1.27}$$

whose solutions are

$$Q^{(l)}(t) = Q^{(l)}(0)e^{-l(l+1)Dt}. \tag{1.28}$$

As examples we can calculate the Legendre moments for $l = 1, 2$; we get

$$Q^{(1)}(t) = \langle \cos\theta\rangle_{f(\theta,t)} = Q^{(1)}(0)e^{-2Dt} \tag{1.29}$$

and

$$Q^{(2)}(t) = \frac{\langle 3\cos^2\theta - 1\rangle_{f(\theta,t)}}{2} = Q^{(2)}(0)e^{-6Dt}. \tag{1.30}$$

If we assumes that at time $t = 0$ the distribution function is described by $f(\theta, t = 0) = \delta(\theta)$, i.e. the particle is known to be aligned with the z-axis, then all the Legendre moments reduce to $Q^{(l)} = 1$, $\forall l$ and the moment $Q^{(1)}$

$$\langle \cos\theta\rangle = \langle \mathbf{s}(t)\cdot\mathbf{s}(0)\rangle = e^{-2Dt}. \tag{1.31}$$

corresponds to the time correlation function representing the conditional probability that the rod is in the direction $\mathbf{s}$ at time t, given that it was in the direction $\mathbf{s}'$ at time $t = 0$.

By the last equation it follows

$$\langle(\mathbf{s}(t) - \mathbf{s}(0))^2\rangle = 2 - 2\langle \mathbf{s}(t)\cdot\mathbf{s}(0)\rangle = 2\left(1 - e^{-2Dt}\right) \tag{1.32}$$

that for $Dt \ll 1$ reduces to Eq. 1.13, giving a clear physical meaning of D.

1.5 Dispersive Forces and Torques Induced by Light on Anisotropic Particles

Small dielectric objects develop an electric dipole moment in response to the light's electric field. This dipole $\mathbf{d}$ is given by

$$\mathbf{d} = \tilde{\alpha}\mathbf{E}, \tag{1.33}$$

$\mathbf{E}$ being the electric field and $\tilde{\alpha}$ is a tensor representing the polarizability of the particle [6, 7]. This dipole interacts with the electric field itself and is subject to a dipole force. This force is named "gradient force" and is given by

$$\mathbf{F} = (\mathbf{d} \cdot \nabla)\,\mathbf{E} = \frac{1}{2}\tilde{\alpha}\nabla\mathbf{E}^2 \tag{1.34}$$

since it is proportional to the gradient of the intensity of the field.

For anisotropic particles the induced dipole is in general not parallel to the electric field [6]. In such a case, the interaction between the electric field carried by the light and the dipole gives rise to a torque acting on the particle, given by

$$\boldsymbol{\tau} = \mathbf{d} \times \mathbf{E} \tag{1.35}$$

which tends to align the dipole in the direction of the field or orthogonal to it, depending on the relative magnitude of the polarizability tensor eigenvalues.

Bibliography

[1] Perrin, F. *Phys. Radium* **1934**, *5*, 497.

[2] Zwanzig, R. *J. Chem. Phys.* **1978**, *68*, 4325–4326.

[3] Hu, C.-M.; Alavi, R. *J. Chem. Phys.* **1974**, *60*, 4354–4357.

[4] Kirkwood, J. G.; Auer, P. L. *J. Chem. Phys* **1951**, *19*, 281.

[5] Doi, M.; Edwards, S. F. *The Theory of Polymer Dynamics;* Oxford Univ. Press: Oxford, 1986.

[6] Boyd, R. W. *Nonlinear Optics;* Academic Press: San Diego, 1992.

[7] Shen, Y. R. *The Principles of Nonlinear Optics;* John Wiley & Sons: New York, 1984.

Chapter 2

Rotational Dynamics of Rodlike Dye Molecules in Liquid Solutions and Interaction with Light

2.1 Rodlike Dye Molecules Brownian Motion, SED model and Effects of Specific Interactions

The nature of the rotational motion of molecules in solution is an interesting topic in physical chemistry because such motion directly reflects the interactions between a solute molecule and its solvent surroundings. Studies of rotational dynamics provide a useful starting point for exploring the molecular friction and its influence on other more complex mechanisms.

The rotational motion of molecules can be usually described by the theory of the Brownian motion of small rods described in Sect. 1.3 The diffusion constant is usually estimated by the so-called Stokes-Einstein-Debye (SED) model which associates the molecular level friction with the solvent viscosity, as given in Eq. 1.5, providing a reasonable estimate of the diffusion constant D of a molecule in solution.

The SED theory therefore treats the solute as a smooth ellipsoid rotating in a continuous fluid, and solves a linearized Navier-Stokes hydrodynamic equation (assuming slow, steady motion of the solute) to calculate the mechanical friction [1]. This leads to the prediction that the rotational diffusion constant D should be proportional to the ratio between the solvent absolute temperature T and the solvent viscosity η; more specifically,

$$D = \frac{kT}{6C_s\eta f V} \tag{2.1}$$

where V is the solute molecular volume, the factor f considers deviation of the solute shape from the spherical one and C is a factor determined by boundary conditions assumed in hydrodynamic calculations of the friction. The boundary conditions used in the hydrodynamic calculation usually ranges from "slip" to "stick", as anticipated in Sect. 1.1.

The stick boundary condition, requiring zero relative velocity between the surface of the molecule and the first layer of solvent, is appropriate for macroscopic objects and macromolecules. The slip boundary condition, so named because it specifies that the solvent can exerts no tangential stress on an object, is considered appropriate for small and medium sized molecules in nonpolar, weakly interacting solvents. These boundary conditions allow to take into account effects as the specific intermolecular interactions, completely neglected by the hydrodynamic approach.

However, the coupling between a molecular solute and its surrounding cannot be quantitatively described in terms of macroscopic hydrodynamics. Several experimental results suggest that this theory breaks down when the size of the solute molecules approaches that of the solvent molecules or become smaller; this regime includes the important case of pure materials. In this range the SED model can still provide an

useful language for discussing data. However, its predictive power is severely limited and this becomes especially evident when tiny changes of the solute molecular structure in a given unmodified solvent lead to large variations of its rotational mobility.

2.2 Intermolecular interactions

Intermolecular interactions are the forces exerted by molecules on each other. Intermolecular forces are responsible for many physical properties of matter as melting point, boiling point, density, heat of fusion, vapor pressure, evaporation, viscosity, surface tension, and solubility. Intermolecular forces pin gigantic molecules like enzymes, proteins, and DNA into the shapes required for biological activity.

Such forces may be either attractive or repulsive in nature. They are conveniently divided into two classes: short-range forces, which operate when the centers of the molecules are separated by 3 angstroms or less, and long-range forces, which operate at greater distances. Generally, if molecules do not tend to interact chemically, the short-range forces between them are repulsive. These forces arise from interactions of the electrons associated with the molecules and are also known as exchange forces. Molecules interacting chemically have attractive exchange forces; these are also known as valence forces. Mechanical rigidity of molecules and effects such as limited compressibility of matter arise from repulsive exchange forces. Long-range forces, or "van der Waals forces" as they are also called, are attractive and account for a wide range of physical phenomena such as friction, surface tension, adhesion and cohesion of liquids and solids, viscosity, and the discrepancies between the actual behavior of gases and that predicted by the ideal gas law. Van der Waals forces act between molecules having closed shells. These forces are much weaker than chemical bonds, and random

thermal motion around room temperature can usually overcome them. They operate only when molecules pass very close to each other, during collisions or near misses. The van der Waals forces consist of several types of interaction:

- interaction between permanent dipoles;
- interaction between a permanent dipole and a temporary dipole, or the induction effect;
- interaction between temporary dipoles and induced dipoles known as dispersion effect or the London force.

The strongest intermolecular forces occur when both molecules contain groups or regions permanently electron-rich or electron poor. We refer to them as permanent forces. When the molecule has a distinctly positive end and a negative end, the permanent force is referred to as a dipole-dipole attraction. Weaker (but still noticeable) permanent forces can act between any molecules with polar bonds. The interaction energy of two permanent dipoles depends on their relative orientation, and might be expected to be zero overall for a compound if all orientations are possible. This would be true if the molecules were completely free to rotate, but they are not and some orientations are preferred over others. The energy of interaction varies as $1/r^6$, the force between the dipoles as $1/r^7$. It is inversely dependent upon the temperature.

A polar molecule can also induce a temporary dipole in a nonpolar molecule. The electron cloud around a nonpolar molecule responds almost instantaneously to the presence of a dipole, so this "dipole-induced dipole" force is not as orientation-dependent as the dipole-dipole interaction. This also varies as $1/r^6$, but unlike the

previous case it is independent of temperature. Its magnitude depends on the polarizability of the molecule.

Transitory forces arise from a temporary dipole inducing a complementary dipole in an adjacent molecule. A temporary dipole can be generated when electron clouds oscillate in step on two molecules at close range. Bond vibrations in molecules may produce these oscillations. The electron-rich and electron-poor regions on the molecule may not persist for more that 10^{-14} or 10^{-15} seconds, but if they can polarize the electron distribution on an adjacent molecule, electron clouds on the two molecules may begin to oscillate cooperatively with each other. The dipoles are transitory but aligned and induced in phase. They give a net attractive force pulling the molecules together. At closer range, the oscillation becomes even more effective. Transitory forces are sometimes called "London forces" in honor of their discoverer. These are the only forces of interaction in non-polar molecules. They depend on the molecular polarizability and vary as $1/r^6$. They are usually weaker than the permanent forces. However, molecules with large, diffuse electron clouds can have London forces that are at least as strong as permanent forces are. The effect is often called the dispersion effect since the same electronic movement originating London forces also causes dispersion of light, that is the variation of refractive index of a substance with the frequency of the light.

2.2.1 Hydrogen Bonding

One of the most important intermolecular interactions is the hydrogen bond or H-bond [2]. It is an abnormally strong dipole-dipole force. A hydrogen bond is the attractive force between the hydrogen attached to an electronegative atom of one

molecule and an electronegative atom of a different molecule. Usually the electronegative atom is oxygen, nitrogen, or fluorine, which has a partial negative charge.

The possibility for a molecule of hydrogen bonding can be roughly recognized by the examination of the Lewis structure of the molecule. The electronegative atom must have one or more unshared electron pairs as in the case of oxygen and nitrogen, and has a negative partial charge. Hydrogen atoms are very small. When a bonded electronegative atom pulls electrons away from the hydrogen atom, the positive charge that results is tightly concentrated. The hydrogen is intensely attracted to small, electron-rich O, N, and F atoms on other molecules. This forms the basis for the hydrogen bond.

Even if hydrogen bonding is usually stronger than normal dipole forces between molecules, of course it is not nearly as strong as normal covalent bonds within a molecule; it is only about few tenth as strong. This is still strong enough to have many important ramifications, for example on the properties of water. The bond lengths give some indication of the bond strength. A normal covalent bond is 0.96 Å, while the hydrogen bond length is 1.97 Å.

Hydrogens bonded to either oxygen or fluorine typically form strong hydrogen bonds with a suitable partner. Hydrogens bonded to certain types of nitrogen can also generate hydrogen bonding, and many hydrogen-bonded systems are based on this type of hydrogen. Hydrogens bonded to carbon, namely CH_n groups, rarely, if ever, form strong hydrogen bonds. On the other side, only nitrogen and oxygen atoms seem to give to neutral compounds the capability to hydrogen bond. Therefore, most hydrogen bonds look like $O{-}H\cdots X$ or $N{-}H\cdots X$, (where X = N or O, $-$ and $\cdots$ correspond to covalent and hydrogen bonds, respectively). An example of the

O−H$\cdots$O pattern can be found in water. Several examples of the N−H$\cdots$X pattern appear in double-stranded DNA. Hydrogen bonds are essential for building biological systems: they are strong enough to bind biomolecules together but weak enough to be broken, when necessary, at the temperatures that typically exist inside living cells.

2.3 Dye Molecule Photophysics

All the organic compounds having a high absorption in the visible part of the electromagnetic spectrum are generally called "dye" [3]. In this Section we discuss the main processes at the root of the interactions of dye molecules with light.

2.3.1 Light Absorption

The absorption properties of the dye molecules are due to the fact that they possess several conjugate double bonds. A peculiarity of the spectra of organic dyes is the width of the absorption bands, which usually covers several tens of nanometers. This is immediately comprehensible when one recalls that a typical dye molecule may possess tens of atoms, and each of them gives rise to three normal vibrations of the molecular skeleton. Many of these vibrations are coupled to the electronic transition. Furthermore, collisional and electrostatic perturbations, caused by the surrounding solvent molecules broaden the individual lines of such vibrational series. Moreover, every vibronic sublevel of every electronic state, including the ground state, has superimposed on it a ladder of rotationally excited sublevels. These are extremely broadened because of the frequent collisions with solvent molecules which

hinder the rotational movement so that there is a quasicontinuum of states superimposed on every electronic level. Thus the absorption is practically continuous all over the absorption band. This can be better understood with the help of a Jabłoński diagram.

A typical Jabłoński diagram is shown in figure 2.1. The singlet ground, first and

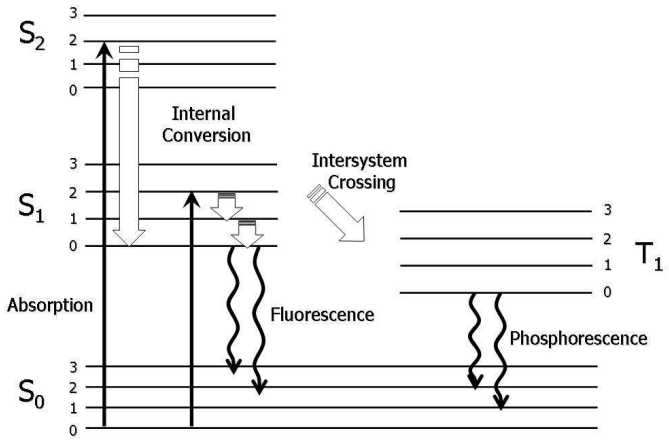

Figure 2.1: A typical Jabłoński diagram.

second electronic states are depicted by S_0, S_1 and S_2 respectively. At each of these electronic energy levels the fluorophores can exist in a number of vibrational energy levels, denoted by 0, 1, 2, etc. The transitions between states are depicted as vertical lines to illustrate the instantaneous nature of light absorption. Transitions generally occur in times too short for significant displacement of atomic nuclei. This is the Franck-Condon principle.

The energy spacing between the various vibrational energy levels is typically larger than the thermal energy at room temperature, hence only the lowest vibrational state is significantly populated. Therefore absorption occurs from molecules with the lowest

vibrational energy. The even larger energy difference between the S_0 and S_1 electronic states explain why light is used to induce electronic excitation.

2.3.2 Nonradiative Relaxation and Fluorescence Emission

Following light absorption several processes can occur. A fluorophore is usually excited to some higher vibrational level of the excited state. With few rare exceptions, molecules in condensed phases rapidly relax to the lowest vibrational level of S_1. This process is called internal conversion and generally occurs in 10^{-12}s or less.

Fluorescence is the phenomenon of emission of light from electronically excited singlet states of any substance. In excited singlet state, the electron in the excited orbital is paired to the second electron (of opposed spin) in the ground-state orbital. Consequently, selection rules allow the transition to the ground state and it occurs rapidly by the emission of a photon.

Since fluorescence lifetimes are typically of the order of nanoseconds, internal conversion is generally complete prior to emission. Hence, fluorescence emission results from a thermally equilibrated excited state.

Return to the ground state typically occurs to a higher excited vibrational excited-state level, which then quickly reaches the thermal equilibrium. An interesting consequence of emission to higher vibrational ground states is that the emission spectrum is a red-shifted mirror image of the absorption spectrum of the $S_0 \rightarrow S_1$ transition (Fig. 2.2). This similarity occurs because electronic excitation does not great alter the nuclear geometry. Hence, the spacing of the vibrational energy levels of the excited state is similar to that of the ground state. As a result, the vibrational structures seen in the absorption and emission spectra are similar.

The red-shift of the emission spectrum with respect to the absorption spectrum, (i.e. the energy of the emission is less than that of absorption) was first observed by Sir G. G. Stokes in 1852 [4], and it is named Stokes' shift. The cause of this effect is the rapid decay to the lowest vibrational level of S_1. Furthermore fluorophores generally decay to higher vibrational levels of S_0, resulting in further loss of excitation energy by thermalization of the excess vibrational energy. In addition to these effects, further Stokes' shift can be due to several mechanisms as solvent effects, excited-state reactions, complex formation and energy transfer.

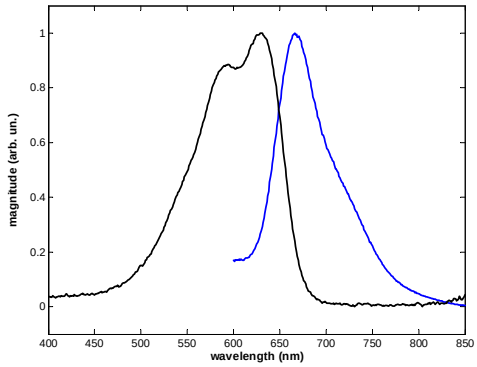

Figure 2.2: Absorption and fluorescence spectra of the anthraquinone dye HK271 (see text for its structure) in ethanol. The fluorescence has been collected at a pump wavelength of 630nm.

2.3.3 Quantum Yields and Fluorescence Lifetimes

Among the parameters involved in the fluorescence emission, the fluorescence lifetime and the quantum yield are perhaps the most important in characterizing a fluorophore. The quantum yield is the number of emitted photons relative to the number of absorbed photons. Substances with the largest quantum yields, approaching unity, such as rhodamine, displays the brightest emission. The lifetime is also important,

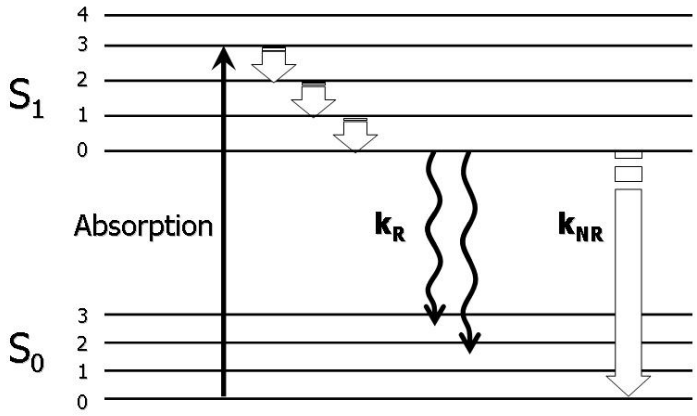

Figure 2.3: A simplified Jabłoński diagram.

as it determines the time available for the fluorophore to interact with or diffuse in its environment, and hence the information available from its emission.

The meaning of the quantum yield and the lifetime is best represented by a simplified Jabłoński diagram (Fig. 2.3).

In the diagram we do not explicitly illustrate the individual relaxation processes leading to the S_1 state. Instead, we focus our attention on those processes responsible for return to the ground state. In particular, we are interested in the emissive rate of the fluorophores (k_R) and its rate of nonradiative decay to S_0 (k_{NR}). The fluorescence quantum yield is the ratio of the number of photons emitted to the number absorbed. The processes governed by the rate constants k_R and k_{NR} both depopulate the excited state. The fraction of fluorophores which decay through emission, and hence the quantum yield, is given by

$$\Phi = \frac{k_R}{k_R + k_{NR}}. \tag{2.2}$$

For convenience all the possible nonradiative decay processes have been grouped with the single rate constant k_{NR}.

The lifetime of the excited state is defined by the average time the molecule spends in the excited state prior to return to the ground state. Following the diagram in fig. 2.3 it is given by

$$\tau_e = \frac{1}{k_R + k_{NR}}. \tag{2.3}$$

One should remember that fluorescence emission is a random process and the lifetime is an average value of the time spent the in excited state.

The quantum yield and the lifetime can be modified by factors affecting either of the rate constants.

2.4 Absorption of a Polarized Light Short Pulse and Polarization of the Ensuing Fluorescence

In the previous chapter we discussed the Smoluchowski equation describing the rotational diffusion dynamics of rodlike particles. In the following we present a molecular model based on the Smoluchowski equation able to describe the rotational diffusion dynamics of a mixture of dye molecules in a liquid solvent under influence of light. For low-energy light pulse we can neglect their effect on the solvent molecules (Kerr effect). Since the dye molecules absorb light with wavelength lying in their absorption spectrum and photoexcitation can considerably change electronic and dynamical properties of the dye molecules, in the model two dye molecules populations are considered, i.e. ground- and excited-state dye molecules. By means of this model it is possible to give an expression for the time dependence of the fluorescence intensity due to short-duration and low-energy pulse excitation that will be very useful in the following.

2.4.1 Molecular Model

Consider an absorbing liquid obtained by dissolving a small amount of dye in a transparent host. If linearly polarized light, with a wavelength lying in the absorption spectrum of the dye, passes through the mixture, part of the dye molecules are excited; we assume that only the first-excited electronic state S_1 is involved. In describing the molecular process we have to deal with two populations of molecules: ground- and excited-state dye molecules. We refer to them with the subscript $\alpha = g, e$. The number of molecules per unit volume and solid angle in function of the time t and the molecular orientation $\mathbf{s}$ is $f_\alpha(\mathbf{s}, t)$ and the number of molecules per unit volume is therefore given by $N_\alpha = \int d\Omega f_\alpha$.

Starting from the Smoluchowski equation (1.20) it is possible to obtain a dynamical equation for f_α. Owing to the isotropy of the mixture, in this case the system exhibits azimuthal symmetry around the optical electric field direction. Therefore the physical quantities involved depend only on the angle between the molecular axis direction $\mathbf{s}$ and the electric field direction. If we assume the electric field vector $\mathbf{E}$ parallel to the z-axis of a cartesian frame of reference we can retain only the dependence on the angle θ and the dynamical equations are then given by

$$\frac{\partial f_\alpha}{\partial t} + \hat{\Lambda} f_\alpha = W_\alpha, \tag{2.4}$$

where the operator $\hat{\Lambda}$ is defined in Eq. 1.23. In the Eq. 2.4 we neglected the external field term instead present in Eq. 1.20. Such a term in this case would take into account of

- light-induced orientational modifications due to the electromagnetic torque;
- intermolecular orientational interactions.

Both this orientation mechanisms are however higher order effect respect to the term due to the absorption-induced anisotropy explicitly considered by the factors W_α.

The terms W_α are in fact the light induced transition rates between ground and excited state of the dye molecules ($W_h = 0$). To have an explicit expression for W_e and W_g, we consider dye molecules with $S_0 \rightarrow S_1$ transition dipole for light absorption parallel to their axes $\mathbf{s}$; the absorption probability per unit time will be then given by

$$p(\theta) = \frac{3\alpha_0}{h\nu N_d} I \cos^2\theta \tag{2.5}$$

where $N_d = N_g + N_e$, h is the Planck constant, ν the light frequency and c is the light speed in vacuum and $I = \frac{|\mathbf{E}|^2}{2}\frac{nc}{4\pi}$ is the light intensity. The decay probability from the excited state S_1 to the ground state S_0 is instead given by the inverse of the S_1 state lifetime τ_e. The transition rates can therefore be written as:

$$W_e(\theta) = p(\theta) f_g(\theta) - \frac{1}{\tau_e} f_e(\theta). \tag{2.6}$$

This expression is based on two important assumptions. One is that the stimulated emission is negligible. This is reasonable as, in most dyes, the Stokes' shift between absorption and fluorescence spectra brings the excited molecules completely off resonance. The other assumption is that the process of vibrational relaxation immediately following each electronic transition has no significant effect on the molecule orientation. This assumption has been verified experimentally [5], as we will see in the following.

The symmetry allows us to expand the distributions functions f_α in a series of Legendre polynomials P_l (Eqs. 1.25 and 1.26). Because the system also exhibits inversion symmetry, all odd-l moments identically vanish. The infinite set of moments $Q_\alpha^{(l)}$ provides an equivalent description of the system dynamics; in particular the

zeroth-order moments $Q_\alpha^{(0)} = N_\alpha$ are the total number densities of the populations and the ratios $Q_\alpha^{(2)}/N_\alpha = S$ are their orientational order parameters.

2.4.2 Short-duration and low-energy light pulse solution

Now we discuss the solutions of Eq. 2.4 in the form of an equivalent set of equations for the corresponding Legendre moments, in analogy with Eqs. 1.27. We restrict our discussion to the case of a short-duration light pulse with sufficiently small intensity.

Before the light pulse impinges on the absorbing liquid, the system is at equilibrium; all the molecules have an isotropic distribution ($Q_e^{(l)} = Q_g^{(l)} = 0$) and all the dye molecules are in the ground state ($N_e = 0, N_g = N_d$). If the duration of the light pulse is much shorter of the typical response times of the system (τ_e, τ_d, $\frac{1}{6D_e}$ and $\frac{1}{6D_g}$) we can consider the pulse as instantaneous and describe the time dependence of its intensity as a δ-function

$$I(t) = \mathcal{E}\delta(t), \tag{2.7}$$

where $\mathcal{E}$ is the energy per unit area carried by the light pulse. Owing to the short-duration and low-intensity of the pulse, we can neglect the quantities $N_e(t)$, $Q_g^{(2)}(t)$ and $Q_e^{(2)}(t)$ with respect to $N_g(t)$ while the pulse interacts with the system and then describe its dynamics by

$$\begin{aligned} \dot{N}_e &= \frac{\alpha_0 I}{h\nu} \\ \dot{Q}_e^{(2)} &= \frac{2\alpha_0 I}{5h\nu}. \end{aligned} \tag{2.8}$$

The latter equations have been obtained by expanding the transition rates W_α in Legendre polynomials serie. We can moreover assume that the ground-state distribution is not significantly modified, i.e. $f_g \simeq N_d/4\pi$.

Eqs. 2.8 by using 2.7 can be trivially integrated with initial conditions given by $N_e = Q_e^{(2)} = Q_g^{(2)} = 0$; we have

$$\begin{aligned} N_e &= \frac{\alpha_0 \mathcal{E}}{h\nu} \\ Q_e^{(2)} &= \frac{2\alpha_0 \mathcal{E}}{5h\nu} \end{aligned} \tag{2.9}$$

.

After the interaction with the pulse ($I = 0$), the dynamic equations for the system are given by

$$\begin{aligned} \dot{N}_e + \frac{N_e}{\tau_e} &= 0 \\ \dot{Q}_e^{(2)} + \frac{Q_e^{(2)}}{\tau_d} &= 0. \end{aligned} \tag{2.10}$$

with

$$\tau_d = \left(\tau_e^{-1} + 6D_e\right)^{-1}. \tag{2.11}$$

This set of equations, with initial conditions given by Eqs. 2.9 can be integrated giving the relaxation dynamics of the system after the interaction with the light. We obtain

$$\begin{aligned} N_e &= \frac{\alpha_0 \mathcal{E}}{h\nu} e^{-\frac{t}{\tau_e}} \\ Q_e^{(2)} &= \frac{2\alpha_0 \mathcal{E}}{5h\nu} e^{-\frac{t}{\tau_d}} \end{aligned} \tag{2.12}$$

.

2.4.3 Polarization of the Ensuing Fluorescence

Looking at the Eqs. 2.12 it is clearly seen that the time-dependent dynamics of our system is fully defined by the parameters τ_e, τ_d and D_g. In particular, the quantities

τ_e and τ_d characterizing the excited-state dye-molecules dynamics, are also important in defining the fluorescence intensity time decay.

Assume that $\boldsymbol{\mu}_f$ is the $S_1 \rightarrow S_0$ transition dipole of a fluorophore; for rodlike dye molecules we can consider that this dipole is parallel to the long axis direction $\mathbf{s}$. The fluorescence light emitted by this fluorophore in a given direction with polarization parallel to $\mathbf{e}_f$ is given by

$$I(\mathbf{s}) = k\left(\mathbf{e}_f \cdot \mathbf{s}\right)^2. \tag{2.13}$$

The fluorescence intensity due to all the molecules contained in a unit volume emitted in a given direction with polarization direction parallel to $\mathbf{e}_f$ is given by

$$I(t) = \int I(\mathbf{s}) f_e(\mathbf{s}, t) d\Omega \tag{2.14}$$

and, by using 2.13, can be cast in the form

$$I(t) = \frac{k}{3}\Big[N_e(t) + (3\cos^2\gamma - 1)Q_e^{(2)}(t)\Big] \tag{2.15}$$

where γ is the angle of the fluorescence polarization direction $\mathbf{e}_f$ with respect to the z-axis which we recall is taken parallel to the excitation polarization.

By substituting the solutions of the dynamical equation 2.12 in 2.15 we have

$$I(t) = \frac{k}{3}\frac{\alpha_0 \mathcal{E}}{h\nu}\left[e^{-\frac{t}{\tau_e}} + \frac{2}{5}(3\cos^2\gamma - 1)e^{-\frac{t}{\tau_d}}\right]. \tag{2.16}$$

It is possible to see that, as already anticipated, the fluorescence time-decay is driven by the characteristic times τ_e and τ_d. In particular, for the value $\gamma = 54.7°$, the so-called "magic" angle solving the equation $\cos^2\gamma = \frac{1}{3}$, we have

$$I_{\text{magic}} = \frac{k}{3}\frac{\alpha_0 \mathcal{E}}{h\nu}e^{-\frac{t}{\tau_e}} \tag{2.17}$$

and the fluorescence intensity decay shows a single-exponential behavior in which the decay-time is the excited state lifetime τ_e. Moreover we have

$$\begin{aligned} \gamma_f = 0 \qquad & I_{\parallel} = \frac{k}{3}\frac{\alpha_0 \mathcal{E}}{h\nu}\left[e^{-\frac{t}{\tau_e}} + \frac{4}{5}e^{-\frac{t}{\tau_d}}\right] \\ \gamma_f = \frac{\pi}{2} \qquad & I_{\perp} = \frac{k}{3}\frac{\alpha_0 \mathcal{E}}{h\nu}\left[e^{-\frac{t}{\tau_e}} - \frac{2}{5}e^{-\frac{t}{\tau_d}}\right], \end{aligned} \tag{2.18}$$

and rightly combining the expression for $I(t)$ obtained in 2.18 it is possible to obtain

$$I_e = \frac{1}{3}(I_{\parallel} + 2I_{\perp}) = \frac{k}{3}\frac{\alpha_0 \mathcal{E}}{h\nu}e^{-\frac{t}{\tau_e}} \tag{2.19}$$

and

$$I_d = (I_{\parallel} - I_{\perp}) = \frac{2k}{5}\frac{\alpha_0 \mathcal{E}}{h\nu}e^{-\frac{t}{\tau_d}} \tag{2.20}$$

for which we again have a single exponential time-behavior.

Bibliography

[1] Alavi, D. S.; Waldeck, D. H. *J. Phys. Chem.* **1991**, *95*, 4848–4852.

[2] Jeffrey, G. A. *An Introduction to Hydrogen Bonding;* Oxford Univ. Press: Oxford, 1997.

[3] Schäfer, F. P. *Dye Lasers;* Springer Verlag: Berlin - Heidelberg - New York, 1973.

[4] Stokes, G. G. *Phil. Trans. R. Soc. London* **1852**, *142*, 463–562.

[5] Manzo, C.; Paparo, D.; Marrucci, L. *Phys. Rev. E* **2004**, *70*, 051702.

Chapter 3

Nematic Liquid Crystals and Their Photoinduced Collective Reorientation

3.1 Orientational Interactions of Rodlike Molecules and the Nematic Phase

In the following we will deal with a special class of materials in which intermolecular orientational interactions are so strong to induce, in suitable conditions, the appearance of long-range orientational correlations and order. These materials are called liquid crystals; they possess phases with an order that is intermediate between that of a crystalline solid (long range, tridimensional both positional and orientational order) and that of a liquid (neither positional order nor orientational order).

The simplest and least ordered liquid crystal phase is the nematic phase, in which there is no positional order, but in which there is long range order of the direction of the molecules. This phase precedes the transition to the isotropic liquid which occurs at the so-called "clearing point".

The name nematic comes from the Greek word *nemátikos*, meaning woven, because of the thread-like discontinuities which can be observed under the polarizing microscope for this phase.

Cyanobiphenil molecules have the feature to show a nematic liquid crystalline phase in a certain temperature range. They assume a molecular arrangement such that there is no positional order of their centers of mass, like in the isotropic liquid, but there is a long-range orientational order. The molecules tend to orient on the average along a preferred direction indicated by a unit vector called the molecular director $\mathbf{n}$, with $\mathbf{n}$ and $-\mathbf{n}$ being physically equivalent.

The ordering of the molecules in the nematic phase is completely described by the time or ensemble average of the orientation of a molecule-fixed axis system with respect to the director $\mathbf{n}$.

However, the mechanisms responsible for this orientational ordering in liquid crystalline systems are not completely understood. In going from an isotropic state, in which both position and orientation are random, to a nematic state, in which position is random but there is a preferred orientation, there must be a reduction in the orientational entropy of the system, associated with the freedom of a molecule to be oriented in any arbitrary direction. So in order for the nematic state to have a lower free energy than the isotropic state, there must be another term in the free energy which favors orientation. Then, as the temperature changes, the relative importance of the two terms changes, leading to a phase transition. This is likely to occur in melts of rodlike objects for two reasons:

- favorable attractive interactions arising from van der Waals forces between the molecules will be maximized when they are aligned;

- it is easier to pack rodlike molecules when they are aligned.

The first factor is perhaps most important for melts of relatively small molecules which form nematic phases; the second factor is the major factor underlying the transitions that occur as a function of concentration for very long rigid molecules and supramolecular assemblies. In both cases, simple statistical mechanical theories can be formulated on the basis of these ideas.

One of the most successful descriptions of nematic orientational order is the theory proposed by Maier and Saupe. [1–3] This theory, which yield predictions about the nature of the transition between the isotropic and nematic states, is a mean-field theory. The intermolecular potential is approximated by a single-molecule potential function. They propose that the long-range anisotropic attractive interactions resulting from dispersion forces are responsible for nematic formation. The starting point for this theory is to write down an expression for the entropy lost when molecules become oriented.

3.1.1 The Maier-Saupe Theory

As already anticipated, the molecular field method has proved to be extremely useful in developing a theory of spontaneous long range orientational order and in explaining the related properties of the nematic phase. In this approach, each molecule is assumed to be in an average orienting field due to its environment, but otherwise uncorrelated with its neighbors. The most widely used treatment based on the molecular field approximation is that due to Maier and Saupe.

We begin by defining the long range orientational order parameter in the nematic phase. Since the liquid crystal is composed of rodlike molecules we can assume that

the distribution function is cylindrically symmetric about the axis of preferred orientation $\mathbf{n}$ and that the directions $\mathbf{n}$ and $-\mathbf{n}$ are fully equivalent. Subject to these two symmetry properties, and assuming the rods to be cylindrically symmetric, the simplest way of defining the degree of alignment is by the scalar order parameter

$$S = \frac{1}{2}\langle 3\cos^2\theta - 1\rangle, \tag{3.1}$$

where θ is the angle which the long molecular axis makes with $\mathbf{n}$, and the angular brackets denote a statistical average. For perfectly parallel alignment $S = 1$, while for random orientation $S = 0$. In the nematic phase, S has an intermediate value which is strongly temperature dependent. Since the order parameter must be covariant respect to the operations of the rotation symmetry group a more general definition is the order parameter tensor

$$S_{ij} = S\left(n_i n_j - \frac{1}{3}\delta_{ij}\right). \tag{3.2}$$

We assume that each molecule is subject to an average internal field which is independent of any local variations or short range ordering. Consistent with the cylindrical distribution of the molecular axis about the nematic axes and the absence of polarity, the orientational energy of a molecule can be postulated to be

$$U(\mathbf{s}) = -U_0\frac{1}{2}\left(3(\mathbf{n}\cdot\mathbf{u})^2 - 1\right)S = -U_0\frac{1}{2}\left(3\cos^2\theta - 1\right)S. \tag{3.3}$$

The exact nature of the intermolecular forces need not to be specified for the development of the theory, however in their original presentation Maier and Saupe [1–3] assumed that the stability of the nematic phase arises from the dipole-dipole part of the anisotropic dispersion force.

Since we make the phenomenological assumption that the energetic interaction between molecules is that given in Eq. 3.3, the total internal energy of the system

comes out to be simply a quadratic function of the order parameter; we can then write the Helmholtz free energy F in order to find the distribution function which minimizes the free energy for a given value of the order parameter S. By substituting this most probable distribution function in the expression of F we obtain the free energy as a function of the order parameter. From the plots of F versus S corresponding to different values of U_0/kT it is possible to distinguish tree regimes.

For relatively small values of the U_0/kT , the minimum of the free energy function is found for a value of the order parameter of zero; in this regime the free energy is dominated by the orientational entropy term, and the equilibrium state is isotropic. But as the coupling parameter value is increased, a minimum of the free energy is found for a nonzero value of S and the equilibrium phase is nematic. The critical value of U_0/kT for the transition is around 4.55. This correspond to the transition temperature for the nematic/isotropic transition. By calculating the value of the order parameter S as a function of U_0/kT we can investigate the character of the transition. At the value of $U_0/kT = 4.55$ there is a discontinuous change of the order parameter from $S = 0$ to $S = 0.44$. This is the nematic/isotropic phase transition; since the change of the order parameter is discontinuous, it is a first order phase transition. Since the entropy change at the transition is not very great, the transition can be said to be only weakly first order.

The Maier-Saupe theory is based on few simple assumptions; nevertheless there is quite good qualitative agreement with experimentally observed transition temperature.

An important assumption is that U is independent of temperature; this would be the case if the coupling arose entirely from van der Waals forces. This turns out to be

a reasonable approximation for small molecule liquid crystals; while the theory captures the relatively small degree of order at the transition and gives a good account of the increase of order with decreasing temperature, there are clearly systematic deviations from the predictions of theory, particularly close to the transition. There are a number of reasons why there are discrepancies between the experimental data and the predictions of Maier-Saupe theory. Two possible factors are: $(i)$the intrinsic temperature dependence of U. This could arise, for example, because the excluded volume entropic interaction is significant. (ii) Being the Maier-Saupe theory a mean-field theory, it neglects the effects of fluctuations in the order parameter. These are likely to become important close to the transition point.

3.2 Laser-Induced Collective Reorientation of Nematics and Corresponding Giant Optical Nonlinearity

When a linearly polarized optical field interacts with a nematic liquid crystal (NLC) an angular momentum exchange takes place due to the anisotropy of the material polarizability.

The light polarization and propagation, which determine the angular momentum carried by the electromagnetic wave, are affected by the medium birefringence. Concurrently, since the induced material polarization $\mathbf{P}$ is not parallel to the electric field $\mathbf{E}$, a net torque $\mathbf{P} \times \mathbf{E}$ per unit volume acting on the medium is developed, corresponding to the average of the dipole torque (Eq. 1.35) per unit volume. This is the main mechanism for giant optical nonlinearity in transparent liquid crystals

(LC). It can be shown that this torque exactly compensates the change of the angular momentum carried by the light, so that the total angular momentum is conserved. The molecular reorientation induced by this optical torque and the ensuing change of refractive index and birefringence is the root of the giant optical nonlinearity of transparent liquid crystals.

3.2.1 Jánossy Effect, Basic Phenomenology and Current Molecular Understanding

In 1990 Jánossy and his coworkers reported a surprising result [4]: adding small amounts (0.1% w/w) of a dichroic dye of the family of anthraquinone derivatives to a transparent nematic LC could enhance the orientational optical nonlinearity, i.e. the optical torque, up to two orders of magnitude without affecting significantly the birefringence [5–8]. Nonlinear effects, in all respects similar to those observed in transparent materials with laser beams of hundreds of milliwatts, could be induced by means of a laser with only few milliwatts of power. Later experiments demonstrated beyond any doubt that the nonlinearity was still orientational and not due to a trivial thermal effect [5–7].

Since light absorption by itself does not give rise to angular momentum exchange, two problem are concerned with this effect: first, where does the angular momentum come from?, and second, what is the mechanism responsible of the effect on the molecular scale? A first attempt to give a theoretical explanation of the effect was presented by Jánossy [4]; even if the physical picture behind the model of Ref. [4] provides a plausible answer to the second of the above questions, the correct interpretation of the effect has been given later by Marrucci and Paparo [9]. First they

extend the Jánossy molecular model obtaining a correct molecular expression of the dye-induced torque; a schematic description of this model is given in the following of this section. Moreover they approach the problem by a macroscopic point of view, by using symmetry and continuum theory, addressing the question concerning the angular momentum conservation. This model is discussed in Sect. 3.2.2.

The molecular model proposed [9,10] is based on the following two processes: (a) light absorption generating an anisotropy in the dye population; (b) the guest-host intermolecular interactions and dye molecule dynamical parameters are electronic-state dependent and transfer the anisotropy to the liquid crystals. The resulting effect is a dye-induced optical torque that is superimposed to the usual dielectric-anisotropy one and enhances the nonlinear orientational response of the host.

Consider an absorbing nematic LC obtained by dissolving a small amount of dye in a transparent host. If linear polarized light, with a wavelength lying in the absorption spectrum of the dye, passes through the mixture part of the dye molecules are excited and populate the first-excited electronic level. If we consider, for the sake of simplicity, a dye molecules with transition dipole for light absorption parallel to their long axis, the absorption probability per unit time will be proportional to the cosine square of the angle between the polarization direction of the light and the molecular long axis direction. Then linear polarized light excites preferentially dye molecules oriented parallel to the electric field. In such a way, by light excitation, we obtain a population of excited dye molecules with a strongly anisotropic orientational distribution (see the left panel of Fig. 3.1). At this point we need some mechanism able to transfer this orientational anisotropy tho the whole system. We can assume that the light

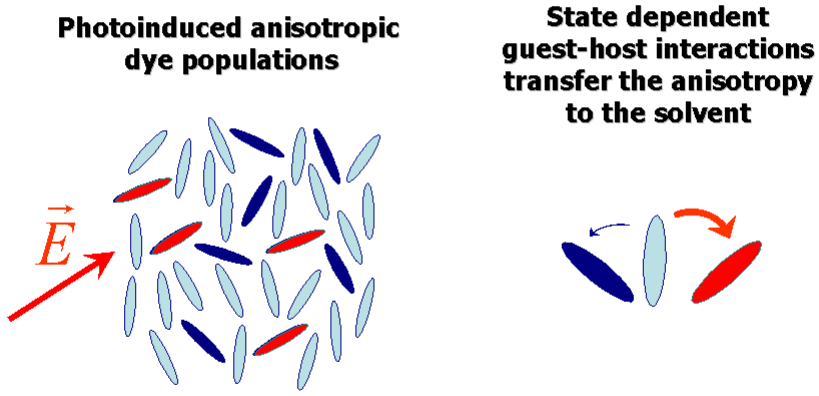

Figure 3.1: Qualitative explanation of the mechanisms leading to the Jánossy effect.

excitation considerably changes both the potential describing the orientational dye-host interactions and the rotational diffusion constant of dye molecules.

Let us first assume, as postulated by Jánossy [4], that the excited molecules attract (from an orientational point of view) the liquid crystal molecules stronger than the ground-state dye molecules, as schematically shown in the right panel of Fig. 3.1. This lead to an additional mechanism in the alignment of the host molecules in the direction of the electric field. The effect of a state-dependent rotational diffusion constant on the orientation of the host molecules can be depicted in these terms: if we assume that the excited molecules diffuse to the equilibrium slower then those in the ground state, we have that the excited molecules tend to "remain" aligned with the polarization direction whereas the ground-state molecules, diffusing faster, restoring their isotropic orientational distribution. This results in a net accumulation of dye molecules, in both the electronic states, along the direction of the electric field. Then, the dye-host orientational interactions (even if assumed to be equal for the two electronic states) transfer the anisotropy to the solvent molecules.

By this qualitative descriptions we see that both the proposed mechanisms, even if considered separately, give rise to an additional torque on the liquid crystal molecules. Nevertheless, the quantitative match between theory and experiments can be obtained only assuming that both the effects are present.

The detailed model accounting for both the mechanism [9] leads to the following expression of the photoinduced torque:

$$\boldsymbol{\tau}_{ph} = -\int d\Omega \left(f_g \frac{kT}{D_g} \boldsymbol{\omega}_g + f_e \frac{kT}{D_e} \boldsymbol{\omega}_e \right), \tag{3.4}$$

where k is the Boltzmann constant, T the absolute temperature, D the rotational diffusion constant, $\boldsymbol{\omega}$ the average angular velocity[1], f the distribution function in the orientation space and the subscripts g and e refer respectively to ground- and excited-state dye molecules.

In principle the equation above can be used to calculate explicitly the photoinduced torque but this is a very difficult task. By introducing some approximations [9] it is possible to obtain for the photoinduced torque the expression:

$$\boldsymbol{\tau}_{ph} = \frac{\zeta}{4\pi} \langle (\mathbf{n} \cdot \mathbf{E})(\mathbf{n} \times \mathbf{E}) \rangle. \tag{3.5}$$

where $\mathbf{n}$ is the nematic director, $\mathbf{E}$ the electric field and the constant ζ turns out to be given by

$$\zeta = \frac{16\pi}{15} \sigma N_d S \frac{\tau_e N_h}{1 + 6 D_e \tau_e} \left(u_{eh} - \frac{D_e}{D_g} u_{gh} \right). \tag{3.6}$$

In the last expression σ is the absorption cross section, N_d and N_h are the number of, respectively, dye and host molecules per unit volume, S is the order parameter, τ_e the dye excited-state lifetime, and u_{eh} and u_{gh} are coefficients describing the dye-host

[1]The angular velocity considered here can be formally defined as the average over the partial angular velocity quasiequilibrium distribution for a given orientation. For further details see Ref. [9].

orientational interaction strength. Since ζ depends trivially on the light absorption coefficient of the dye, it is useful to drop out the dependence on the cross section σ introducing the dimensionless figure of merit

$$\mu = \frac{2\tau_d D_e}{15h}\left(\frac{u_{eh}}{D_e} - \frac{u_{gh}}{D_g}\right), \tag{3.7}$$

where τ_d has been defined in Eq. 2.11. The merit figure μ gauges the ability of a single dye molecule to contribute to the torque provided that it has absorbed a photon.

The value of μ has been measured for various dye-LC mixtures, varying several parameters [11, 12]. This has been done, for example, by measuring the nonlinear phase shift induced in a probe beam by the molecular reorientation due to a pump laser beam. The cross section is instead obtained by linear absorption measurements.

3.2.2 Angular Momentum Conservation Issue

In a transparent nematic LC, the optical electromagnetic torque acting on the molecular director $\mathbf{n}$ owing to the polarizability anisotropy is given by

$$\boldsymbol{\tau}_{em} = \langle \mathbf{P} \times \mathbf{E} \rangle = \frac{\epsilon_a}{4\pi}\langle (\mathbf{n}\cdot\mathbf{E})(\mathbf{n}\times\mathbf{E})\rangle \tag{3.8}$$

where $\epsilon_a = n_e^2 - n_o^2$ is the optical dielectric anisotropy, and n_e and n_o are respectively the extraordinary and ordinary refractive indices; the angular brackets denote time average over an optical cicle. By adding a small amounts of dye to the LC, in order to make it absorbing the total optical torque $\boldsymbol{\tau}_o$ increases; the experimental results [5–7] are consistent with a total torque $\boldsymbol{\tau}_o = \boldsymbol{\tau}_{em} + \boldsymbol{\tau}_{ph}$ where $\boldsymbol{\tau}_{ph}$ is the dye-induced torque given by

$$\boldsymbol{\tau}_{ph} = \frac{\zeta}{4\pi}\langle (\mathbf{n}\cdot\mathbf{E})(\mathbf{n}\times\mathbf{E})\rangle. \tag{3.9}$$

The similarity between Eq. 3.9 and Eq. 3.8 (except for the substitution of ϵ_a with the dimensionless material constant ζ) is not accidental: the dependence of the optical torque on the electric field $\mathbf{E}$ and the director $\mathbf{n}$ is fully constrained by simmetry. We can now cast the torque balance equation controlling the molecular director dynamics in this form: [13, 14]

$$I \cdot \mathbf{n} \times \frac{d^2\mathbf{n}}{dt^2} = \boldsymbol{\tau}_{el} + \boldsymbol{\tau}_v + \boldsymbol{\tau}_{em} + \boldsymbol{\tau}_{ph}. \tag{3.10}$$

On the left side of Eq. 3.10 it is shown the inertial contribution, usually negligible. On the right side there are:

- the elastic torque $\boldsymbol{\tau}_{el}$, a complicated function of the molecular director gradient. [13, 14];
- the viscous torque given by $\boldsymbol{\tau}_v = -\gamma_1 \mathbf{n} \times (d\mathbf{n}/dt)$;
- the electromagnetic torque $\boldsymbol{\tau}_{em}$, including the polarization optical torque and eventually the static electric and/or magnetic torque;
- the photoinduced torque $\boldsymbol{\tau}_{ph}$.

Equation 3.10 describes the change in time of the angular momentum associated with molecular orientation. The angular momentum conservation law forces each torque to be generated by an angular momentum exchange with: (i) the director field in the surrounding; (ii) other degrees of freedom carrying linear momentum as the fluid flow and the electromagnetic field. This can be stated by the following equation:

$$(\boldsymbol{\tau})_i = \frac{\partial}{\partial x_j}(\epsilon_{ihk} n_h s_{jk}) + \epsilon_{ihk} t_{hk}, \tag{3.11}$$

where ϵ_{ihk} is the Levi-Civita antisymmetric tensor, t_{hk} is a stress tensor associated with fluid displacement without any director rotation and s_{jk} is another material tensor.

The term with the total divergence on the right side of Eq. 3.11 takes into account the exchange in the angular momentum as in (i) whereas the stress tensor term refers to the angular momentum exchange mechanism described in (ii). Since only the elastic torque $\boldsymbol{\tau}_{el}$ among those in Eq. 3.10 has both the contributions, angular momentum conservation requires the existence of a photoinduced stress tensor. Its antisymmetric part can be determined by means of Eqs. 3.9 and 3.11 :

$$t_{ij}^{ph} = \frac{\zeta}{8\pi}\langle(\mathbf{n}\cdot\mathbf{E})(n_iE_j - n_jE_i)\rangle. \tag{3.12}$$

This photoinduced stress must be a mechanical stress tensor, describing short-range forces exchanged through the material surfaces, similar to those giving rise to pressure or viscosity, then acting on molecule center-of-mass degrees of freedom. The reason of this is that it cannot be associated with a momentum flux carried by the electromagnetic field since it is totally taken into account by t_{ij}^{em}. The photoinduced torque, therefore, must correspond to an angular momentum transfer from the molecular center-of-mass degrees of freedom to the orientational one (director).

3.2.3 Further effects

The model presented above has been recently confirmed by several quantitative tests [11, 15–18]. Nevertheless, some features of the Jánossy effect remain still obscure. One of them is the anomalous wavelength dependence exhibited by certain dyes [12, 19]. Based on the model, one would expect a dye-induced torque scaling just

as the dye absorption spectrum. What one finds instead in these dyes is that an excess photon energy reduces the torque, in some cases even leading to its sign-inversion (reorientation perpendicular to the electric field) [19]. Different possible explanations have been proposed for this phenomenon [11, 19], but this issue remains unsettled.

Bibliography

[1] Maier, W.; Saupe, A. *Z. Naturforsch. A* **1958**, *13*, 564.

[2] Maier, W.; Saupe, A. *Z. Naturforsch. A* **1959**, *14*, 882.

[3] Maier, W.; Saupe, A. *Z. Naturforsch. A* **1960**, *15*, 287.

[4] Jánossy, I.; Lloyd, A. D.; Wherrett, B. S. *Mol. Cryst. Liq. Cryst.* **1990**, *179*, 1–12.

[5] Jánossy, I.; Lloyd, A. D. *Mol. Cryst. Liq. Cryst.* **1991**, *203*, 77.

[6] Jánossy, I.; Csillag, L.; Lloyd, A. D. *Phys. Rev. A* **1991**, *44*, 8410–8413.

[7] Jánossy, I.; Kósa, T. *Opt. Lett.* **1992**, *17*, 1183–1185.

[8] Khoo, I. C.; Li, H.; Liang, Y. *IEEE J. Quantum Electron.* **1993**, *29*, 1444.

[9] Marrucci, L.; Paparo, D. *Phys. Rev. E* **1997**, *56*, 1765–1772.

[10] Jánossy, I. *Phys. Rev. E* **1994**, *49*, 2957.

[11] Marrucci, L.; Paparo, D.; Maddalena, P.; Massera, E.; Prudnikova, E.; Santamato, E. *J. Chem. Phys.* **1997**, *107*, 9783–9793.

[12] Paparo, D.; Maddalena, P.; Abbate, G.; Santamato, E.; Jánossy, I. *Mol. Cryst. Liq. Cryst.* **1994**, *251*, 73.

[13] de Gennes, P. G. *The Physics of Liquid Crystals;* Oxford University Press: Oxford, 1974.

[14] Chandrasekhar, S. *Liquid Crystals;* Cambridge University Press: Cambridge, 1977.

[15] Kreuzer, M.; Hanisch, F.; Eidenschink, R.; Paparo, D.; Marrucci, L. *Phys. Rev. Lett.* **2002**, *88*, 013902.

[16] Kreuzer, M.; Benkler, E.; Paparo, D.; Casillo, G.; Marrucci, L. *Phys. Rev. E* **2003**, *68*, 011701.

[17] Truong, T. V.; Xu, L.; Shen, Y. R. *Phys. Rev. Lett.* **2003**, *90*, 193902.

[18] Truong, T. V.; Xu, L.; Shen, Y. R. *Phys. Rev. Lett.* **2004**, *93*, 039901.

[19] Kósa, T.; Jánossy, I. *Opt. Lett.* **1995**, *20*, 1230.

Part II

Experimental Methods

Chapter 4

Materials and Preparations

4.1 Dyes and Liquid Hosts

In our experiments we used molecules belonging to two classes of organic compounds: anthraquinone dyes and cyanobiphenyls. These molecules are anisotropic and elongated objects; their length is of the order of tens of angstroms.

Cyanobiphenyls are constituted by two aromatic rings with a cyano group CN at one end and a C_nH_{2n+1} group at the other end. This kind of structure is shown in Fig. 4.1. These molecules show a planar structure; their length is $\sim$ 15Å and their width $\sim$ 5Å.

Figure 4.1: Molecular structure of the 4'-*n*-pentyl-4-cyanobiphenyl (5CB).

In our experiment we mainly used the 4'-*n*-pentyl-4-cyanobiphenyl (5CB). The structure formula of 5CB is reported in Fig. 4.1. We also used a mixture of cyanophenyls

produced by Merck and denoted as E63(see Ref. [1] for its composition). This kind of molecules shows a strong polar head, namely the cyano group CN, capable of dipole-dipole interactions or even hydrogen bonding with other polar groups such as hydroxyl OH, carbonyl CO, or amino NH_2. These materials moreover show a liquid-crystalline nematic phase for temperatures below 34°C (5CB) and 89°C (E63).

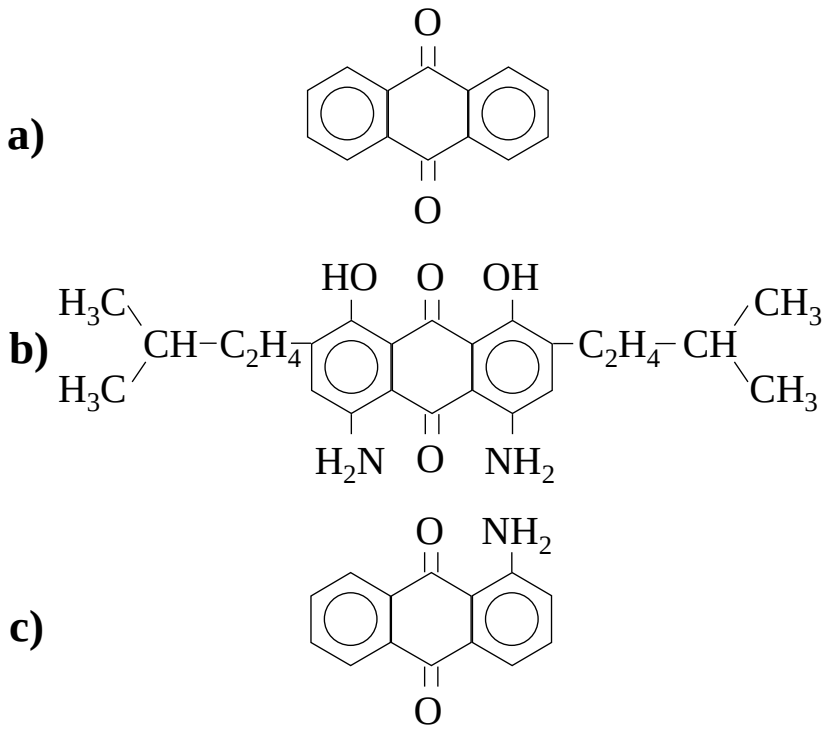

Figure 4.2: Molecular structure of the anthraquinone (a) and of the anthraquinone-derivated dyes HK271 (b) and 1AAQ (c).

The dye molecules used in our experiments are anthraquinone derivatives. The anthraquinone unsubstituted molecule is shown in Fig. 4.2(a). The derivatives we used are the 1,8-dihydroxy 4,5-diamino 2,7-diisopentyl anthraquinone (HK271, provided by Nematel, Mainz, Germany) and the 1-amino anthraquinone (1AAQ, available, e.g., from Aldrich Chem. Company, Inc.). For the molecular structure see Fig. 4.2(b) and

(c). The molecule of HK271 is a factor 1.6 larger in weight than the molecule of 5CB. The molecule of 1AAQ is 10% smaller than that of 5CB. These relative sizes will be important for the rotational diffusive experiments that will be discussed in chapter 7.

From a rough steric point of view, both kinds of molecules can be treated as rigid rods; since we are mainly interested in their rotational dynamics, it is useful to define the versor **s** parallel to the long axis of the rod, to indicate its direction.

4.2 Preparation Techniques

Our samples are prepared by mixing dyes and hosts at room temperature. The mixtures are then sonicated for 1 hour at a temperature of 60°C in order to obtain complete mixing and homogenization of the solvents. Solutions were prepared at several concentrations ranging from 10^{-6} to 10^{-3} mol/L. In all measurements, we identified the concentration below which nonlinear effects on the absorption and fluorescence spectra were negligible, and in our discussions we consider only results obtained in this range.

4.2.1 Isotopic Substitution

We prepared the deuterated forms by making an emulsion of the dye-liquid solution in heavy water D_2O, allowing it to stand overnight, and reseparating the two components by centrifugation. This procedure will effectively replace with deuterium atoms only the hydrogens of the amino and hydroxyl side groups of dye molecules, not altering the alkyl and aromatic moieties of dyes and hosts [2]. The final dye deuteration was verified by looking at the blue-shift in the absorption spectrum, as

shown in fig. 4.3. We find a shift of about 7 nm, consistent with that reported for

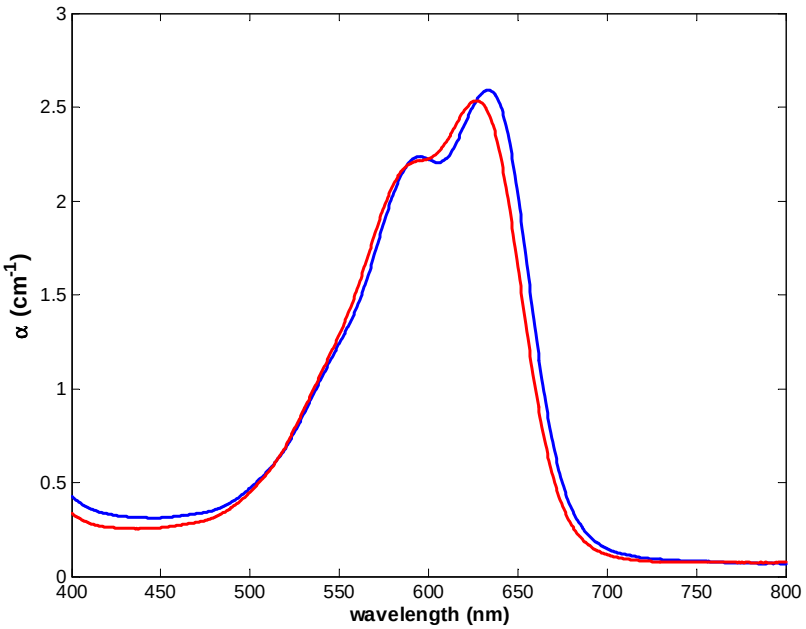

Figure 4.3: Absorption spectrum of HK271-5CB deuterated (blue) and protonated (red) mixtures. The deuteration-induced blue shift is $\sim$ 7nm.

similar molecules after complete deuteration of the amino and hydroxyl groups [3]. The complete deuteration is further confirmed by our measurements of excited-state lifetime (Fig. 4.4) as discussed in the following. Although our samples were kept sealed, the deuteration usually lasted for no more than a few days, owing to exchange with atmospheric humidity. Control samples were also prepared following the same procedure as for deuterated samples, but using ordinary pure water H_2O instead of heavy water. In all our measurements these control samples produced results which were undistinguishable from those obtained with normal non-deuterated samples.

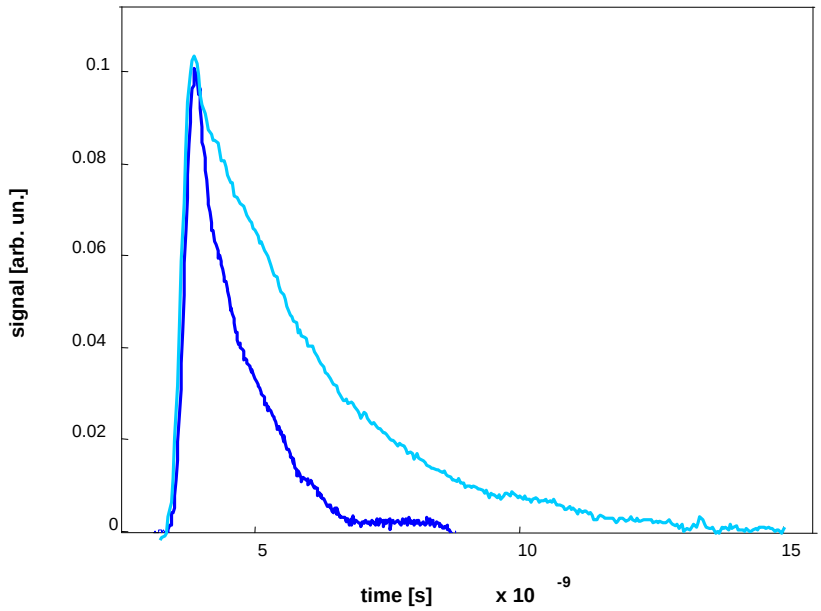

Figure 4.4: Deuteration-induced variation of the excited-state lifetime τ_e of HK271 in 5CB. The fluorescence intensity decay I_e collected at excitation wavelength $\lambda =$ 532nm for deuterated (cyan, $\tau_e = 2410 \pm 30$ps) and protonated (blue, $\tau_e = 871 \pm 7$ps) mixtures are shown.

4.2.2 Liquid Crystal Droplets

Some of the experiments described in the following have been carried out on liquid crystals and dye-doped liquid crystals droplets. The droplets are obtained by dispersion of the pure and dye-doped liquid crystals in distilled water. Due to the hydrophobic nature of the liquid crystal it is possible to observe the formation of droplets with diameters of $\sim 1 \div 10\mu$m. The concentrations of the dye-liquid crystals mixtures are quite higher than those described previously and range from $0.5\% \div 2\%$ w/w.

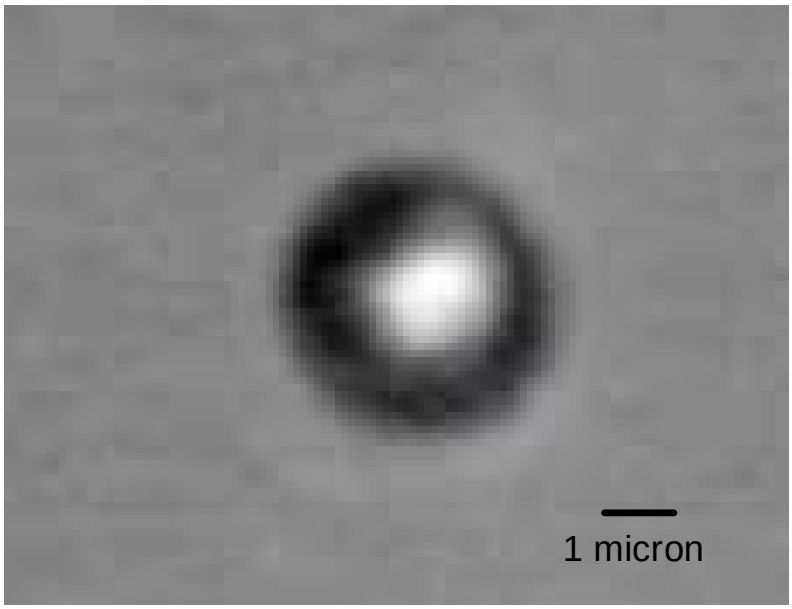

Figure 4.5: Image of a dye-doped liquid crystal droplet. The diameter is of 3.4μm.

Bibliography

[1] Jákli, A.; Kim, D. R.; Kuzma, M. R.; Saupe, A. *Mol. Cryst. Liq. Cryst.* **1991**, *198*, 331.

[2] Alder, R. W.; Baker, R.; Brown, J. M. *Mechanisms in Organic Chemistry;* Wiley-Interscience: London, 1971.

[3] Palit, D. A.; Pal, H.; Mukherjee, T.; Mittal, J. P. *J. Chem. Soc. Faraday Trans.* **1990**, *86*, 3861.

Chapter 5

Fluorescence Experiments

5.1 Steady-State Fluorescence Spectroscopy

Steady-state fluorescence spectroscopy is widely used in several fields of research to study molecular interactions and kinetics. This technique relies on monitoring changes in the intensity of fluorescence at a given wavelength or changes in the emission spectrum. By means of steady-state fluorescence it is possible to record excitation and emission spectra. An emission spectrum is the wavelength distribution of the emission, measured at a single excitation wavelength. Conversely, an excitation spectrum is the dependence of emission intensity, measured at a single emission wavelength, upon the excitation wavelength.

5.1.1 Instruments for steady-state fluorescence

A typical spectrofluorometer generally consists in a xenon lamp as source of exciting light; the instrument is equipped with monochromators to select both the excitation and emission wavelengths. The fluorescence is detected with photomultipliers tubes and quantified with appropriate electronic devices.

For an ideal instrument, the directly recorded emission spectra would represent the photon emission rate or power emitted at each wavelength over a determined wavelength interval. Similarly, the excitation spectrum would represent the relative emission of the fluorophore at each excitation wavelength. Since for most fluorophores the quantum yield and emission spectra are independent of excitation wavelength, the excitation spectrum of a fluorophore is typically superimposable on its absorption spectrum. However, this is rarely observed because the wavelength responses of almost all spectrofluorometers are dependent on wavelength. Excitation spectra are distorted primarily by the wavelength dependence of the intensity of the exciting light, since light sources do not yield a constant photon output at all wavelengths. This intensity can be converted to a signal proportional to the number of incident photons by the use of a quantum counter [1]. Quantum counters are those mixtures having an emission spectrum independent on the excitation wavelength. Rhodamine B in ethylene glycol (3g/L) [2] or in ethyl alcohol (10^{-6} mol/L) [3] is one of the best known quantum counter.

Moreover, also the other components of a spectrofluorometers with "ideal" characteristics are not available and we must consider that the quantum efficiency of monochromators and detectors (photomultiplier tubes) depends on photon wavelength. The wavelength-dependent responses of the emission monochromator and phototube do not affect the excitation spectra because the emission wavelength is unchanged during a scan of the excitation wavelength. Indeed they can significantly modify the emission spectra. In order to take into account of these effects one reliable method is to compare the observed emission spectrum of a standard substance with the known corrected spectrum for this same substance. Other ways to obtain the correction

factors are either to observe the wavelength-dependent output from a calibrated light source or to calibrate the excitation lamp in the spectrofluorometer for its spectral output by means of a quantum counter and a scatterer [1].

5.1.2 Calibration and Test Measurements

For the steady-state fluorescence measurements we used a Varian Cary Eclipse fluorescence spectrofluorometer; this allowed us to obtain both excitation spectra, collecting at several emission wavelengths, and emission spectra induced by several excitation wavelengths. These spectra have been measured in the right-angle geometry in a standard fused-quartz cuvette with reduced path-length.

In order to check the instrument calibration and the effectiveness of the correction factors we carried out test measurements on known solutions. Fluorescence spectra at different excitation wavelength have been collected for Rhodamine B dissolved in ethyl alcohol; in Fig. 5.1 is possible to see the spectrum collected at $\lambda = 500$nm. It superimposes almost perfectly to the one given in Ref. [4].

Absorption spectra of all samples have been measured with a JASCO's V-series UV-Visible spectrometer. Also for such kind of measurements several test have been made. Even in this case our measurements match with others reported in literature [4] as it is possible to see in Fig. 5.2 for the Rhodamine B. In the same figure we plotted the excitation spectrum for the same solution at λ=630nm. It shows a shape very close to that of the absorption spectrum as expected because of the quantum counter property of the solution.

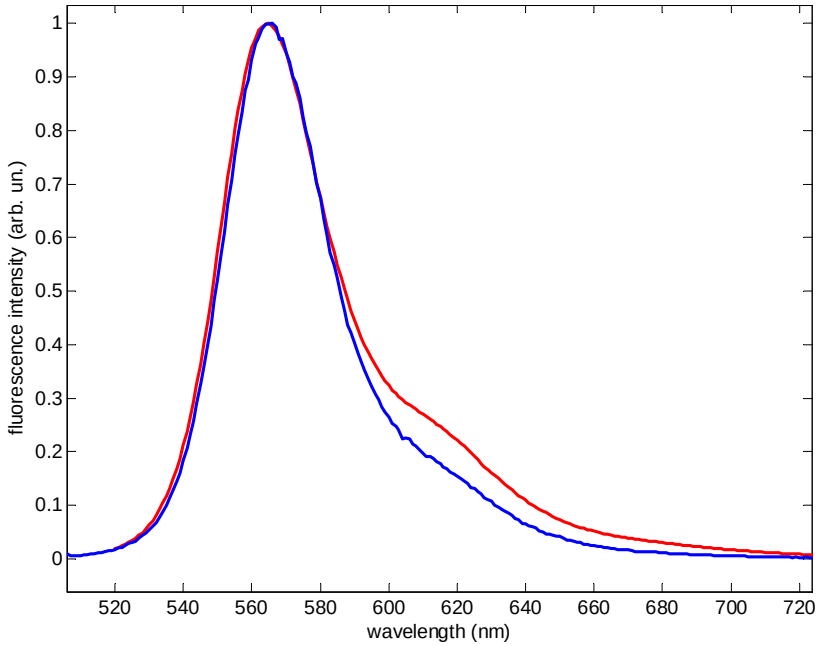

Figure 5.1: Fluorescence spectrum of Rhodamine B in ethyl alcohol (red) compared with that given in Ref. [4](blue).

5.1.3 Measurements of Quantum Yield

We defined the quantum yield as the total number of emitted photons divided by the total number of absorbed photons; even if a more general definition should consider the fraction of molecules that emit a photon after direct excitation by the source, in many instances the two quantities are nearly equal. Quantum yields are of the central importance for studies of radiationless processes, for correlation of predicted lifetimes with the observed lifetimes and for making assignments of electronic transitions.

The most common method employed for the determination of quantum yield is by using of dilute solutions and a spectrofluorometer as detector. The technique is relatively simple and reasonably accurate.

The optical dilute measurements rest on Beer's Law: the fraction of light absorbed

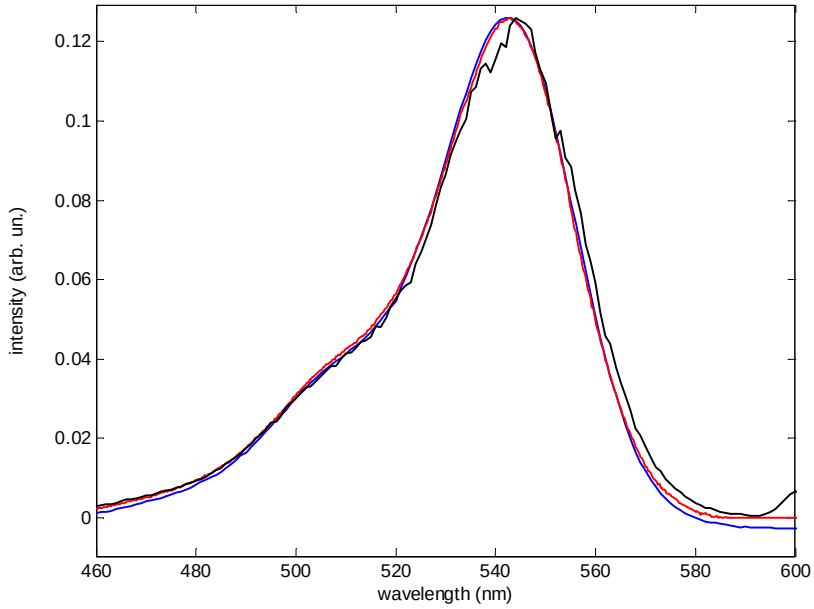

Figure 5.2: Absorption (red) and excitation (black) spectra of Rhodamine B in ethyl alcohol, compared with the absorption spectrum given in Ref. [4](blue).

by a sample of length L of a solution with absorbance α is

$$I_a = I_0 \left(1 - e^{-\alpha L}\right), \tag{5.1}$$

where I_0 is the intensity of incident light. If the fluorescence intensity is proportional to the absorbed light I_a, then the expression for the quantum yield becomes

$$\Phi = \frac{1}{I_a(\lambda_a)\lambda_a} \int \frac{dI_f(\lambda_a)}{d\lambda} \lambda_f d\lambda_f. \tag{5.2}$$

In these equation λ_i with $i = a, f$ is the wavelength at which, respectively, absorption and fluorescence emission occur, I_f is the fluorescence intensity and the integral is carried on the whole fluorescence spectrum and n is the average refractive index of the solution. In order to perform absolute quantum yield measurements, the quantum yield of a reference substance needs to be measured. It takes into account of

systematic errors induced by the experimental setup. For a better determination of the absolute quantum yield, the reference substance must have absorption and fluorescence spectrum as similar as possible to those of the sample.

The equation 5.2 is correct if the mixture concentration is low enough to avoid nonlinear effect in the absorption and/or the emission processes. Errors can be introduced by reabsorption or reemission or simply by deviation from the Beer's law due to high concentrated solutions.

From the Eq. 5.2 is also possible to see that the fluorescence quantum yield can depend on the absorbtion wavelength only if the the total fluorescence intensity is not proportional to the absorbed light intensity or in presence of a wavelength-dependent fluorescence spectrum shape variation. Generally the quantum yield is not expected to vary with the excitation wavelength.

In Fig. 5.3 is shown the λ-dependence of the quantum yield for rhodamine B in ethyl alcohol obtained with the above discussed method. As expected $\Phi(\lambda)$ does not show any dependence and this ensures us about the reliability of the method and provide a further test of the instruments calibration.

5.2 Time-Resolved Fluorescence Depolarization

Time-resolved fluorescence spectroscopy provides measurements of the time dependence of fluorescence intensity after a short excitation pulse which can also be made as a function of emission wavelength. The time dependence of fluorescence emission is far more sensitive to changes in the environment of the fluorescent residues than steady state measurements of peak emission wavelength or intensity. In addition to this increased sensitivity to conformational changes or interactions, the technique can also

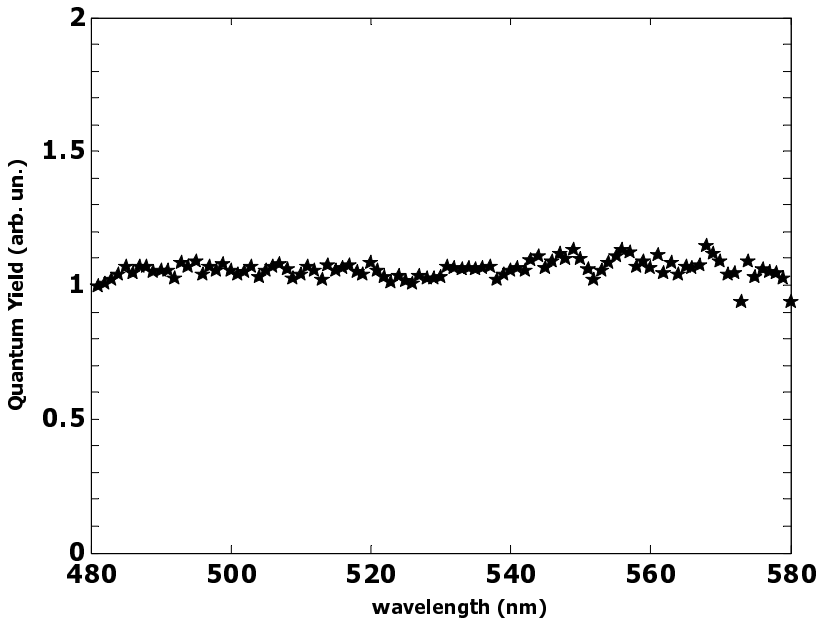

Figure 5.3: Quantum yield wavelength dependence $\Phi(\lambda)$ of Rhodamine B in ethyl alcohol.

be performed using polarized light to provide time resolved fluorescence anisotropy measurements. The analysis of fluorescence anisotropy measurements can provide information about residue freedom within a local environment as well as global motion of the molecules in solution.

5.2.1 Time-Resolved Fluorescence Measurements

There are several ways to perform time-resolved fluorescence measurements. Basically the sample is excited with a light pulse. The pulse duration is needed as short as possible and preferably much shorter than the decay time τ_e of the sample. The time-dependent intensity is measured following the excitation pulse and by fitting the decay curve (expected to be a single exponential decay) it is possible to calculate

the decay time τ_e.

A definition of the decay time can be obtained by considering an infinitely sharp light pulse (δ-function) exciting at the time $t = 0$ an initial population N_0 of fluorophores in the excited state. The excited state population decays with a rate k_R+k_{NR} according to

$$\frac{dN(t)}{dt} = -\left(k_R + k_{NR}\right) N(t) \tag{5.3}$$

where $N(t)$ is the number of excited molecules at the time $t > 0$. Emission is a random event, and each excited fluorophore has the same probability of emitting in a given period of time. This results in an exponential decay of the excited state population $N(t) = N_0 \exp(-t/\tau_e)$. In a fluorescence experiment we observe a fluorescence intensity rather than the number of excited molecules. Since the fluorescence intensity is proportional to the number of emitting molecules we can write

$$I(t) = I_0 \exp\left(-\frac{t}{\tau_e}\right), \tag{5.4}$$

where I_0 is the intensity at time $t = 0$.

Fluorescence emission of a molecule can be further characterized by the direction of polarization. The polarization of the radiation in a fluorescent sample is indeed dependent on the orientation of the emission transition dipole and therefore on the molecular motions (rotation and flexibility of segments within the molecule).

A fluorescence anisotropy measurement is very useful to achieve information on the rotational mobility of the molecules; it can be sketched in the following way: assume to excite a sample with vertically polarized light and to measure the fluorescence intensity trough a polarizer. When the analysis polarizer is oriented parallel ($\|$) to the direction of the polarized excitation, the observed intensity is called $I_\|$. Likewise,

when the polarizer is perpendicular ($\perp$) to the excitation polarization direction, the intensity is called $I_\perp$. The anisotropy is then a dimensionless quantity given by

$$r = \frac{I_\parallel - I_\perp}{I_\parallel + 2I_\perp} = \frac{I_d}{3I_e}, \tag{5.5}$$

and is independent of the total intensity of the sample. Introducing in the last equation the time-dependent expression obtained for I_e and I_d we get

$$r = r_0 e^{-\frac{t}{\tau_r}}, \tag{5.6}$$

with $\tau_r = (\tau_d^{-1} - \tau_e^{-1})^{-1} = 1/6D_e$ so the rotational time can be seen as the decay time of the molecular anisotropy. The constant r_0, hereafter called *initial degree of anisotropy*, gauges the degree of excited-state dye orientational anisotropy (or "order parameter") at the beginning of the fluorescence signal. It can be show that it is given by $r_0 = \langle(3\cos^2\theta - 1)/2\rangle = Q_e^{(2)}(0+)$, i.e. it is the value that the order parameter assume immediately after the light excitation, where θ is the angle between the direction of the molecule fluorescence transition dipole and that of the excitation light electric field, and where the angular brackets denote an average over the ensemble of excited dye molecules. For rodlike molecules with fluorescence dipole parallel to the molecular axis, the initial anisotropy is expected to be $r_0 = 2/5$.

5.2.2 Time-Resolved Fluorescence Anisotropy Measurements of Dye Molecules in Liquid Solutions

The technique we are going to present allows to measure the parameters characterizing the time dependence of the excited-state molecules rotational diffusion and fluorescence emission. As we have seen in Sect.2.4.3 the fluorescence intensity $I(t)$ decays as a double exponential function which decay times are τ_e and τ_d; collecting the

fluorescence emitted with polarizations parallel ($I_{\|}$) and perpendicular ($I_{\perp}$) to that of the pump pulse, combining these signals we have the single exponential curves I_e and I_d, easier to handle to obtain the parameters above.

Before entering in the details of the technique, let us first describe the set-up. It is shown in fig. 5.2.2. As excitation light to induce fluorescence, we used the pulses generated by a frequency-doubled Nd:YAG laser, having a duration of about 20 ps. The frequency-tripled pulses of same laser are also used to pump an optical parametric generator in order to obtain excitation-light tunable in the whole visible range of the electromagnetic spectrum. The dye-doped liquid is hosted in a cell of thickness 1.0±0.1 mm placed into an oven allowing temperature control to within 0.1K.

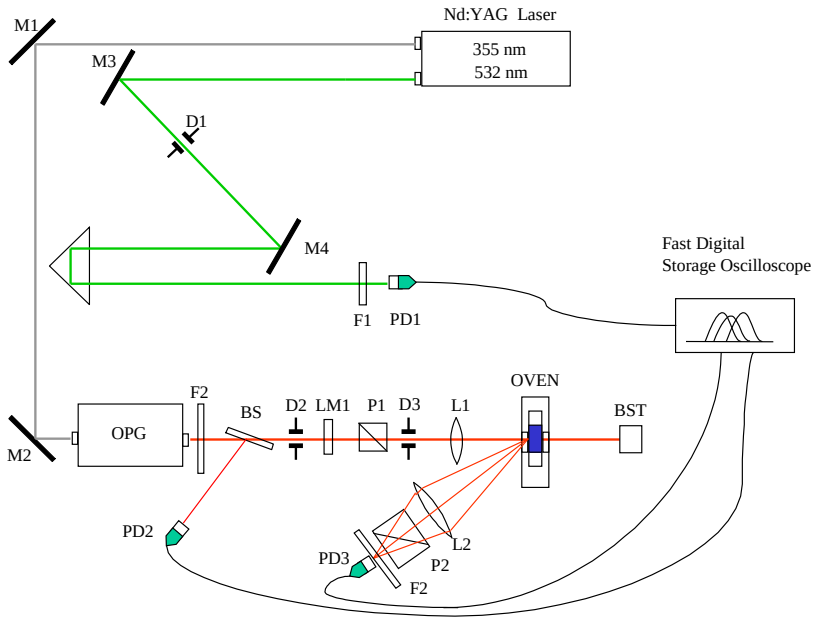

Figure 5.4: Schematic picture of the time-resolved fluorescence experimental setup.

The transient fluorescence was then detected by means of a fast photodiode (about

100 ps rise-time) and sampled by 2 GHz analog bandwidth electronics. A polarizer was used to select parallel ($\|$), perpendicular ($\perp$), or "magic-angle" (i.e., 54.7°) linear polarizations of the detected fluorescence light with respect to that of the excitation light.

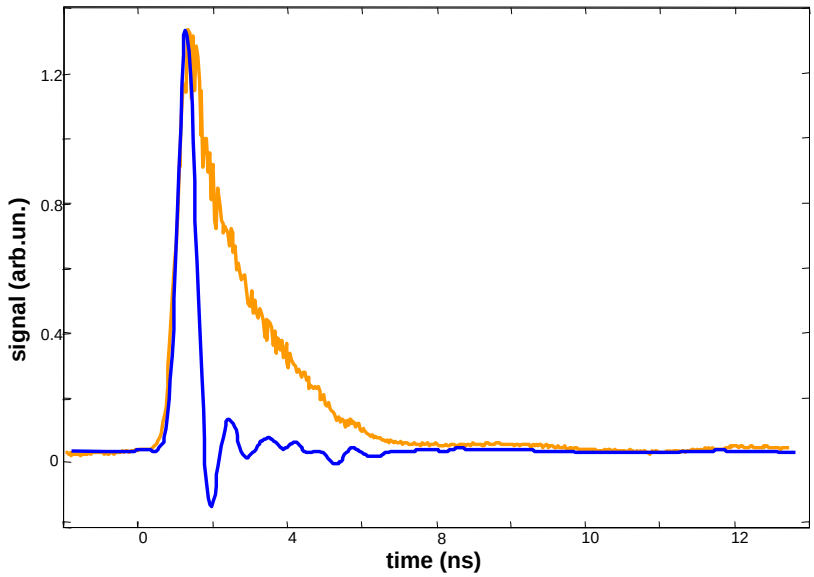

Figure 5.5: Typical response function (blue line) and fluorescence decay (orange line).

As the detection apparatus has a finite response time, the signal $S(t)$ we measure is actually the convolution of the fluorescence intensity $I(t)$ with the instrumental response function $R(t)$ [5]:

$$S_i(t) = \int I_i(t')R(t-t')dt', \tag{5.7}$$

with $i = e, d$.

To measure this response function, we replaced the sample with an opaque plate and collected the scattered light, which has essentially the same time-duration as the laser pulse and therefore can be considered as a delta-function input to the detection

system,

$$I_{scat}(t) \propto \delta(t - t_0); \tag{5.8}$$

what we measure is then

$$S_{scat}(t) = \int I_{scat}(t')R(t - t')dt' \propto R(t - t_0). \tag{5.9}$$

We measured the response function at wavelengths ranging within the whole fluorescence spectrum of our dye, and found that its shape and temporal parameters (e.g., rise time, FWHM) remained approximately constant. Therefore, we used the response function averaged over all detected wavelengths for our subsequent data analysis.

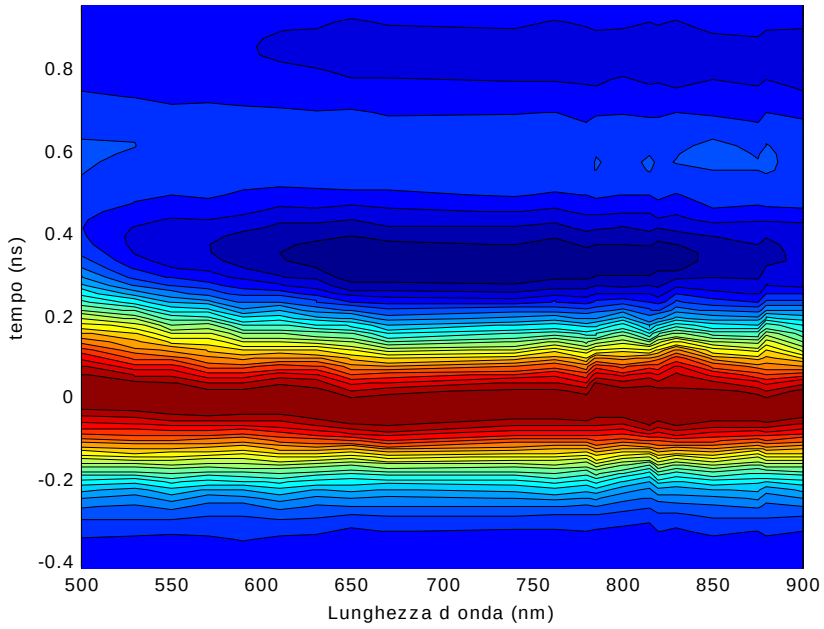

Figure 5.6: Contour plot of the response functions collected at several wavelengths.

In the data analysis, the parallel and perpendicular signals, $S_{\parallel}(t)$ and $S_{\perp}(t)$, were first combined into $S_e(t) = (S_{\parallel} + 2S_{\perp})/3$ and $S_d(t) = S_{\parallel} - S_{\perp}$. We verified that $S_e(t) = S_{\text{magic}}(t)$ as expected, thus confirming that the detection efficiency of our

apparatus was independent of light polarization. Each of the two combinations $S_e(t)$ and $S_d(t)$ was then best-fitted by a single exponential decay of the form

$$I_i(t) = c_i\theta(t-t_0)e^{-\frac{t-t_0}{\tau_i}}, \tag{5.10}$$

where $\theta(t)$ is the Heavyside step function, convoluted with the measured response function $R(t)$. The Fourier transform for this expression give

$$\widetilde{S}_i(\omega) = c_i\frac{\widetilde{R}(\omega)}{\frac{1}{\tau_i}+i\omega}e^{-i\omega t_0}. \tag{5.11}$$

By means of a FFT (*Fast Fourier Transform*) algorithm [6] we numerically evaluate $\widetilde{R}(\omega)$ from the measured $R(t)$; then, after fixing the starting value for t_0 e τ_i, from 5.11 we obtain $\widetilde{S}_i^{th}(\omega)$. The latter is changed into the time-domain predicted signal $S_i^{th}(t)$ by the FFT procedure; by minimizing the function χ^2 given by

$$\chi^2(\tau_i, c_i, t_0) = \sum_j \left(S_{i,j}^{exp}(t) - S_{i,j}^{th}(t)\right)^2 \tag{5.12}$$

where the sum is carried on the index j referring to the experimentally collected points, with respect to the parameters τ_i, c_i and t_0.

The fit parameters with relevant physical meaning for the dynamics, are the excited-state lifetime τ_e and the effective time $\tau_d = (\tau_e^{-1} + \tau_r^{-1})^{-1}$, where τ_r is the rotational diffusion time [5], and the two preexponential factors c_e and c_d.

In the diffusion approximation, the rotational time is given by $\tau_r = 1/(6D)$, where D is the rotational diffusion constant [7].

The ratio $r_0 = c_d/3c_e$ gauges the degree of excited-state dye orientational anisotropy (or "order parameter") immediately after the laser pulse absorption, i.e. at the beginning of the fluorescence signal. It is independent of dye-concentration and laser intensity. More precisely, it can be shown that $r_0 = \langle(3\cos^2\theta - 1)/2\rangle$, where θ is the

angle between the direction of the molecule fluorescence transition dipole and that of the excitation light electric field, and where the angular brackets denote an average over the ensemble of excited dye molecules, sampled at a time of the order of our temporal resolution ($\simeq$ 100 ps) after the excitation. In the case of HK271, the dipole moment is indeed along the longest molecular axis [8], which should be reflected into an initial anisotropy $r_0 = 2/5$ [5]. In 1AAQ, the direction of the transition dipole is theoretically calculated to form an angle of about 15° with the molecule longest axis [9, 10], small enough to be neglected in our decay-time analysis. The predicted initial anisotropy is however reduced to $r_0 = 0.36$.

We tested the set-up and the analysis procedure by measuring the fluorescence lifetime τ_e of Rhodamine 6G at 10^{-4} mol/L in ethylene glycol and in ethyl alcohol, finding in both cases $\tau_e = 3.6 \pm 0.1$ ns, in agreement with values reported in the literature for the case of negligible energy transfer [11, 12]. This ensures that energy transfer effects can be neglected for our experimental geometry [12]. As a further test, we verified that the fluorescence lifetimes and that the value of r_0 of HK271 and 1AAQ were independent of laser intensity and dye concentration in the range $10^{-4} \div 10^{-3}$ mol/L.

Bibliography

[1] Lakowicz, J. R. *Priciples of Fluorescence Spectroscopy;* Kluver Academic/ Plenum Publisher: New York, 1999.

[2] Melhuish, W. *J. Opt. Soc. Am.* **1962**, *52*, 1256–1258.

[3] Taylor, D. G.; Demas, L. N.; Phillips, D. *An. Chem.* **1979**, *51*, 717.

[4] Du, H.; Fuh, R. A.; Li, J.; Corkan, A.; Lindsey, J. S. *Photochem. Photobiol.* **1998**, *68*, 141–142.

[5] O'Connor, D. V.; Phillips, D. *Time-correlated single photon counting;* Academic Press: London, 1984.

[6] Press, W. H. *Numerical Recipes;* Cambridge University Press: Cambridge, 1986.

[7] Debye, P. *Polar Molecules;* Reinhold: New York, 1929.

[8] Myrvold, B. O.; Spanget-Larsen, J.; Thulstrup, E. W. *Chem. Phys.* **1986**, *104*, 305–313.

[9] Inoue, H.; Hoshi, T.; Yoshino, J.; Tanizaki, Y. *Bull. Chem. Soc. Japan* **1972**, *45*, 1018–1021.

[10] Myrvold, B. O.; Klæboe, P. *Acta Chem. Scand. A* **1985**, *39*, 733–747.

[11] Philips, L. A.; Webb, S. P.; Clark, J. H. *J. Chem. Phys.* **1985**, *83*, 5810–5821.

[12] Scully, A. D.; Matsumoto, A.; Hirayama, S. *Chem. Phys.* **1991**, *157*, 253–269.

Chapter 6

Optical Tweezers Experiment

6.1 Optical Trapping

In this chapter we will briefly present one of the most powerful optical manipulation techniques, consisting in a single-beam optical trap and known as optical tweezers. Since their discovery [1] they have been used in many field of research as biology, chemistry, physics and engineering and they continue to undergo interesting developments in a number of areas.

The techniques of optical trapping and manipulation of neutral particles by laser light provide unique means to control the dynamics of small particles. They are based on the forces of radiation pressure, arising from the momentum of light itself. In essence, optical tweezers rely upon the extremely high gradient in the electric field produced close to the waist of a strongly focused laser beam. In such a way it is possible to catch and hold particles of dielectric material in a size range from tens of nanometers to tens of micrometers. This technique makes it possible to study and manipulate particles like atoms, molecules (even large), cells, viruses, organelles and dielectric spheres.

This technique has been successfully used to align and spin calcite particles [2] and nematic liquid crystal droplets [3–5]. This rotational manipulation is possible because of the birefringent nature of these materials, which leads to a coupling with the light polarization.

Although the theory behind the optical tweezers is still being developed, the basic principles are straightforward for objects either much smaller or much larger than the wavelength of the light.

For particles much larger than the wavelength of the trapping light, ray optics analysis of the deviated light path gives the change in momentum flow and hence the reaction force acting on the object. To show that the transverse force is originated from radiation pressure as well as the axial component, consider two typical rays r_1 and r_2 from a mildly focused Gaussian beam impinging simmetrically on a spherical object of higher refractive index than the bathing medium (Fig. 6.1). Most of the rays refract trough the particle giving rise to forces F_1 and F_2 in the direction of the momentum change. Because the intensity of the ray r_1, closest to the center of the beam, is higher than that of the ray r_2, the force F_1 is greater than F_2. Adding all such symmetrical pairs of rays striking the sphere it is possible to resolve the force into two components F_{scat} pointing in the direction of the incident light and F_{grad} arising from the beam intensity profile and pointing trasversely towards the high intensity region of the beam.

For a low index particle placed off-axis, the refraction through the particle reverses and it should be pushed out of the beam. For a particle on axis there is no net gradient force component. Fig. 6.2 shows the typical optical tweezers arrangement; the laser light is strongly focused by means of a microscope objective with a high numerical

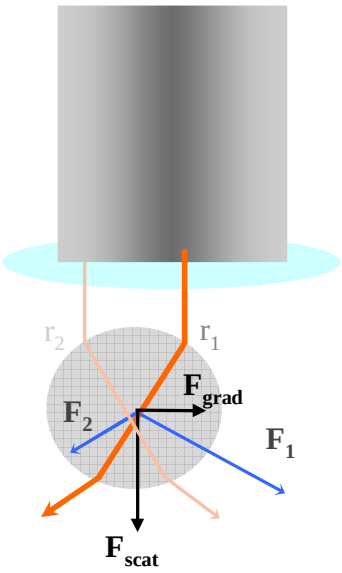

Figure 6.1: Origin of scattering and gradient forces for high index sphere displaced from TEM_{00} beam axis.

aperture. In the figure it is also possible to see the origin of the backward light force in the case which the center of the particle is located below the lens focus.

6.2 Orientational Manipulation and Light Induced Rotation

In 1936, Beth first observed the angular momentum of the light reporting a tiny torque developed in a quartz wave-plate owing to the change in polarization of trasmitted light [6]. Fifty years later, by using the optical tweezers it has been possible to exert a

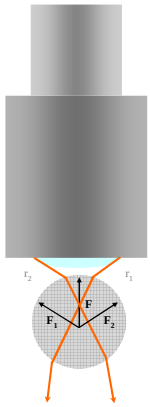

Figure 6.2: Origin of backward restoring force for sphere located below tweezers focus.

larger torque on a microscopic wave-plate, i.e. calcite particles obtained by crushing a small crystal [2]. The key of the effect is the birefringent nature of both quartz and calcite; when passing through a birefringent media the ordinary and extraordinary components of the incident light will undergo different phase shift. If this results in a change in the angular momentum carried by the light, there will be a corresponding torque on the material. Owing to this torque, birefringent particles held by laser tweezers formed by linearly polarized light can be oriented [2, 7] and if the light is circularly polarized they will rotate and the rotation direction is determined by that of the circular polarization [2, 7]. Evidences of such mechanism have been reported recently also on nematic liquid crystal droplets [3–5].

The effect can be depicted in a simple plane-wave model. In the case of optical tweezers, the particles are trapped near the focal point of the beam and the plane-wave approximation is valid. A general polarization state of the light can be expressed as the combination of a circularly polarized and plane polarized components; it results

in an elliptical polarization state, that can be described by:

$$\mathbf{E} = E_0 e^{i\omega t} \cos\phi \hat{\mathbf{x}} + iE_0 e^{i\omega t} \sin\phi \hat{\mathbf{y}} \tag{6.1}$$

where ϕ describes the degree of ellipticity of the light (plane polarized light for $\phi = 0, \pi/2$, circularly polarized for $\phi = \pi/4$). In order to calculate the change in the angular momentum of the light after passage through a birefringent material it is better to express the incident light in terms of the components parallel and perpendicular to the optic axis of the material by:

$$\begin{aligned} \mathbf{E} = E_0 e^{i\omega t}(\cos\phi\cos\theta - i\sin\phi\sin\theta)\hat{\mathbf{i}} + \\ + iE_0 e^{i\omega t}(\cos\phi\sin\theta + i\sin\phi\cos\theta)\hat{\mathbf{j}} \end{aligned} \tag{6.2}$$

where θ is the angle between the optic axis of the birefringent material and the fast axis of the quarter-wave plate producing the elliptically polarized light. The passage through a thickness d of material having refractive index n induces a phase shift kdn and the expression for the electrical field becomes

$$\begin{aligned} \mathbf{E} = E_0 e^{i\omega t} e^{ikdn_e} \cos\phi\cos\theta - i\sin\phi\sin\theta)\hat{\mathbf{i}} + \\ + iE_0 e^{i\omega t} e^{ikdn_o}(\cos\phi\sin\theta + i\sin\phi\cos\theta)\hat{\mathbf{j}}. \end{aligned} \tag{6.3}$$

where the subscripts e and o stand for extraordinary and ordinary and refer to the different refractive indices experienced by the extraordinary and ordinary rays.

The angular momentum of a plane monochromatic wave of angular frequency ω is given by the integration of:

$$\mathbf{J} = \frac{\epsilon}{2i\omega} \int \mathbf{E}^* \times \mathbf{E} d^3 r \tag{6.4}$$

where ϵ is the permittivity. By means of the last formula it is possible to calculate the change in the angular momentum and hence the torque per unit area:

$$\tau = -\frac{\epsilon}{2\omega} E_0^2 \sin(kd(n_o - n_e)) \cos 2\phi \sin 2\theta + \\ + \frac{\epsilon}{2\omega} E_0^2 \{1 - \cos(kd(n_o - n_e))\} \sin 2\phi. \tag{6.5}$$

In the equation 6.5 the first term represents the effect due to the plane-polarized component of the incident light while the second term represents the polarization change due to the passage through the medium. For plane polarized light, $\phi = 0$ or $\pi/2$, the torque acting on the particle is proportional to $\sin 2\theta$; for circularly polarized light the first term vanishes but the particle experience a constant torque due to the second term. The equation that describes the motion of a spherical particle with volume V in a medium of viscosity η is:

$$\boldsymbol{\tau} = I \frac{d\boldsymbol{\omega}}{dt} + \varsigma \boldsymbol{\omega} \tag{6.6}$$

where $\boldsymbol{\tau}$ is the overall torque, $\varsigma = 6\eta V$ is the drag coefficient for the rotation, I the momentum of inertia and $\boldsymbol{\omega}$ the angular velocity; in the steady-state the time-derivative drops out and the particle will rotate with constant angular frequency $f = \boldsymbol{\omega}/2\pi$. In the case of light of power P and optical frequency ω, the rotation frequency f is given by

$$f(d, \phi) = \frac{P}{2\pi\omega\varsigma} \sqrt{\left\{ [1 - \cos kd(n_o - n_e)]^2 \sin^2 2\phi - \sin^2 kd(n_o - n_e) \cos^2 2\phi \right\}}. \tag{6.7}$$

Clearly the fastest spinning is obtained when particle thickness d (or diameter $d = 2R$, in the case of spherical particles) corresponds to a $\lambda/2$ wave-plate and the light is circularly polarized.

6.3 "Double Wavelength" Optical Tweezers

The particular configuration of the set-up allows us to trap and manipulate the droplets by means of infrared and visible laser light. The light of two laser beam

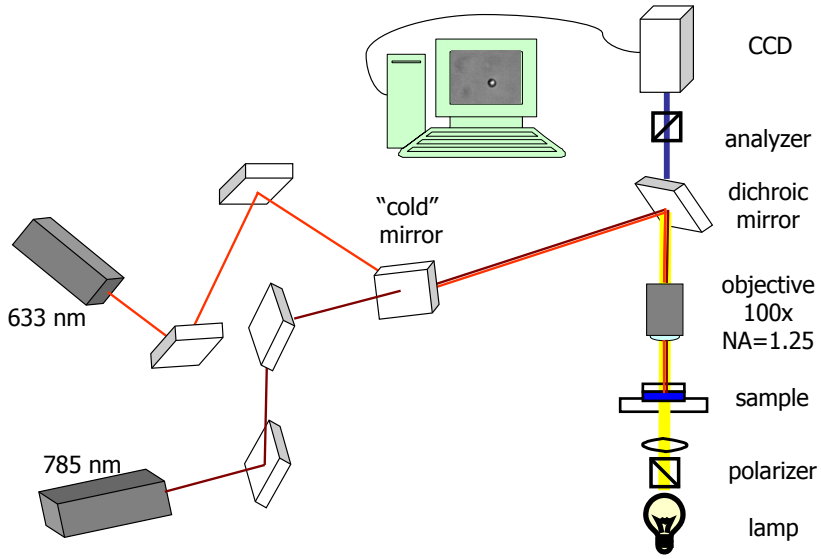

Figure 6.3: "Double Wavelength" optical tweezers setup.

with wavelength 785nm and 633nm is strongly focused by means of a microscope objective with magnification 100x and N.A.= 1.25; the polarization of the beams is controlled by a $\lambda/2$ and a $\lambda/4$ wave-plate (not shown in figure). Both the retarders are needed to compensate the birefringence of the mirror. The two beams, starting with perpendicular directions are superimposed by mean of a "cold" mirror, transparent to the infrared light and reflecting the visible light. A beam expander allows us to match the size of the beam impinging on the objective to the objective window size. The light of a lamp, placed under the microscope is used to illuminate the sample. Part of this light, trasmitted by a dicroich mirror, is collected on a CCD camera.

Two polarizers, the first below the sample (polarizer) and the second just in front of the CCD, can be crossed in order to have a polarizing microscope. It is possible to record picture and movie at a maximum speed of 50 frame/s. A further dichroic mirror, placed between the microscope objective and the first dichroic mirror, can be used to direct the laser light backscattered by the droplets toward a photodiode to measure rotation frequency higher than 10 Hz.

Bibliography

[1] Ashkin, A.; Dziedzic, J. M.; Bjorkholm, J. E.; Chu, S. *Opt. Lett.* **1986**, *11*, 288–290.

[2] Friese, M. E. J.; Nieminen, T. A.; Heckenberg, N. R.; Rubinsztein-Dunlop, H. *Nature* **1998**, *394*, 348–350.

[3] Juodkazis, S.; Shikata, M.; Takahashi, T.; Matsuo, S.; Misawa, H. *Jpn. J. Appl. Phys.* **1999**, *38*(5), L518–L520.

[4] Juodkazis, S.; Shikata, M.; Takahashi, T.; Matsuo, S.; Misawa, H. *Appl. Phys. Lett.* **1999**, *74*(24), 3627–3629.

[5] Juodkazis, S.; Matsuo, S.; Murazawa, N.; Hasegawa, I.; Misawa, H. *Appl. Phys. Lett.* **2003**, *82*(26), 4657–4659.

[6] Beth, R. A. *Phys. Rev.* **1936**, *50*, 115–125.

[7] Cheng, Z.; Chaikin, P. M.; Mason, T. G. *Phys. Rev. Lett.* **2002**, *89*, 108303.

Part III

Results and Discussion

Chapter 7

Large Deuterium Effect in Rotational Diffusion of Dye in Liquid Solution

7.1 Introduction and Motivations

Our interest in studying the effect of hydrogen-deuterium substitution on the rotational dynamics of the anthraquinone dyes arises from the fact that for the same dyes dissolved in the 5CB nematic phase, the isotopic substitution was found to approximately double the magnitude of the optical nonlinearity arising from photoinduced molecular reorientation [1]. The molecular model proposed in order to explain the optical nonlinearity of dye-doped mixtures deals with an expression for the nonlinearity (given in the formula 3.7) depending, to first approximation, on the effective excited-state lifetime τ_d and to the photoinduced variations of two molecular parameters: the orientational mean-field potential energy u and the rotational diffusion constant D.

If we assume for D the expression given in Sect. 2.1, obtained by means of the SED model [2–9] no significant changes would be expected either owing to the electronic

excitation or to the isotopic substitution. Nevertheless a significant photoinduced change of D has been recently reported [1] and ascribed to a strength variation of specific intermolecular interactions. Since our molecules have the possibility to perform hydrogen bonding and this interaction is sensitive to the isotopic substitution, our discussion seems to indicate a possible explanation of the isotopic substitution enhanced nonlinearity.

Moreover, as already discussed, the validity of the SED model is expected to loose its validity when the size of the solute molecules approaches that of the solvent molecules or becomes smaller exactly for the same reason, i.e., the specific intermolecular interactions between solute and nearest-neighbor solvent molecules become important in this regime. [6–12].

Our materials are well suited to study possible deviations from simple SED behavior, in connection with the presence of specific interactions. Indeed, the molecule of HK271 is only a factor 1.6 larger in weight than the molecule of 5CB. The molecule of 1AAQ is 10% smaller than that of 5CB. Moreover, we anticipated the possibility that the amino groups of the dyes could hydrogen-bond to the cyano group of 5CB (see Fig. 7.1). Since hydrogen bonds are sensitive to isotopic substitution [13, 14], a significant deuterium effect in the rotational mobility is conceivable.

Deuterium-substitution effects on the S_1 excited-state lifetime τ_e have already been reported for other dyes [15–17]; since $\tau_d = (\tau_e^{-1} + \tau_r^{-1})^{-1}$ such a variation can contribute to the nonlinearity enhancement.

A direct measurement of the deuterium-hydrogen substitution effect on the rotational diffusion dynamics of photoexcited dye molecules may then definitely clarify the question, a fact that motivated the work described in this Chapter.

7.2 Experimental Procedure

We used the dyes HK271 and 1AAQ dissolved in liquid 5CB. As a reference solvent which cannot hydrogen-bond to the dyes, we used a mixture of alkanes $C_nH_{2(n+1)}$ with $n = 20 \div 30$ (paraffin with a melting point in the range 325-327 K, from Merck, Darmstadt, Germany). The viscosity of paraffin has been measured by means of a stress controlled rheometer in the Couette geometry.

The deuterated forms have been obtained by means of the procedure described in Sect. 4.2.1. During the measurements the sample is placed into an oven (see Fig. 5.2.2) allowing temperature control to within 0.1K. Although 5CB is a liquid crystalline material that has a nematic phase between 297 and 308 K, our study was limited to the temperature range 311-368 K, in which 5CB is in its ordinary isotropic liquid phase.

The technique employed to detect the rotational diffusion is the time-resolved fluorescence, described in Sect. 5.2.

7.3 Results

The measured values of the excited-state lifetime τ_e and the rotational diffusion time τ_r as a function of temperature, for the protonated and deuterated solutions HK271-5CB, 1AAQ-5CB, and HK271-paraffin are shown in Figs. 7.2**A**, 7.2**B** and 7.3, respectively.

The main figures report, in semilogarithmic scale, the rotational times versus inverse absolute temperature (error bars are for a confidence-level of 99%, not including the statistical uncertainty on the response function). The solid lines are best-fits to

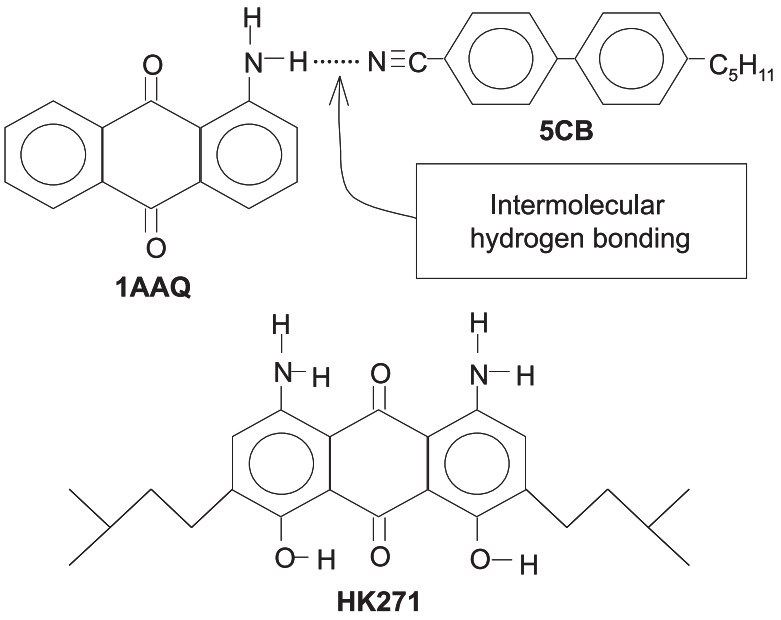

Figure 7.1: Molecular structures of 1AAQ, HK271 and 5CB. Top panel, possible hydrogen-bond between the amino-moiety of dye molecules and the cyano group of 5CB.

data based on the phenomenological Arrhenius law $\tau_r = \tau_0 \exp(E_a/kT)$, where k is the Boltzmann constant, E_a is an activation energy (best-fit values are given in the figures), and τ_0 is a constant.

The fluorescence lifetimes τ_e of the corresponding samples are plotted in the figure insets. A very large isotopic effect of both lifetime τ_e (see also Fig. 4.4) and rotational time τ_r in both 5CB solutions, and of τ_e only in the paraffin solution, is evident in our data.

The isotopic effect of τ_r is our main result and the following part of this section will be devoted to its discussion. First, however, let us comment briefly the isotopic

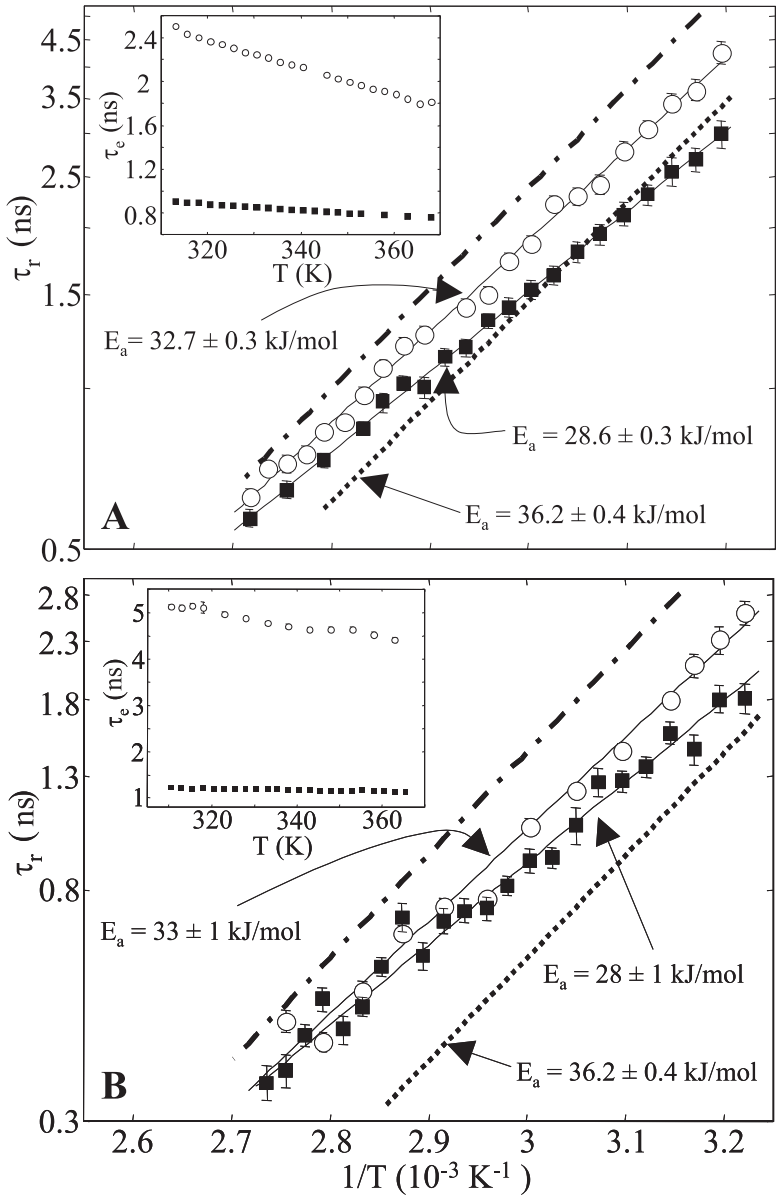

Figure 7.2: Semilog plot of τ_r vs $1/T$ for protonated (filled squares) and deuterated (open circles) mixtures, respectively. Subplots (**A**) and (**B**) refer to HK271-5CB and 1AAQ-5CB mixtures, respectively. Solid lines are Arrhenius fits. E_a are the resulting activation energies. The dotted and dot-dashed lines are the predictions of the SED model for stick boundary conditions: (**A**) $\rho = 2.43$, and V_{eff}= 388Å^3 (dotted line) and V_{eff}=632Å^3 (dot-dashed line); (**B**) $\rho = 2.2$, V_{eff}=174Å^3 (dotted line) and V_{eff}=414Å^3 (dot-dashed line). Inset: fluorescence lifetime τ_e vs T for the same samples (same meaning of symbols).

effect of the excited-state lifetime τ_e. The ratio of lifetimes for deuterated and protonated samples at the lowest working temperatures is of 2.8 at 313 K, 4.2 at 311 K, and 1.6 at 328 K for HK271-5CB, 1AAQ-5CB, and HK271-paraffin, respectively. We have checked that these ratios do not further increase when the exchange phase of the deuteration procedure is prolonged or the whole procedure is repeated, indicating that our procedure leads to complete deuteration of the amino and hydroxyl dye groups. Similar deuterium effects in the S_1-state lifetime τ_e have been already reported, for related dyes [15–17]. Probably the nonradiative decay channels of state S_1 associated with nuclear vibrations are suppressed by the deuterium substitution. Intermolecular interactions and possibly hydrogen bonding must also play an important role in this phenomenon, as we found that the deuterium effect on τ_e of HK271 is much larger in 5CB than in paraffin. Solvent-dependent nonradiative decay attributed to intermolecular hydrogen bonding has been already reported for anthraquinone dyes [18, 19].

Let us turn now to the isotopic effect of the rotational time τ_r observed for both dyes in 5CB (Fig. 7.2). The increase of τ_r induced by deuteration in both cases is of about 40% at the lowest investigated temperatures (313 K for HK271 and 311 K for 1AAQ). To our knowledge, this is the largest isotopic effect of diffusional rotational dynamics ever reported. It is about twice as large as that reported for pure benzene (referring to its diffusional degree of freedom) [20]. Moreover, unlike the case of benzene, in our dyes deuteration leads to an increase of rotational times (decrease of rotational mobility). The isotopic effect on τ_r vanishes completely (within the uncertainties) when HK271 is dissolved in liquid paraffin (Fig. 7.3). This shows unambiguously that specific polar interactions, most likely hydrogen bonding, between HK271 and 5CB are the main cause of the effect. The temperature dependence of τ_r

for the two dyes in 5CB also shows a significant deuterium effect, with a difference of 4-5 kJ/mol in the best-fit activation energies.

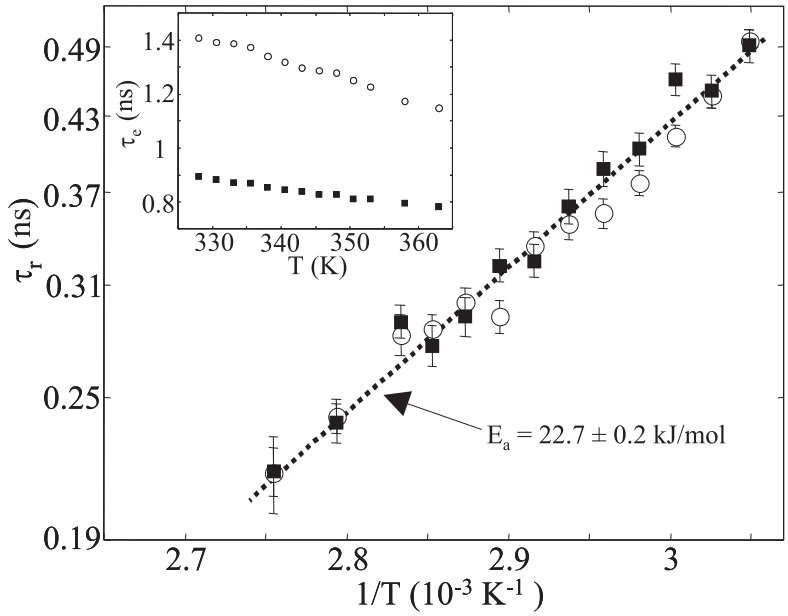

Figure 7.3: Semilog plot of τ_r vs $1/T$ for protonated (filled squares) and deuterated (open circles) HK271-paraffin. The dotted line is the prediction of SED model with "slip" boundary conditions, $\rho = 2.43$ and V_{eff}= 388Å^3. The Arrhenius activation energies of both data sets are consistent with that of SED, given in the figure. Inset: corresponding fluorescence lifetimes.

The activation energy that we obtain from our fits is a phenomenological parameter that has no simple microscopic interpretation. Nonetheless, it is interesting to compare our results with the effect of deuteration on the hydrogen bond energy. Typically, this energy change is of about 1 kJ/mol or less [14], that is not enough to explain our results. One could ascribe this discrepancy to a cooperative effect of more than one hydrogen-bonds. However the dye 1AAQ is unlikely to make more than one intermolecular bond (and in any case no more than two), because one of the

two hydrogens of the amino group is probably already involved into a intramolecular hydrogen bond with the carbonyl group of the anthraquinone core [15, 16]. Although HK271 has the possibility of forming more than one intermolecular bonds (but it is unlikely to have more than two, for the same reason as for 1AAQ), it shows almost the same isotopic change in activation energy. This leads us to associate the observed isotopic effect to the breaking of a single hydrogen bond. Therefore, since the isotopic shift of equilibrium energy is not enough to explain our findings, the main contribution to the variation of activation energy must arise from the change of potential barrier for the breaking of the hydrogen bond, perhaps in connection with the diminished quantum delocalization of deuterium [21].

The complexity of the intra-molecular photophysics of these dyes, revealed for example in the strong isotopic effect of lifetimes, imposes maximum care in order to exclude that we are actually observing some artifact due to an incorrect interpretation of the fluorescence signal. That this is not the case is first confirmed by our data in paraffin, where the isotopic effect on lifetime (still large, although smaller than in 5CB) does not result in any apparent isotopic effect of rotational diffusion. Moreover, our interpretation is confirmed by the analysis of the initial anisotropy r_0 as a function of temperature, deuteration, solute and solvent. The results are shown in Fig. 7.4.

The experimental values of r_0 ($\approx$0.32 for HK271 and $\approx$0.25 for 1AAQ) are slightly smaller than the predicted ones (0.4 for HK271 and 0.36 for 1AAQ). This is typical for this sort of experiments, and it could be explained for example with fast dynamical effects occurring immediately after excitation, hidden by our limited time resolution, or with some degree of distortion of the dye molecular structure in its excited state. However, no significant dependence of r_0 on deuteration, solvent, and temperature is

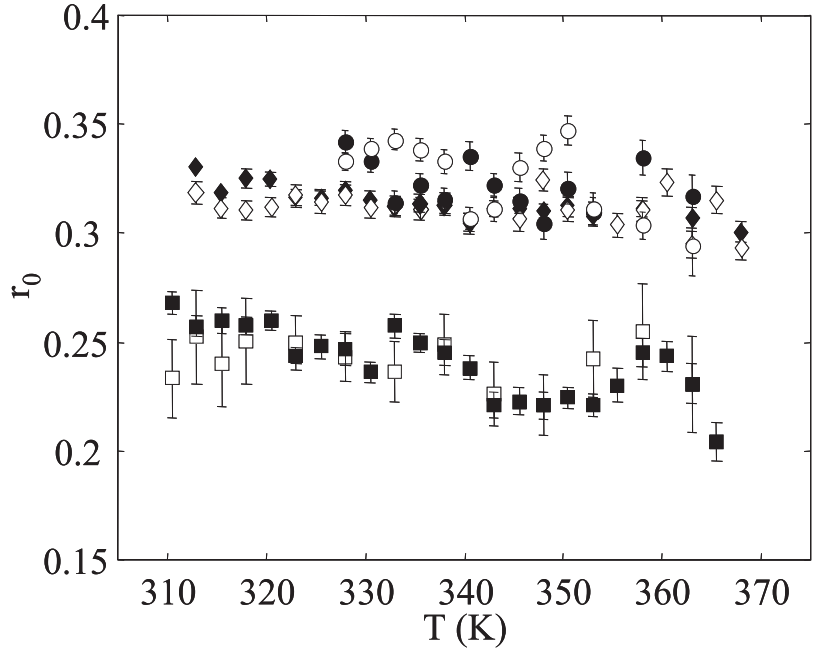

Figure 7.4: Initial anisotropy r_0 as a function of temperature, deuteration, solute, and solvent: deuterated and protonated HK271-5CB (open and filled diamonds, respectively); deuterated and protonated HK271-paraffin (open and filled circles, respectively); deuterated and protonated 1AAQ-5CB (open and filled squares, respectively).

observed, so that no artifact on decay times can be possibly induced. Experiments of time-resolved dichroism on HK271 in 5CB [22], have fully confirmed the deuterium-isotope effect reported here. As these experiments probe the dye rotational dynamics also in the ground-state, they are less sensitive to the excited-state lifetime.

7.4 Comparison with the SED model

Let us now compare our results with the predictions of the SED model. According to the latter, the rotational time is given by $C_s \eta V_{\text{eff}}/kT$, where η is the shear viscosity

of the host liquid, C_s a factor accounting for the anisotropic shape of the molecule and depending on the assumed hydrodynamic boundary conditions, and V_{eff} is the effective volume of the solute molecule. For the $\eta(T)$ of 5CB we used the values reported in Refs. [23,24], while the viscosity of paraffin has been measured by means of a stress controlled rheometer in the Couette geometry. The factor C_s is tabulated in the literature, as a function of the ratio ρ between the major and minor axis of the molecule "equivalent ellipsoid" [2,8,9,25]. The molecule volumes V and ratios ρ have been calculated by using the van der Waals packing radii for each atom, and covalent bond lengths and angles [26, 27]. We obtained V(1AAQ)=174 Å^3, V(HK271)=388 Å^3, V(5CB)=244 Å^3, and ρ(1AAQ)=2.2. Owing to the flexible alkyl chains at the ends of HK271, ρ(HK271) is not well defined and can range from 2.3 to 2.7. For comparison, we calculated also the average molecular volume of the paraffin solvent, $V(C_{25}H_{52})$=475 Å^3.

In the case of HK271-paraffin (Fig. 7.3), we find that the activation energy predicted by the SED model (E_a = 22.7±0.2 kJ/mol) is in excellent agreement with the best-fit Arrhenius energies found for deuterated and protonated samples (E_a = 22±1 kJ/mol and E_a = 23±1 kJ/mol, respectively). Moreover, the SED prediction (dotted line) for the absolute values of τ_r fits well our data if one assumes the so-called "slip" boundary conditions [2, 3, 9] and sets ρ(HK271)=2.43, corresponding to C_s = 0.7. Based on this result, we used ρ(HK271)=2.43 also when analyzing HK271-5CB data.

In HK271-5CB and 1AAQ-5CB, the SED predictions for "stick" boundary conditions [2, 3, 9] (that give C_s = 1.83 for HK271 and C_s = 1.67 for 1AAQ) are plotted in Fig. 7.2 as dotted lines. We can see that for the 5CB solvent our systems are in the so-called "super-stick" regime, i.e., almost all data lie above the SED line for

stick boundary conditions. This behavior has no explanation within a pure hydrodynamic model [9]. A simple way to circumvent this difficulty is to assume that the rotating solute molecule is strongly attached to one or more molecules of the host, thus behaving as if its effective volume is actually larger than the true molecular one. In Fig. 7.2 we have also plotted, as dash-dotted lines, the predictions of SED for V_{eff}=V(dye)+V(host), without changing C_s. We see that all our data lie below these new lines, indicating that the situation is somewhat in between the two effective SED behaviors. Moreover, the Arrhenius activation energies of τ_r for both deuterated and protonated samples are significantly smaller than the predictions of SED model. We may interpret phenomenologically these findings by introducing a microscopic effective solvent viscosity η_m "sensed" by our dye molecules [12]. η_m is a manifestation of the interactions between the solute and solvent molecules. The fact that in our case η_m is larger than the viscosity of 5CB but it has a lower activation energy implies that the average enthalpic contribution to these dye-5CB interactions is smaller than for 5CB-5CB, even though the resulting friction is larger.

Bibliography

[1] Kreuzer, M.; Hanisch, F.; Eidenschink, R.; Paparo, D.; Marrucci, L. *Phys. Rev. Lett.* **2002**, *88*, 013902.

[2] Hu, C.-M.; Alavi, R. *J. Chem. Phys.* **1974**, *60*, 4354–4357.

[3] Zwanzig, R. *J. Chem. Phys.* **1978**, *68*, 4325–4326.

[4] Hynes, J. T.; Kapral, R.; Weinberg, M. *J. Chem. Phys.* **1978**, *69*, 2725–2733.

[5] Myers, A. B.; Pereira, M. A.; Holt, P. L.; Hochstrasser, R. M. *J. Chem. Phys.* **1987**, *86*, 5146–5155.

[6] Ben-Amotz, D.; Drake, J. M. *J. Chem. Phys.* **1988**, *89*, 1019–1029.

[7] Alavi, D. S.; Waldeck, D. H. *J. Phys. Chem.* **1991**, *95*, 4848–4852.

[8] Hartman, R. S.; Alavi, D. S.; Waldeck, D. H. *J. Phys. Chem.* **1991**, *95*, 7872–7880.

[9] Williams, A. M.; Jiang, Y.; Ben-Amotz, D. *Chem. Phys.* **1994**, *180*, 119–129.

[10] Blanchard, G. J.; Wirth, M. J. *J. Chem. Phys.* **1985**, *82*, 39.

[11] Blanchard, G. J.; Cihal, C. A. *J. Phys. Chem.* **1988**, *92*, 5950–5954.

[12] Blanchard, G. J. *J. Phys. Chem.* **1988**, *92*, 6303–6307.

[13] Jeffrey, G. A. *An Introduction to Hydrogen Bonding;* Oxford Univ. Press: Oxford, 1997.

[14] Scheiner, S.; Cŭma, M. *J. Am. Chem. Soc.* **1996**, *118*, 1511–1521.

[15] Inoue, H.; Hida, M.; Nakashima, N.; Yoshihara, K. *J. Phys. Chem.* **1982**, *86*, 3184.

[16] Benthem, M. H. V.; Gillispie, G. D.; Haddon, R. C. *J. Phys. Chem.* **1982**, *86*, 4281.

[17] Palit, D. A.; Pal, H.; Mukherjee, T.; Mittal, J. P. *J. Chem. Soc. Faraday Trans.* **1990**, *86*, 3861.

[18] Yatsuhashi, T.; Inoue, H. *J. Phys. Chem. A* **1997**, *101*, 8166.

[19] Yatsuhashi, T.; Nakajima, Y.; Shimada, T.; Tachibana, H.; Inoue, H. *J. Phys. Chem. A* **1998**, *102*, 8657.

[20] Hardy, E. H.; Merkling, P. J.; Witt, R.; Doelle, A. *Z. Phys. Chem.* **2000**, *214*, 1687–1698.

[21] Guillot, B.; Guissani, Y. *J. Chem. Phys.* **1998**, *108*, 10162–10174.

[22] Kreuzer, M.; Benkler, E.; Paparo, D.; Casillo, G.; Marrucci, L. *Phys. Rev. E* **2003**, *68*, 011701.

[23] Martinoty, P.; Kiry, F.; Nagai, S.; Candau, S. *J. de Physique* **1977**, *38*, 159–162.

[24] Boettger, A.; Frenkel, D.; van de Riet, E.; Zijlstra, R. *Liq. Cryst.* **1987**, *2*, 539–547.

[25] Philips, L. A.; Webb, S. P.; Clark, J. H. *J. Chem. Phys.* **1985**, *83*, 5810–5821.

[26] Israelachvili, J. *Intermolecular and Surface Forces;* Academic Press: London, 1985.

[27] *CRC Handbook of Chemistry and Physics, 55th ed.;* CRC: Cleveland, 1974.

Chapter 8

Effect on the Fluorescence of the Photon Excess Energy and of the Ensuing Vibrational Excitation

8.1 Introduction and Motivations

Our interest in the investigation of the effect of the excitation light wavelength on the dynamics and the fluorescence of dye molecules in liquid solvent arises from two still open questions; the first is related to the possible effects of the nonradiative energy released by the molecule following the absorption, while relaxing from an excited vibrational level to either the bottom of the electronic excited state or to the ground state. Moreover, as already anticipated, some dye-liquid crystal systems show a non-constant wavelength dependence in their dye-induced nonlinearity relative to the absorbance. Both these questions are still not understood; several models, proposed in the past, seem to provide plausible explanations but experimental tests have never been carried out in order to test their validity. In the following we present separately the theoretical backgrounds behind the two problems, in both cases underlying the

potential role of our measurements in improving our understanding.

8.1.1 Photoinduced Molecular Reorientation

Besides electronic excitation, another general consequence of photon absorption is a relatively large vibrational excitation of the molecule. This occurs already when the molecule is in its photo-excited electronic state, due to Franck-Condon effect: a significant fraction of the photon energy is immediately converted into vibrational energy. However, the vibrational excitation may become even stronger when the molecule relaxes back nonradiatively to its electronic ground-state: in this case the photon energy is entirely converted into vibrational energy. The latter is then rapidly redistributed among many different degrees of freedom of the molecule and of its neighbor molecules, approaching a Boltzmann distribution. One can then approximately describe this process as a "local heating", heating which may be very large (in the order of several hundreds Kelvin's, as estimated by dividing the photon energy by the heat capacity of a molecular volume of material), although also very short-lived in condensed materials, due to rapid heat diffusion (typically, few picoseconds) [1].

The possibility of photoinduced molecular reorientation (PMR) driven by this local heating effect was first proposed, in our knowledge, by A. C. Albrecht in the mid fifties [2]. Albrecht's idea was that the local heating may strongly enhance rotational diffusion, thus leading to a partial or total orientational randomization. This randomization occurs preferentially for molecules oriented with their transition dipole more parallel to the optical electric field. Therefore, molecules are more often reoriented *away* from the field direction and a net orientation in the plane perpendicular to it can be achieved by cumulating many randomization events.

To our knowledge Albrecht's effect, although theoretically possible, has never been demonstrated experimentally. This is probably because the rapidity of heat diffusion makes it highly ineffective in most materials, as discussed for example in Ref. [3]. However, the idea that a significant contribution to PMR can be due to photoinduced local heating keeps surfacing in the scientific literature whenever other models seem to fail or to leave room for doubts. In some works, this randomization mechanism has been proposed *in combination* with other PMR effects. For example, in amino-anthraquinone dye solutions, the possibility of a large sudden random reorientation of photo-excited molecules relaxing back to the ground state has been recently considered in Ref. [4]. The extent of this orientational randomization was parametrized by a constant F ranging from 0 to 1, with $F = 1$ meaning no randomization and $F = 0$ complete randomization. However, the data reported in Ref. [4] did not allow a good estimate of F (on this issue, see in particular the related *Erratum* [5]). A similar idea was put forward also in Ref. [6] to explain a peculiar excitation wavelength dependence of the photoinduced reorientation of certain azodye-doped liquid crystals. In this case, the assumption was that a partial random molecular reorientation occurs directly in the excited electronic state, due to the fast release of vibrational energy. The magnitude of this effect was then thought to depend on the amount of photon energy (hence the wavelength dependence) in excess of the minimum required for electronic excitation, which is converted in vibrational energy. A very fast random reorientation of the molecule after excitation due to the local heating (or more generally nonradiative vibrational energy dissipation) effect may reduce the initial anisotropy r_0. Such reduction should however depend strongly on the amount of dissipated heat, which in turn depends on the photon extra energy. Therefore, by measuring the dependence

of r_0 on the excitation wavelength, as resulting from time-resolved fluorescence, we address this issue directly.

8.1.2 Jánossy Effect Wavelength Dependence

In Sect. 3.2.1 the approximate expression of the dye-induced optical nonlinearity is obtained, expressed in terms of the molecular merit-figure μ given in 3.7 as:

$$\mu = \frac{2\tau_d D_e}{15h}\left(\frac{u_{eh}}{D_e} - \frac{u_{gh}}{D_g}\right). \tag{8.1}$$

In this expression, τ_e is the dye excited state lifetime, D_e (D_g) the diffusional rotational constant for the excited (ground) state, h the Planck constant, and u_e (u_g) the mean field intermolecular interaction potential for the excited (ground) state. The diffusional rotational constant is related to the rotational time τ_r by means of the relationship $D_e = 1/(6\tau_r)$. Equation 8.1 is based on the assumption that there is a single relevant excited state (presumably the first-excited singlet state S_1). Based on Eq. 8.1 and assuming that the excited-state presents no kind of polymorphism, no excitation-wavelength dependence of μ is expected. This in turn implies that the dye-induced torque magnitude is simply proportional to the absorption coefficient [7]. Nevertheless, some dyes exhibit an anomalous wavelength dependence [6,8] where this proportionality does not hold. To explain this anomalous wavelength dependence, we clearly have to go beyond this simple model. All ground-state parameters cannot of course depend on λ. Perhaps the simplest possible extension of the model is that the excited state changes somehow its nature when it is excited with an excess-energy photon. Possible modifications are long-lived internal vibrations excited by the photon extra-energy, or variations in the intramolecular or intermolecular hydrogen-bond

or other physical interactions (e.g., an excess photon energy may lead to breaking a hydrogen bond) [7]. Another possibility could be that there are actually more than one close-lying excited electronic states (although it is uncommon that any electronic excited state higher in energy than S_1 is long-lived). All these forms of polymorphism of the excited state of the dye could lead to an excitation-wavelength variation of some of the molecular parameters appearing in Eq. 8.1. By time-resolved fluorescence, we could directly check if either τ_e and/or $\tau_r = 1/(6D_e)$ depend on the excitation-light wavelength. A second possibility, first proposed in Ref. [6], is that the fast vibrational relaxation immediately following the photon absorption, whose magnitude depends on the photon excess energy, could lead to a significant random reorientation of the excited dye molecules. This in turn would naturally lead to a wavelength dependence of the Jánossy effect, as the diminished anisotropy of the excited dye population is reflected into a smaller orientational mean-field acting on the host. As already discussed, a rapid loss of orientational order after excitation would be reflected into a reduced initial degree of anisotropy r_0 in the time-resolved fluorescence data. Therefore, if this effect is significant, we should see an excitation-light wavelength dependence of r_0. A third possible explanation of the wavelength dependence of the nonlinearity merit figure μ is that a λ-dependent fraction of the excitations is "wasted", for example because they are followed by an immediate nonradiative relaxation back to the ground state or because they are immediately followed by an intersystem-crossing to an ineffective triplet state. If it occurs, this effect is usually more likely at higher photon energies (lower λ's), where more decay channels are present. This effect should be however reflected also into a λ-dependence of the fluorescence quantum yield Φ, that monitors the S_1-fluorescent state population induced by absorption.

8.2 Experimental Procedure

This experiments have been carried out by using the technique of time-resolved fluorescence depolarization and steady-state fluorescence on amino-anthraquinone dyes in liquid solutions at varying excitation wavelength. For the time-resolved fluorescence measurements, this is made possible by means of an optical parametric generator (Fig. 5.2.2); it allows us to obtain light pulses at a tunable wavelength in the visible part of the electromagnetic spectrum.

We used the dye HK271 (which shows a significant wavelength dependence of the Jánossy effect [8]) in the isotropic liquid phase of 5CB.

Moreover we performed separate experiments of steady-state fluorescence. For these measurements we used also the deuterated form of HK271. In order to investigate the dependence of fluorescence on the host molecular structure, these measurements have been performed also in ethyl alcohol and in a liquid paraffin (a mixtures of alkanes, melting point 18°C) as solvents. All the solutions have concentrations sufficiently low to avoid nonlinear effects on the absorption and/or in the emission spectra (HK271 in: 5CB at 10^{-4} mol/L, paraffin at 3×10^{-6} mol/L and ethanol at 10^{-4} mol/L) .

The quantum yield $\Phi(\lambda)$ has been obtained by taking the ratio of the number of fluorescence photons as deduced from the excitation steady-state fluorescence spectrum (i.e., fluorescence intensity at a fixed emission wavelength for a varying excitation wavelength) to the number of absorbed photons as deduced from the absorption spectrum.

As a check, we measured also the $\Phi(\lambda)$ of RhB, known to be a good quantum counter [9]. Our results in RhB dissolved in ethanol (at 10^{-6} mol/L) are reported in

the inset of Fig. 8.5 and show the expected λ-independent behavior of Φ.

8.3 Results

We varied the excitation wavelength in the range 480-630 nm, corresponding to photons having an energy in the range 2.0-2.6 eV. This is approximately the same range in which wavelength dependence of the Jánossy effect has been observed [8, 10].

For HK271 dissolved in 5CB, the absorption peak is at 633 nm, so that our photons had an excess energy with respect to the absorption peak ranging from 0 up to approximately 0.62 eV.

In Fig. 8.1, we plotted our results for the initial anisotropy factor r_0 versus excitation wavelength and photon excess energy. In this and in the following figures, error bars correspond to one standard deviation. It can be seen that r_0 is indeed smaller than the ideal value 0.4, confirming that some of the aforementioned mechanisms is operating. Its average value is $r_0 = 0.31 \pm 0.01$ (here and in the following all quoted uncertainties are standard deviations). However, it is also seen in the figure that no significant dependence of r_0 on the photon excess energy is present. A linear fit yields a slope $dr_0/dE = -0.024 \pm 0.021$ eV^{-1}, fully compatible with zero. The maximum negative slope that is compatible with our data is $-(dr_0/dE) = 0.065$ eV^{-1}, at a 95% confidence level.

Actually a small "dip" in r_0 is perhaps seen for wavelengths close to 570 nm, although it is not statistically very significant. Roughly at this wavelength, in the absorption spectrum of HK271 one finds a secondary peak. Moreover, in a narrow range of wavelengths between 570 and 590 nm, the fluorescence was also found to exhibit an additional fast-decaying component (decay time shorter than 100 ps). This

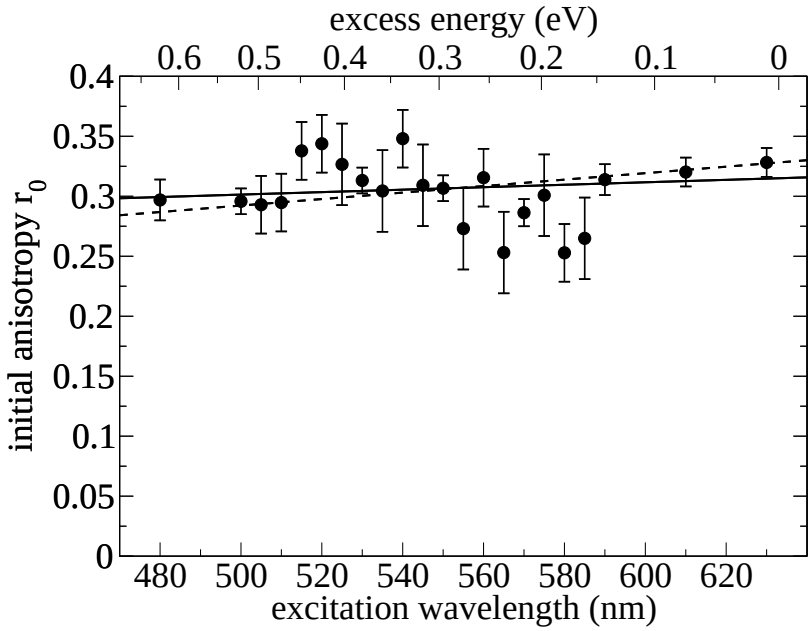

Figure 8.1: Initial anisotropy factor r_0 versus excitation wavelength or photon excess energy. The solid line is a linear best-fit, whose slope (with respect to photon energy) is $dr_0/dE = -0.024 \pm 0.021$ eV^{-1}. The dashed line shows the best-fit line having the maximum slope compatible with our data, at a confidence level of 95%.

additional fluorescence was superposed to the normal one and fully unpolarized. We could not identify its origin. In the data analysis, we could however separate the two components by fitting our $S_e(t)$ signal with a double-exponential decay, one of which almost istantaneous; the anisotropic signal $S_d(t)$ did not show this second component at all, indicating that it is fully unpolarized. The value of r_0 reported in Fig. 8.1 only refers to the ordinary "slow" decay signal.

Fig. 8.2 shows our results for the wavelength dependence of the rotational time τ_r. Error bars correspond to one standard deviation. Data show a small reduction of τ_r with increasing photon energy but, since the slope calculated by a linear fit(1.8 ± 1.5 ps/nm) is compatible with zero within two standard deviations, no definite conclusion

can be drawn.

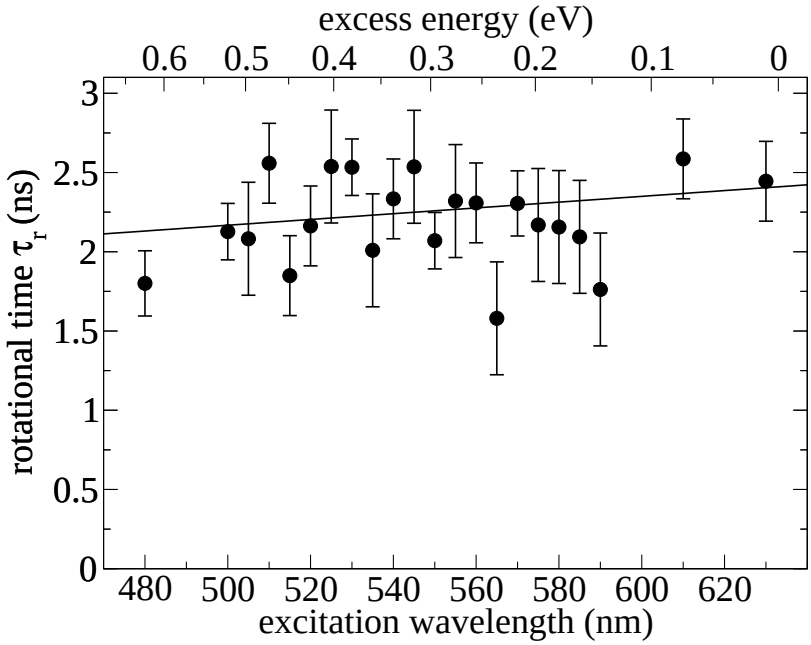

Figure 8.2: Rotational time τ_r versus excitation wavelength or photon excess energy (at a temperature of 45°C). The solid line is a linear best-fit. Its slope is 1.8 ± 1.5 ps/nm, compatible with zero.

Our results for the wavelength dependence of the excited electronic state lifetime τ_e are reported in Fig. 8.3. In this case the wavelength dependence is statistically significant. The linear best-fit slope is -0.57 ± 0.15 ps/nm, corresponding to a reduction of this decay time of about the 10% between the lowest and the highest wavelength at which it has been measured. A possible explanation of this variation, related to the sensitivity to specific interaction is proposed in the next section.

Figure 8.4 illustrates our results for the wavelength dependence of the quantum yield $\Phi(\lambda)$. It results to be strongly dependent on the photon energy. Stimulated by this "positive" result, we also investigated the effect of deuteration on the $\Phi(\lambda)$

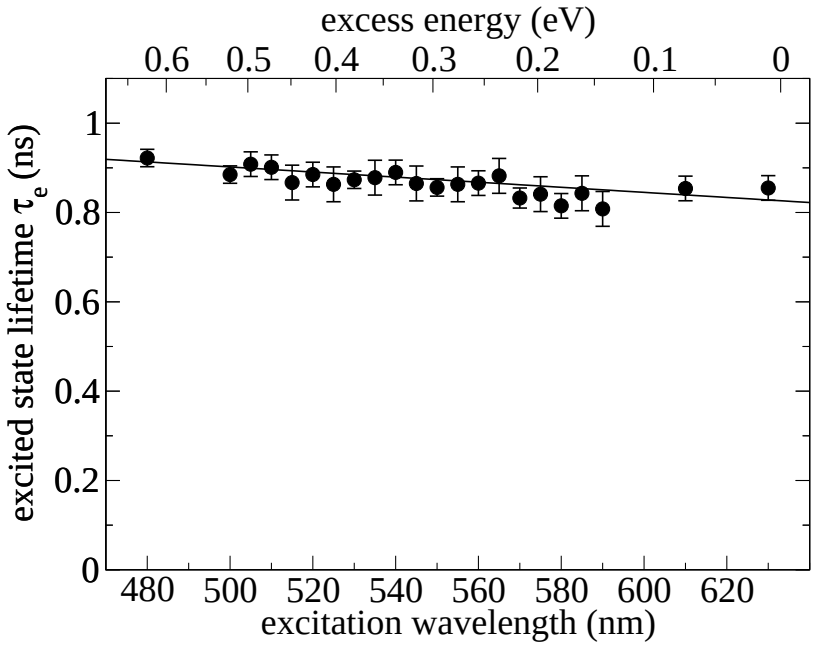

Figure 8.3: Excited state lifetime τ_e versus excitation wavelength or photon excess energy. The solid line is a linear best-fit. Its slope is -0.57 ± 0.15 ps/nm.

behavior for HK271 in 5CB and in paraffin. The data are shown in Fig. 8.4, where it is seen that deuterated samples exhibit the same $\Phi(\lambda)$ as protonated ones except for a λ-independent overall multiplicative enhancement. This enhancement results to be comparable to that induced by the deuteration on the fluorescence lifetime.

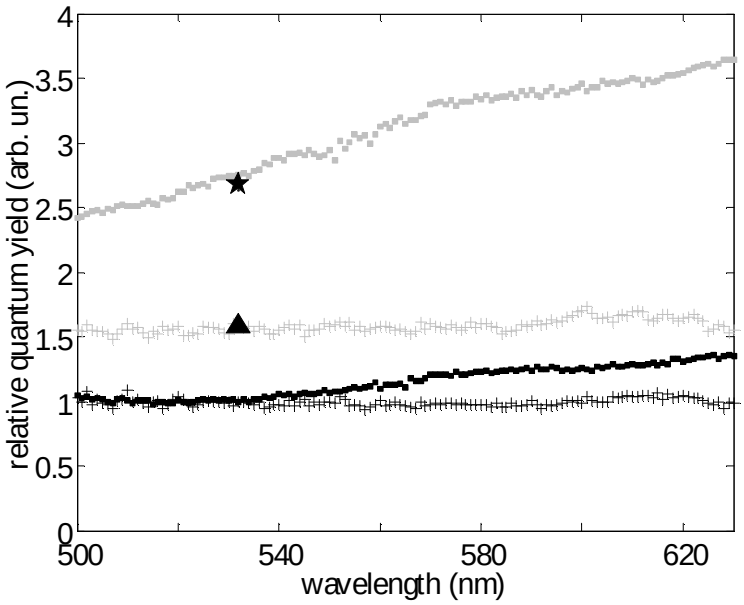

Figure 8.4: Effect of hydrogen-deuterium substitution on the fluorescence quantum yield $\Phi(\lambda)$. Shown are the quantum yield for protonated (black squares) and deuterated (gray squares) HK271-5CB and for protonated (black crosses) and deuterated (gray crosses) HK271-paraffin. The quantum yields of the protonated solutions have been rescaled so as to be superimposed at the lowest wavelengths. The data for the deuterated compounds have been kept in scale with the corresponding protonated ones, so as to show the increased yield associated with deuteration. At $\lambda = 532$ nm, the deuterated-protonated lifetime-ratio is also shown for HK271-5CB (star) and HK271-paraffin (triangle).

As a further test, we investigated the dependence of the quantum yield $\Phi(\lambda)$ behavior on the host. In figure 8.5, we show the measured $\Phi(\lambda)$ for HK271 in 5CB, paraffin and ethanol. It is seen that the $\Phi(\lambda)$ is significantly nonconstant only in 5CB. A very small increase is perhaps present in ethanol, while $\Phi(\lambda)$ is constant in the nonpolar paraffin.

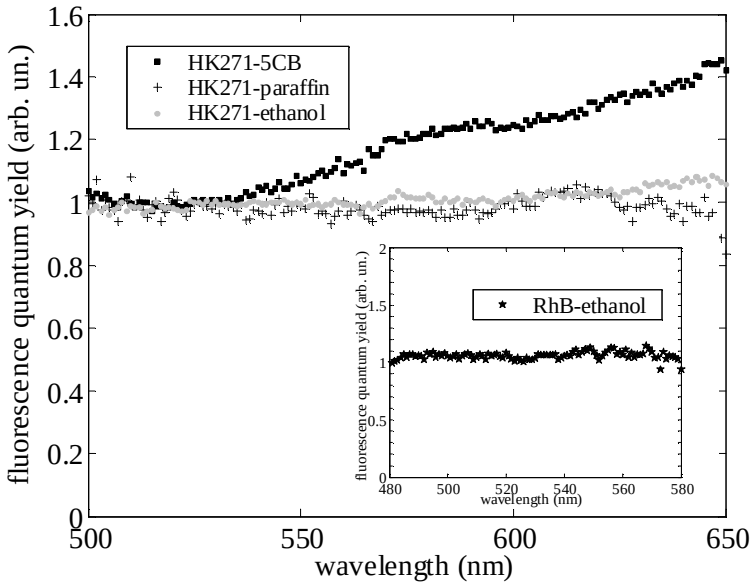

Figure 8.5: Effect of the host on the fluorescence quantum yield excitation-wavelength dependence $\Phi(\lambda)$ of HK271. The hosts are 5CB (black squares), paraffin (crosses) and ethanol (gray circles). The three $\Phi(\lambda)$ curves have been rescaled so as to be superimposed at $\lambda = 532$ nm. Inset: fluorescence quantum yield excitation-wavelength dependence of RhB, known to be a good quantum counter, dissolved in ethanol.

8.4 Discussion in Connection with Proposed Models for Photoinduced Random Reorientation via Local Heating

From our measurements (Fig. 8.1), as already pointed out, no significant dependence of r_0 on the photon excess energy is present. If one models the orientational randomization as a diffusion process in angular space with root-mean-square (rms) angular rotation $\Delta\theta$, the r_0 after the randomization $r_0(\Delta\theta)$ is given by the following equation:

$$r_0(\Delta\theta) = r_0(0)e^{-\frac{3}{2}\Delta\theta^2}, \tag{8.2}$$

where $r_0(0)$ is the anisotropy before the randomization. These results are obtained trivially using the theory of rotational diffusion given in Sect. 1.4.

The average value obtained for r_0 corresponds to a rms $\Delta\theta = 24°$ randomization of the transition dipole direction with respect to the ideal case. The best-fit slope corresponds to a further rms angular randomization of 10° at $E = 0.6$ eV, or, if combined (by adding the angular variances) with the energy-independent rms angle 24°, a total rms angle of 26°. The maximum negative slope compatible with our data corresponds to an experimental upper limit for the rms angular randomization due to radiationless energy relaxation of 17° at $E = 0.6$ eV, or equivalently to an upper limit for the angular variance per unit energy of about 0.15 rad^2/eV.

To estimate the expected orientational randomization effect of the nonradiative energy relaxation we combined a simple continuum model of heat diffusion to estimate the temperature dynamics (i.e., the local heating versus time) around the molecule

with the measured dependence of the molecular rotational diffusion constant on temperature. Our approach is very similar to that outlined in the Appendix of Ref. [3].

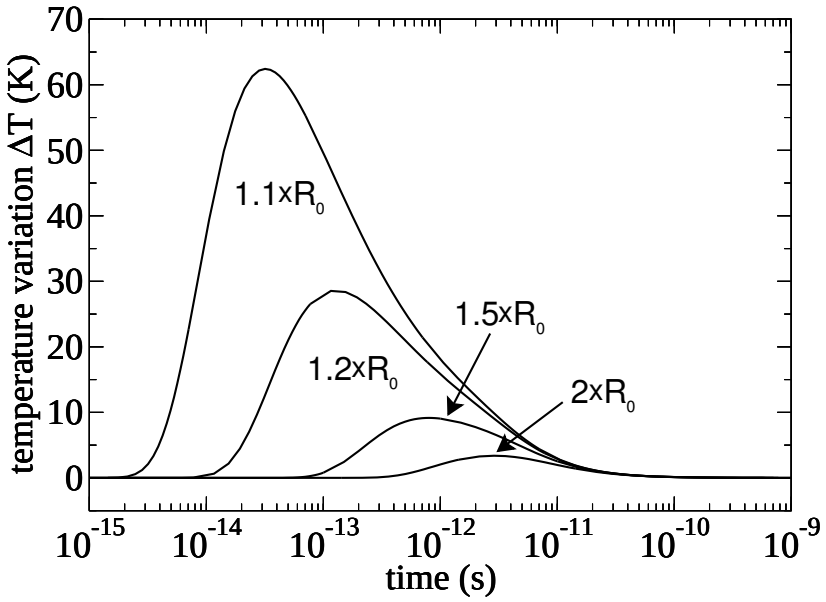

Figure 8.6: Temperature variation induced locally by the sudden release of 0.6 eV of heat on the surface of a spherical molecule of radius $R_0 = 7.3$ Å, in $5CB$ host at several distances R from the center of the molecule, ranging from $R = 1.1 \times R_0$ to $R = 2 \times R_0$.

Let us consider a spherical molecule of radius R_0 surrounded by an infinite continuous medium having thermal conductivity λ, specific heat c (we neglect here the small difference between constant-volume and constant-pressure heat capacity), and mass density ϱ. At time $t = 0$ an excess energy ΔE, corresponding to the photon excess energy, suddenly appears on the external surface of the molecule and starts diffusing in the medium. This is a classic heat diffusion problem that has a simple closed solution. The temperature variation $\Delta T(t)$ at a distance R from the center of

the molecule is the following:

$$\Delta T = \frac{\Delta E}{4\pi^{2/3} R_0 \varrho c \sqrt{at}} \frac{1}{R} \left[\exp\left\{ \frac{-(R-R_0)^2}{at} \right\} - \exp\left\{ \frac{-(R+R_0)^2}{at} \right\} \right] \tag{8.3}$$

where $a = \frac{4\lambda}{c\varrho}$. Inserting in this expression the parameters characterizing our system (i.e., $R_0 = 7.3$ Å, obtained as the cube-root of the HK271 molecule volume estimated in Ref. [11], $c = 1.8$ J/gK [12], $\lambda = 0.15$ W/Km [13] and $\varrho = 1.0024$ g/cm^3 [14], for 5CB in the isotropic phase), we obtain the results shown in Fig. 8.6, where an excess energy excitation $\Delta E = 0.6$ eV has been used. It is seen that at any distance from the molecule the temperature increase becomes essentially negligible (i.e., below few degrees) within 10 ps, a time much shorter than both the fluorescence lifetime τ_e and the diffusion rotational time τ_r.

The time-dependent temperature increase $\Delta T(t)$ leads to a corresponding time-dependent increase of the rotational diffusion constant $\Delta D(t)$. To estimate the latter we used the results of Ref. [11], where the temperature dependence of the rotational diffusion D for our system in the range $313 \div 368$K was found to be well described by an Arrhenius behavior, i.e., $D = D_0 \exp(E_a/kT)$, where $E_a = 28.6 \pm 0.3$ kJ/mol is an activation energy, $D_0 = (3.6 \pm 0.2) \times 10^{12}$ s^{-1}, and k is the Boltzmann constant. We assumed that this Arrhenius behavior remains valid also in our non-equilibrium process and at the much higher temperatures reached in proximity of our molecule (actually the rotational diffusion may only become slower than what predicted by this assumption, owing to the crossover to the inertial regime that may occur at very high temperatures; therefore our results for the orientational randomization can only be overestimated due to this assumption). In the absence of a clear criterion for this choice, we used different values of the radius R at which the temperature is actually "sampled", ranging from $1.1 \times R_0$ to $2 \times R_0$.

Finally, we used these results to compute the total extra angular variance that can be associated with the local heating effect by means of the following equation:

$$\overline{\Delta\theta^2} = 4\int_0^\infty \Delta D(T(t))dt = 4D_0\int_0^\infty \left(\exp\left\{\frac{E_a}{k\left[T_0+\Delta T(t)\right]}\right\} - \exp\left\{\frac{E_a}{kT_0}\right\}\right)dt \tag{8.4}$$

where T_0 is the equilibrium temperature. The square-root of this variance, i.e., the rms angular change $\Delta\theta$ calculated for excess energy ΔE values ranging up to 2 eV (as that typically occurring in a radiationless decay to the ground state) is shown in Fig. 8.7.

It can be seen from this figure that the predicted local-heat-induced orientational effects are very small for any reasonable choice of the model free parameters. In particular, all model predictions fall well within our experimental upper limit for $\Delta\theta$.

The possibility that some randomization mechanism somehow associated with excess energy (i.e., depending on the excitation wavelength) could be present also on a slower time scale, such that instead of being considered "sudden" and thus affecting the initial degree of polarization, it could act continuously during the fluorescence decay. In this case, one should however see it as a change of rotational time τ_r as a function of photon excess energy. Figure 8.2 shows that a small effect could indeed be present in the form of a small reduction of τ_r with increasing photon energy. However the magnitude of this effect is compatible with zero within two standard deviations, so no definite conclusion can be drawn.

We also verified if some excitation wavelength dependence could be seen in the excited electronic state lifetime τ_e. Figure 8.3 shows that in this case a small but statistically significant wavelength dependence is actually found. Its physical meaning

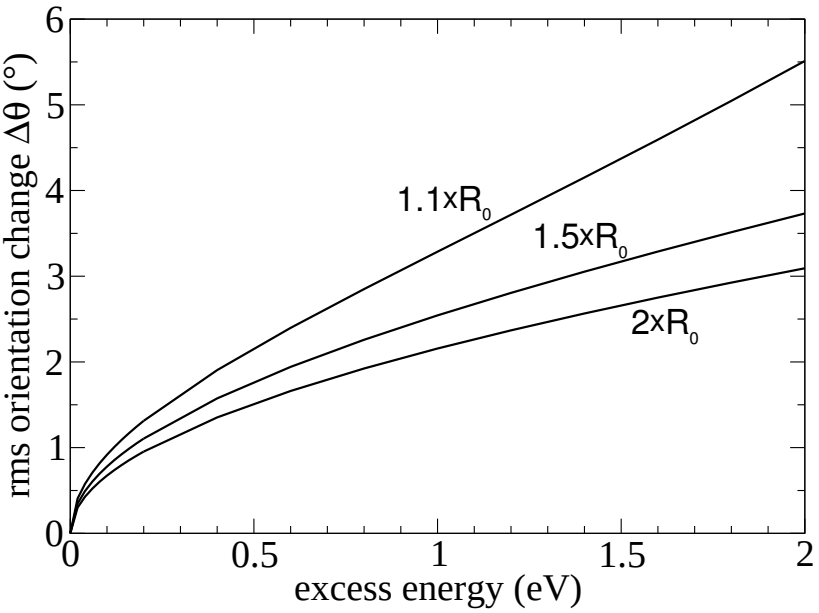

Figure 8.7: Root-mean-square random reorientation angle $\Delta\theta$ predicted by our model as a function of photon excess energy. The distance R taken for the temperature "sampling" to be used in the evaluation of the rotational diffusion is set equal to $1.1\times R_0$, $1.5\times R_0$, and $2\times R_0$.

is not clear. It could be related just with the nature of the excited electronic state. However, since the excited state lifetime in amino-anthraquinones is known to be very sensitive to intermolecular interactions [11], one might also speculate that the photon excess energy may cause some relatively long-lived modifications of these interactions, e.g., breaking an hydrogen bond, which in turn would be reflected in an increase of τ_e. This would indeed be an important side effect of the nonradiative energy relaxation. A long-lived modification of intermolecular interactions should however be visible also in the wavelength dependence of the rotational time τ_r, most likely as a reduction of τ_r with increasing photon energy. In our case we cannot exclude that such an effect is indeed present, but our signal-to-noise ratio does not allow reaching a definite

conclusion about this point.

We have then shown by a direct experiment that, for a solution of amino-anthraquinone dyes in isotropic 5CB, the orientational randomization induced by the nonradiative dissipation of vibrational energy following each photon absorption is negligible within our uncertainties. This was shown for a maximum dissipated energy of 0.6 eV, corresponding to a local heating of the order of 100K. The results are in accordance with a simple model based on continuum heat diffusion and on the measured temperature dependence of molecular rotational diffusion. An experimental upper limit to the orientational randomization has been estimated. We found instead some evidence that small effects of nonradiative energy relaxation on the molecule "behavior" could be present for a longer time-scale, comparable with the state lifetime, but clearly not related with photon-induced local heating.

Based on our experimental result and the associated theoretical understanding, there is no reason to believe that our null result for the orientational effects of photon-induced local heating be specific of our materials: it is probably a rather general result. It is however still possible that a measurable effect may be found in systems having characteristic relaxation times very different from ours. In particular, although the random molecular rotation induced at every excitation remains very small, a cumulative effect might become measurable in suitably rigid systems, as on the other hand was suggested in the original proposal by Albrecht [2].

8.5 Discussion in Connection with Jánossy Effect Anomalous Wavelength Dependence

The measured values of excited-state lifetime τ_e and the rotational time τ_r of HK271 in 5CB versus excitation wavelength λ (plotted in Figs. 8.3 and 8.2, respectively) show variations that are too small respect the observed enhancement of the dye-induced nonlinearity with the excitation wavelength. Therefore, any explanation of

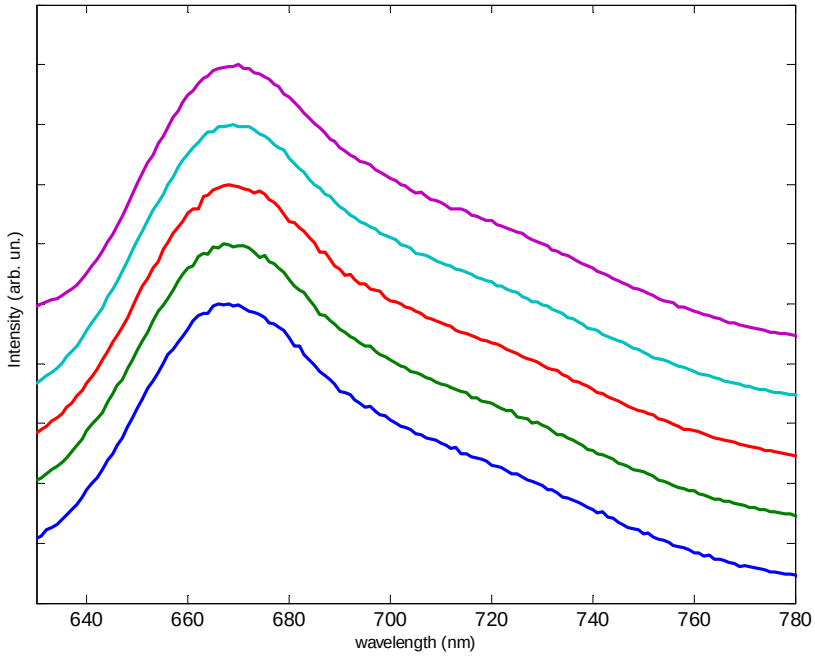

Figure 8.8: Fluorescence spectra of HK271-5CB mixture collected at several excitation wavelengths (The spectra are plotted with different offsets: 500nm (blue), 514nm (green), 550nm (red), 600nm (cyan) and 630nm (magenta)).

the wavelength-dependence of the Jánossy effect based on a long-lived polymorphism of the excited-state is ruled out by these results. We cannot exclude by means of our measurements that the excited-state parameters u_e depend somehow on λ, but

this possibility is extremely unlikely, as changes of u_e would be probably correlated with changes of τ_r. More generally, the possibility of a long-lived polymorphism of the excited state is further excluded by our observation that the shape of the steady-state fluorescence emission spectra does not change for a varying excitation light wavelength (see Fig. 8.8).

The possibility of a wavelength-dependent excited dye anisotropy reflecting into a variation of the orientational mean-field acting on the host is ruled out as well, by the results obtained for the initial degree of anisotropy (Fig. 8.1).

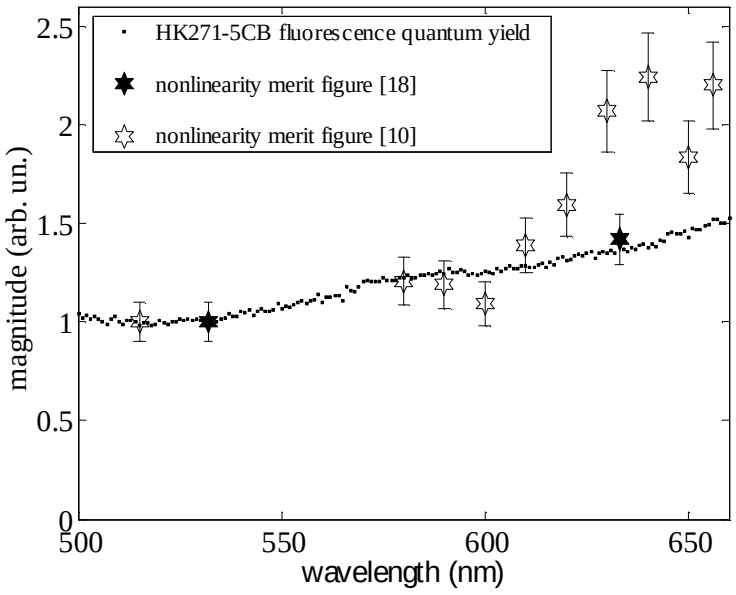

Figure 8.9: Excitation-wavelength dependence $\Phi(\lambda)$ of the fluorescence quantum yield in HK271-5CB compared with the wavelength dependence $\mu(\lambda)$ of the dye-induced optical nonlinearity merit figure in HK271-E63 (E63 is a mixture of cyanophenyls), as reported in Refs. [10] (filled stars) and [8] (open stars). The $\mu(\lambda)$ data are rescaled so as to be superimposed to the $\Phi(\lambda)$ data at the lowest wavelengths.

In contrast, the quantum yield shows a variation compatible with that observed

for the merit figure μ. In Fig. 8.9, we compare $\Phi(\lambda)$ with the $\mu(\lambda)$ of HK271 in E63 reported in two different works (Refs. [8] and [10]). We find a good quantitative correlation with the data of Ref. [10] and a qualitative correlation with the data of Ref. [8] (the discrepancy between the two sets of data has not been explained). This correlation supports the validity of the last explanation given in Sect. 8.1.2. Nonradiative immediate relaxation, more likely to occurr at higher photon energies where more decay channels are present, then seems to be responsible of the effect.

Other important conclusions can be drawn from the deuteration-dependence and the host-dependence of $\Phi(\lambda)$. The deuteration-induced enhancement of Φ is in excellent agreement with the corresponding increase of the excited-state lifetime τ_e measured at $\lambda = 532$ nm, as shown in figure 8.4. Since the quantum yield can be written as $\Phi = k_R \tau_e$, where k_R is the radiative decay rate, this result implies that deuteration affects only the nonradiative decay channels, as expected.

Moreover, the increase of the quantum yield at higher photon energy seems to be somehow related to the polarity of the solvent molecules. This solvent effect may be due to the presence of host-dependent nonradiative decay channels, in connection with intermolecular hydrogen bonds between HK271 and 5CB (see Ref. [11] and references therein).

Bibliography

[1] Hackermüller, L.; et al. *Nature (London)* **2004**, *427*, 711–714.

[2] Albrecht, A. C. *J. Chem. Phys.* **1957**, *27*, 1413–1414.

[3] Pantke, E. R.; Labhart, H. *Chem. Phys. Lett.* **1973**, *23*, 476–481.

[4] Truong, T. V.; Xu, L.; Shen, Y. R. *Phys. Rev. Lett.* **2003**, *90*, 193902.

[5] Truong, T. V.; Xu, L.; Shen, Y. R. *Phys. Rev. Lett.* **2004**, *93*, 039901.

[6] Kósa, T.; Jánossy, I. *Opt. Lett.* **1995**, *20*, 1230.

[7] Marrucci, L.; Paparo, D.; Maddalena, P.; Massera, E.; Prudnikova, E.; Santamato, E. *J. Chem. Phys.* **1997**, *107*, 9783–9793.

[8] Paparo, D.; Maddalena, P.; Abbate, G.; Santamato, E.; Jánossy, I. *Mol. Cryst. Liq. Cryst.* **1994**, *251*, 73.

[9] Taylor, D. G.; Demas, L. N.; Phillips, D. *An. Chem.* **1979**, *51*, 717.

[10] Marrucci, L.; Paparo, D.; Vetrano, M. R.; Colicchio, M.; Santamato, E.; Viscardi, G. *J. Chem. Phys.* **2000**, *113*, 10361–10366.

[11] Paparo, D.; Manzo, C.; Kreuzer, M.; Marrucci, L. *J. Chem. Phys.* **2002**, *117*, 2187–2191.

[12] Iannacchione, G. S.; Finotello, D. *Phys. Rev. E* **1993**, *50*, 4780–4795.

[13] Boudenne, A.; Khaldi, S. *J. Appl. Polym. Sci.* **2003**, *89*, 481–486.

[14] Sen, S.; Brama, P.; Roy, S. K.; abd S. B. Roy, D. K. M. *Mol. Cryst. Liq. Cryst.* **1983**, *100*, 327.

Chapter 9

Optically-Induced Rotation of Dye-Doped Nematic Droplets: a Check of Angular Momentum Conservation

9.1 Introduction and Motivations

In Sect. 3.2.1 we have seen that adding small amounts of dyes to nematic liquid crystals, the light-induced torque acting on the molecular director could be greatly enhanced. This effect has been explained by a model relying on the reversible changes of dye molecules diffusion constant and intermolecular forces occurring between photoexcited dye molecules and liquid crystal host. The understanding achieved with this model has also provided an answer to the fundamental question related to the observed torque enhancement and concerning the total angular momentum conservation (see Sect. 3.2.2). It emerges that the angular momentum transfer associated with light absorption cannot account for the torque magnitude; light absorption however triggers a transfer of angular momentum between different internal degrees of freedom of the liquid crystal, namely from the center-of-mass molecular degrees of freedom

(corresponding macroscopically to fluid flow) to the molecular-orientation degrees of freedom (corresponding to the molecular director). Being an internal transfer, the total angular momentum given to the material as a whole is not affected by the presence of dye. Another consequence of this internal transfer is that, by the force action-reaction principle, in dye-doped liquid crystals there should be an opposite torque acting on the fluid in the form of a photoinduced stress tensor.

Both these predictions however have never been tested directly in an experiment. In the aim of perform such tests, we investigated the rotational behavior of dye-doped liquid crystal droplets of micrometric size, dispersed in water, under the effect of infrared and visible laser light. In particular, we searched for possible enhancements of the droplets light-induced rotation by illumination with light having a wavelength in the dye absorption spectrum. The comparison has been made with the case in which the droplets are illuminated by infrared light, not absorbed by the dye.

9.2 Experimental Results

Most droplets possess a polar arrangement due to the anchoring effect; that is, molecules at the outer regions tend to be oriented along the surface of the droplet, while those at the inner regions tend to sustain their bulk-like orientation. Other droplets have a radial or irregular structure. When viewed in the polarizing microscope the two kind of structures however cause similar cross-like images. The internal molecular arrangement can be further distinguished by judging the response of the droplet to laser manipulation. The mechanism leading to this response is strictly connected with the birefringence of the droplets. Only droplets with polar molecular arrangement can be aligned and rotated by the rotation of the polarization of the incident light.

The spinning can be evidenced by comparing frame by frame the movie recorded by the CCD camera in polarizing microscope. The polar arrangement of the droplets cause a different scattering (depolarization) of the linear polarized light coming by the lamp. After passing through the analyzer, the light scattered by the droplets forms an image of the droplets itself consisting in darker (less scattering) and lighter regions (more scattering). Since a droplet rotation modifies this pattern by monitoring these changes, e.g. by the intensity variation of the light in a given region, we can measure the rotation frequency of the droplets. The CCD frame rate (50 f/s) give us an upper limit for frequency we can measure with this method. Frequency faster than 10 Hz have been measured by looking at the intensity variations of the laser light backscattered by the droplets and collected by a photodiode.

A typical result for this kind of measurements is shown in Fig. 9.1). The signals is best-fitted with sinusoidal curve. A FFT algorithm is used in order to find the frequency of the signal, that is twice the droplet rotation frequency.

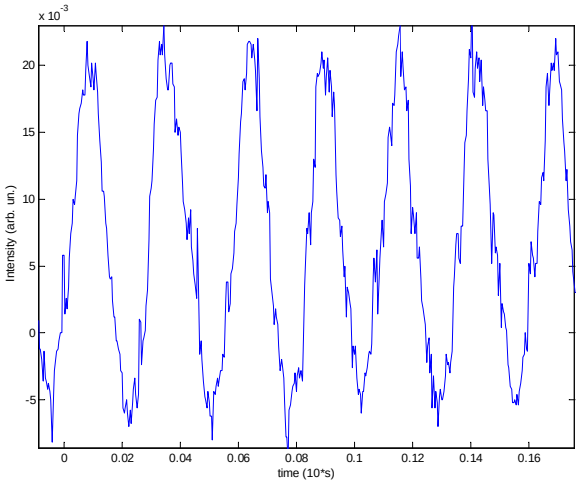

Figure 9.1: Typical measured signal of the laser light back-scattered by a spinning droplet.

For low rotation frequencies measurements have been performed with both the methods; from their comparison we observed a good agreement.

The rotation frequencies of several droplets have been measured varying the angle of the $\lambda/4$ wave plate in order to modify the polarization of the light. On each droplet the measurements have been carried out both for infrared and visible light-induced spinning. In Fig. 9.2 the results for a dye-doped droplet with a diameter of $\sim 3.5\mu$m are shown. The large difference between the two sets of data seems to be only related to the different powers of the two laser beams ($\sim$ 15mW for infrared light and $\sim$ 1mW for visible light). From Eq. 6.7 the rotation frequency is expected to depend linearly on the beam power. The ratio between the two maximum frequencies is compatible with the ratio of the two laser powers.

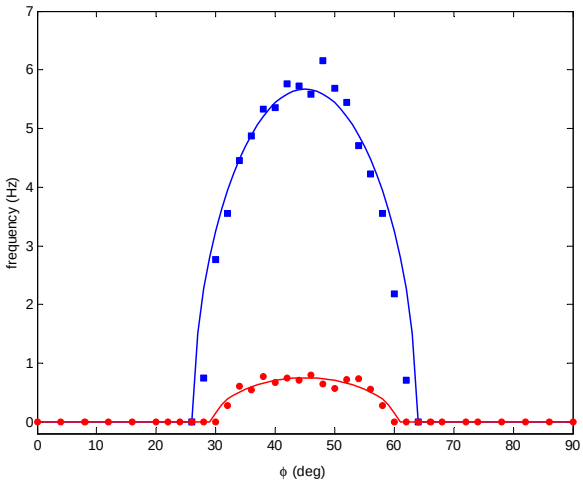

Figure 9.2: Variation of rotation frequency with the polarization of the infrared (in blu, power$\sim$ 15mW) and visible beam (in red, power$\sim$1mW). Solid lines are the best-fit of the data with the function given in Eq. 6.7 for the rotation frequency.

The same kind of measurements performed on pure liquid crystal droplets do not show significative variations with respect to the dye-doped case.

Moreover we measured the frequency rotation induced on dye-doped droplets by both the beams simultaneously and compared to which obtained with only the infrared beam. As it is possible to see in fig 9.3, even in this case no significant variations

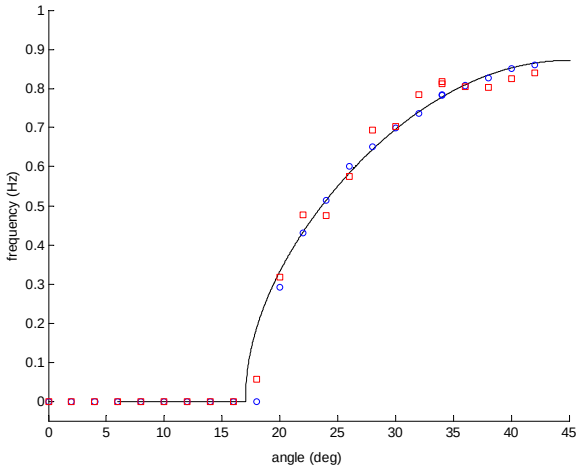

Figure 9.3: Droplet rotation frequency versus the ellipticity of the polarization of the incident light. Circles refer to rotation induced by infrared light whereas data indicated by squares are obtained by adding the visible light to the infrared one, with same polarization. Solid line is the data best-fit obtained by means of the function given in Eq. 6.7 for the rotation frequency.

in the droplet rotational speed are observed.

9.3 Discussion in Connection with Angular Momentum Conservation in Dye-Doped Liquid Crystal Droplet

In general, the dynamical state of a nematic liquid crystal under the action of laser light is defined by the temporal and spatial dependence of the following fields: the

molecular director $\mathbf{n}$ specifying the local molecular alignment, the velocity vector $\mathbf{v}$ defining the flow of matter, and the electric and magnetic fields of the optical wave, $\mathbf{E}$ and $\mathbf{B}$, respectively. These fields will be governed by the director torque balance equation, the Newton equation for the acceleration, and the electromagnetic Maxwell equations [1,2], completed with all the relevant constitutive equations for torques and forces.

In order to write down explicitly these equations, it is convenient to introduce first some standard notations of fluid dynamics. From the velocity field, one can define the deformation-rate tensor $V_{ij} = (\partial_j v_i + \partial_i v_j)/2$, where ∂_j denotes the partial derivative with respect to the coordinate x_j, and the vorticity vector $\mathbf{W} = \nabla \times \mathbf{v}/2$. The vorticity vector gives the local rotational velocity of the fluid. Moreover, it is useful to introduce the "material" or "convective" time derivative, defined as $d/dt = \partial/\partial t + v_j \partial_j$, that corresponds to a derivative taken following the fluid element along its motion. The usual sum convention over repeated indices is understood.

With these definitions, the director torque balance equation can be written as follows:

$$I_n \frac{d}{dt}\left(\mathbf{n} \times \frac{d\mathbf{n}}{dt}\right) = \tau^{el} + \tau^{v} + \tau^{em} + \tau^{ph} \tag{9.1}$$

where τ^{α} with $\alpha = el, v, em, ph$ are the elastic, viscous, electromagnetic, and photoinduced torque densities, respectively, and I_n is the moment of inertia per unit volume of the nematic molecules, actually negligible in most cases, but included in Eq. (9.1) for making its physical significance more transparent.

The constitutive equations for the torques are the following. Introducing the usual Franck elastic free energy density $F^{el}(n_i, \partial_j n_i)$ (see Refs. [1,3] for its expression), the

elastic torque can be written as

$$\tau_i^{el} = -\epsilon_{ijh} n_j \left(\frac{\partial F^{el}}{\partial n_h} - \partial_k \frac{\partial F^{el}}{\partial_k n_h} \right) \tag{9.2}$$

where ϵ_{ijh} is the fully antisymmetric Levi-Civita tensor. The viscous torque is

$$\tau_i^{v} = -\epsilon_{ijh} n_j \left[\gamma_1 \left(\frac{dn_h}{dt} - \epsilon_{ijh} W_j n_h \right) + \gamma_2 V_{hk} n_k \right] \tag{9.3}$$

where γ_1 and γ_2 are two characteristic viscosity coefficients [1,3]. Neglecting magnetic effects at optical frequencies, the electromagnetic torque is given by

$$\tau^{em} = \langle \mathbf{D} \times \mathbf{E} \rangle \tag{9.4}$$

where the average $\langle\rangle$ is to be taken over the optical cycle and where $\mathbf{D}$ is the dielectric displacement field [1]. The latter is given by

$$D_i = \epsilon_{ij} E_j = \epsilon_0 (\epsilon_\perp \delta_{ij} + \epsilon_a n_i n_j) E_j, \tag{9.5}$$

where ϵ_{ij} is the dielectric tensor, ϵ_0 the vacuum dielectric constant, $\epsilon_\perp$ the relative dielectric constant for $\mathbf{E} \perp \mathbf{n}$ and ϵ_a the relative dielectric anisotropy. Finally, the photoinduced torque, appearing in dye-doped absorbing liquid crystals when illuminated, is in the limit of small light intensities identical to the electromagnetic torque except for the replacement of the dielectric anisotropy ϵ_a with a new material constant ζ, proportional to the absorbance (or to dye concentration) [4]. Therefore, its explicit expression can be written as follows:

$$\tau^{ph} = \zeta \epsilon_0 \langle (\mathbf{n} \cdot \mathbf{E})(\mathbf{n} \times \mathbf{E}) \rangle \tag{9.6}$$

Let us now turn to the velocity field dynamical equation, that can be obtained from Newton equation for the acceleration

$$\rho \frac{dv_i}{dt} = \partial_j t_{ji}^{tot} \tag{9.7}$$

where ρ is the mass density and t_{ji}^{tot} is the total stress tensor associated with a fluid displacement with no director rotation (this corresponds to Ericksen's definition of stress tensors in liquid crystals [1]). Eq. (9.7) must actually be written both for the liquid crystal in the droplet and for the surrounding water. In the liquid crystal, the total stress tensor will be given by the following sum [1]:

$$t_{ji}^{tot} = -p\delta_{ji} + t_{ji}^{el} + t_{ji}^{v} + t_{ji}^{em} + t_{ji}^{ph}, \tag{9.8}$$

where p is pressure, δ_{ji} is Kronecker delta, t_{ji}^{el} is the (Ericksen) stress tensor associated with director elasticity, t_{ji}^{v} the viscous (Leslie) stress tensor, t_{ji}^{em} the electromagnetic stress tensor, and t_{ji}^{ph} the photoinduced stress tensor associated with the presence of dye [4]. In water the elasticity and photoinduced stress tensors will vanish identically.

Angular momentum conservation law, in combination with eqs. (9.1) and (9.7), sets the following relationship between each torque acting on the director and the corresponding stress tensors acting on the center-of-mass degrees of freedom:

$$\tau_i^{\alpha} = \epsilon_{ijh} t_{jh}^{\alpha} + \partial_k(\epsilon_{ijh} n_j s_{kh}^{\alpha}) \tag{9.9}$$

where s_{kh}^{α} is a surface torque tensor [1, 3]. To first order, s_{kh}^{α} is nonzero only in the case of the elastic torque. Therefore, in all other cases, owing to angular momentum conservation, the stress tensor defines completely the torque, or conversely, the torque defines the antisymmetric part of the stress tensor. In particular, the expression (9.6) of the torque determines the antisymmetric part of the unknown stress tensor t_{ji}^{ph}. As we will see, this antisymmetric part is all we actually need to determine the induced rotational effects of the stress tensor.

For our purposes it is sufficient to write down the complete expression of the

electromagnetic stress tensor only [2]:

$$t_{ji}^{em} = \left(\tilde{F}_{em} - \rho \frac{\partial \tilde{F}_{em}}{\partial \rho} \right) \delta_{ji} + D_j E_i \tag{9.10}$$

where $\tilde{F}_{em}$ is the electromagnetic free energy at given $\mathbf{E}$ field (magnetic effects are neglected), which in our case can be written as

$$\tilde{F}_{em} = -\frac{1}{2} \epsilon_{ij} E_i E_j = -\frac{\epsilon_0}{2} \left(\epsilon_\perp \delta_{ij} + \epsilon_a n_i n_j \right) E_i E_j \tag{9.11}$$

Equations (9.1) and (9.7) completed with all constitutive equations for torques and stress tensors and with the appropriate boundary conditions at the droplet surface completely define the problem of the light-induced dynamics of the droplet. However, they are clearly very complex and an exact solution can be determined only numerically.

In the following, we instead approach the problem analytically with the help of two different kinds of approximations. In both, we assume that the droplet is perfectly spherical, with a radius R and a total mass M. In the first approximation, we also assume that the droplet behave as a rigid body under the effect of the total external torques. The main reason for the validity of this approximation is that the typical viscosity coefficients of the nematic liquid crystals (for example $\gamma_1 \approx 100$ cP) are much larger than the water viscosity ($\eta \approx 1$ cP at room temperature). So all internal shear and relative rotation of the director with respect to the fluid are much slower than the rigid rotation with respect to the surrounding water. We will call this the *rigid body approximation* (RBA). In the second approximation, we relax the rigidity assumption somewhat by accepting the possibility of a relative motion of the director with respect to the fluid. However we will still consider the fluid motion to coincide with that of a rigid body and we will also assume that the director is perfectly uniform in the

droplet. This second approximation will be called *uniform director approximation* (UDA).

9.3.1 Rigid body approximation (RBA)

Within the RBA, the fluid velocity in the droplet is given by

$$\mathbf{v} = \mathbf{\Omega}\times\mathbf{r}, \tag{9.12}$$

where $\mathbf{\Omega}$ is the droplet angular velocity. Moreover, the molecular director satisfies the following equation

$$\frac{d\mathbf{n}}{dt} = \mathbf{\Omega}\times\mathbf{n} \tag{9.13}$$

so that the vorticity vector $\mathbf{W} = \mathbf{\Omega}$ in the whole droplet.

The rotation of the liquid crystal droplet is then governed by the second cardinal equation for the motion of rigid bodies

$$\frac{d\mathbf{L}}{dt} = \mathbf{M}^{tot} \tag{9.14}$$

where $\mathbf{L}$ is the total angular momentum of the droplet and $\mathbf{M}^{tot}$ is the total external couple (we reserve the term *torque* to indicate the specific couples acting on the director). The two sides of the latter equation can be deduced from Eq. (9.7) by multiplying both sides vectorially by $\mathbf{r}$ and integrating over the whole droplet volume V_d and then adding the volume integral of both sides of Eq. (9.1). In this way we easily obtain

$$\mathbf{L} = \int_{V_d} (\rho\mathbf{r}\times\mathbf{v} + I_n\mathbf{n}\times\frac{d\mathbf{n}}{dt})dV = I\mathbf{\Omega} \tag{9.15}$$

where the total moment of inertia I is given by $I = \int_{V_d} \rho(x^2+y^2)dV = 2MR^2/5$, and where we set $I_n \simeq 0$. The total external couple is instead given by

$$M_i^{tot} = \int_{V_d} (\epsilon_{ijh}x_j\partial_k t_{kh}^{tot} + \tau_i^{tot})dV \tag{9.16}$$

Combining the latter with Eq. (9.9), we readily find

$$M_i^{tot} = \int_{V_d} \epsilon_{ijh} \partial_k (x_j t_{kh}^{tot} + n_j s_{kh}^{tot}) dV = \int_{A_d} \epsilon_{ijh} (x_j t_{kh}^{tot} + n_j s_{kh}^{tot}) dA_k \tag{9.17}$$

where the last integral is extended to the droplet surface A_d and the surface element dA_k is defined as a vector having modulus equal to the surface element area and direction normal to it and pointing outward.

The final expression for the total external couple shows the reason why Eq. (9.9) is needed for angular momentum conservation, as it brings the total external couple in the form of a input flux of angular momentum through the surface. This total external couple can be actually evaluated at a surface that lies just outside the liquid crystal droplet boundary, within water. Being in water, we will have $s_{kh}^{tot} = 0$ and the only nonvanishing contributions to the stress tensor will be the pressure, viscous, and electromagnetic terms. There should not be, instead, any photoinduced contribution, as the photoinduced stress tensor should vanish identically in water, where the dye is absent. This shows that at least within the RBA we do not expect any enhancement of the light-induced rotation or other photoinduced effects associated with the presence of dye, owing to angular momentum conservation.

The pressure stress tensor does not contribute to the external couple, as it can be readily verified by a direct evaluation of the surface integral in (9.17) (this result can be proved for any droplet shape if p is uniform or for any pressure distribution if the droplet is spherical). The viscous term can be easily evaluated by solving the Navier-Stokes equations in water (in the laminar flow limit). The result is the well known Stokes formula for the rotational viscous couple acting on a rotating sphere in a viscous fluid:

$$\mathbf{M}^v = -6\eta V_d \mathbf{\Omega} \tag{9.18}$$

where η is the water viscosity coefficient. The electromagnetic term is the most difficult to evaluate in general. The exact expression is given by the surface integral (9.17) applied to the electromagnetic stress tensor (9.10). However, to obtain a nonvanishing result the electric field to be used with this calculation is the total one, i.e., that resulting from the superposition of the incoming and diffracted (or scattered) waves.

An alternative expression of the electromagnetic couple can be obtained by going back to the volume integral (9.16), as applied to the electromagnetic contribution only. This expression can be evaluated approximately by using the incoming beam only and leads to a nonvanishing first-order result. In particular, the first term of Eq. (9.16) vanishes identically if one neglects all gradients of the molecular director and of the light intensity within the volume of the sphere. With these approximations, the total couple reduces to the second term, i.e., to the volume integral of the electromagnetic local torque acting on the director:

$$\mathbf{M}^{em} \approx \int_{V_d} \tau^{em} dV = \int_{V_d} \langle \mathbf{D} \times \mathbf{E} \rangle dV = \int_{V_d} \epsilon_a \epsilon_0 \langle (\mathbf{n} \cdot \mathbf{E})(\mathbf{n} \times \mathbf{E}) \rangle dV \tag{9.19}$$

This last approximate expression can be evaluated easily for a uniform electric field. Assuming that the director distribution $\mathbf{n}(\mathbf{r})$ within the droplet has cylindrical symmetry around a droplet axis $\mathbf{d}$, one finds

$$\mathbf{M}^{em} \approx \epsilon_a S_d V_d \langle (\mathbf{d} \cdot \mathbf{E})(\mathbf{d} \times \mathbf{E}) \rangle \tag{9.20}$$

where S_d is the order parameter of the director distribution averaged over the droplet volume and is defined as

$$S_d = \frac{3}{2V_d} \int_{V_d} (\mathbf{n} \cdot \mathbf{d})^2 dV - \frac{1}{2} \tag{9.21}$$

In the case of a uniform director one has $\mathbf{d} = \mathbf{n}$ and $S_d = 1$.

However for a light wave crossing a micrometric-sized liquid crystal droplet, the approximation of considering the field as uniform within the droplet is usually too rough. Indeed the birefringence will induce a significant change of light polarization within the droplet, change which must be taken into account to obtain a reasonable estimate of the electromagnetic couple. In general it is rather difficult to calculate this polarization variation within the droplet. A rough estimate can be however gained by replacing the droplet with a plane slab, so that the birefringence effect can be easily calculated. If the laser beam waist is smaller than the droplet radius one may approximate the droplet effect on the light polarization as that of a slab having a thickness equal to the droplet diameter $2R$. This approximation leads to a simple expression of the torque in terms of the incoming polarization. Otherwise, one can approximate the total torque with a suitable average over slabs having different thicknesses. In such approximation we obtain the results shown in Eq. 6.5.

For a circularly polarized beam, if the droplet axis $\mathbf{d}$ remains in the plane of the input field $\mathbf{E}$, i.e., orthogonal to the light propagation direction, the electromagnetic couple will be constant, i.e., independent of director rotation. This result is not approximate, as it can be proved simply by symmetry. In this simple case one obtains a stationary solution corresponding to a uniform rotation of the droplet with constant angular velocity. The stationary solution to Eq. (9.14) is given by the balance of the viscous and electromagnetic couples, that gives the following expression for the rotational velocity:

$$\mathbf{\Omega} = \frac{1}{6\eta V_d}\mathbf{M}^{em} \tag{9.22}$$

9.3.2 Uniform director approximation (UDA)

Assuming from the beginning that the director is always uniform within the droplet, one can release the assumption that the director and the droplet rotations are rigidly connected. The dynamics of **v** and **n** fields will still be taken to be given by Eqs. (9.12) and (9.13), but the two $\mathbf{\Omega}$'s entering these equations may in general be different. Let us then label $\mathbf{\Omega}_v$ and $\mathbf{\Omega}_n$ the angular velocities of the fluid and director rotations, respectively.

By multiplying vectorially both sides of Eq. (9.7) by **r** and integrating over the droplet volume we obtain again a cardinal equation as Eq. (9.14), with $\mathbf{L} = I\mathbf{\Omega}_v$. The total couple $\mathbf{M}^{tot}$ is however now given by

$$M_i^{tot} = \int_{V_d} \epsilon_{ijh} x_j \partial_k t_{kh}^{tot} dV = \int_{A_d} \epsilon_{ijh} x_j t_{kh}^{tot} dA_k - \int_{V_d} \tau_i^{tot} dV \tag{9.23}$$

The first term of this expression can be calculated in a surface within water immediately out the droplet, and is therefore given by the same two total external couples, viscous and electromagnetic, as obtained in the previous subsection within the RBA model.

However, now we also have a term given by the opposite of the torque acting on the molecular director integrated over the whole droplet volume. This term couples the droplet fluid rotation with the director rotation and appears also in the equation for the latter. We will therefore evaluate it below, together with the director dynamical equation.

The director dynamics can be obtained directly from Eq. (9.1). We must now evaluate an explicit expression for each torque entering this equation.

For a perfectly uniform director the elastic torque vanishes identically. However it is not obvious here that one can truly neglect the elastic torque, as it is just this torque

that keeps the director approximately uniform. If all other torques are always uniform then the director will stay uniform spontaneously, and the elastic torque will remain zero. If however one of the other torques is nonuniform this will create a nonvanishing elastic torque to constrain the director to remain approximately uniform. We assume here that all the other torques are at least approximately uniform, so that we may still consider the elastic torque as negligible, at least when integrated over the droplet volume.

The viscous torque under our assumptions is easily calculated and is given by

$$\tau^v = -\gamma_1(\mathbf{\Omega}_n - \mathbf{\Omega}_v) \tag{9.24}$$

This torque is uniform within the droplet, so it gives no problems.

The electromagnetic torque, instead, given by Eq. (9.4), is in general not uniform, mainly due to the changes of light polarization induced by the droplet birefringence. We assume here that the effects of the nonuniformity are anyway sufficiently small to allow us to continue neglecting the elastic torque. Moreover, we replace the electromagnetic torque with its (trivially uniform) volume average over the droplet, thus obtaining

$$\tau^{em} \approx \frac{1}{V_d}\mathbf{M}^{em} \tag{9.25}$$

where $\mathbf{M}^{em}$ is still given by Eq. (9.19).

The photoinduced torque is identical to the electromagnetic torque, except for the replacement of ϵ_a with ζ, i.e., it can be obtained from the electromagnetic torque just by multiplying it times the enhancement factor ζ/ϵ_a. We will also indicate with

$$\mathbf{M}^{ph} = \int_{V_d} \tau^{ph} dV = \frac{\zeta}{\epsilon_a}\mathbf{M}^{em} \tag{9.26}$$

the integrated photoinduced torque.

Putting all these results together, the droplet dynamics within the UDA model can be finally described by the following two coupled equations:

$$\begin{aligned} I\frac{d\mathbf{\Omega}_v}{dt} &= -6\eta V_d \mathbf{\Omega}_v + \gamma_1 V_d(\mathbf{\Omega}_n - \mathbf{\Omega}_v) - \mathbf{M}^{ph} \\ I_n V_d \frac{d\mathbf{\Omega}_n}{dt} &= -\gamma_1 V_d(\mathbf{\Omega}_n - \mathbf{\Omega}_v) + \mathbf{M}^{em} + \mathbf{M}^{ph} \simeq 0 \end{aligned} \tag{9.27}$$

where in the former equation we have cancelled the two electromagnetic terms, which are almost exactly opposite to each other. The director moment of inertia I_n shown in the above equations can actually be always neglected. Adding together the two equations, one recovers exactly the dynamical equation already obtained in the RBA model.

In particular, for circularly polarized light we reecover the stationary solution

$$\mathbf{\Omega}_v = \frac{1}{6\eta V_d}\mathbf{M}^{em} \tag{9.28}$$

showing that the droplet fluid rotation is not affected by the photoinduced torque.

However, at steady state, the rotation of the molecular director is instead governed by the following equation:

$$\mathbf{\Omega}_n = \frac{1}{V_d}\left(\frac{1}{6\eta} + \frac{1}{\gamma_1}\right)\mathbf{M}^{em} + \frac{1}{\gamma_1 V_d}\mathbf{M}^{ph} \tag{9.29}$$

that shows that there can be an effect of the photoinduced torque. The effect of the photoinduced torque is depressed by the large viscosity coefficient γ_1 as compared with the water one η. However at comparable light intensities the photoinduced torque should be enhanced by the large factor $\zeta/\epsilon_a \approx 100$, when compared with the electromagnetic term, so it could still be possible to observe its effects in a suitably designed experiment.

Our results show that the overall angular momentum transfer to the droplets is indeed not affected by the presence of the dye. Although this null result was indeed expected from considerations of angular momentum conservation, from our discussion emerges that it is actually a non-trivial outcome of the rigid coupling that is established in the droplets between the molecular director and the liquid crystal flow. If this coupling can be overcome, highly non-trivial photoinduced effects associated with the dye should take place.

Bibliography

[1] de Gennes, P. G. *The Physics of Liquid Crystals;* Oxford University Press: Oxford, 1974.

[2] Landau, L.; Lifschitz, E. *Electrodynamics of Continuous Media;* Pergamon Press: Oxford, 1984.

[3] Chandrasekhar, S. *Liquid Crystals;* Cambridge University Press: Cambridge, 1977.

[4] Marrucci, L.; Paparo, D. *Phys. Rev. E* **1997**, *56*, 1765–1772.

Conclusions

Our experiments provide a great deal of information about rotational dynamics and photoemissive properties of amino-anthraquinone molecules dissolved in liquid hosts. These results can moreover address some general topics in molecular physics, related to intermolecular interactions, nonradiative relaxations and nonlinear effects.

By measuring the effect of hydrogen-deuterium substitution on the rate of rotational diffusion of anthraquinone dyes dissolved in the isotropic liquid phase of 5CB we observed a reduced rotational mobility of the deuterated species with respect to the protonated ones by up to 43% (at 311 K) and a corresponding increase of 4-5 kJ/mol in the activation energy, as deduced from the temperature dependence. To our knowledge, this is the largest isotopic effect ever reported for the molecular rotational diffusion in liquids. In nonpolar liquids the effect vanishes. We attribute our findings to an isotopic effect in the breaking kinetics of the hydrogen-bond between the amino groups of dye molecules and the cyano group of 5CB that cannot be explained with the known isotopic effect on the hydrogen-bond strength. These findings could be relevant for the modeling of a broad class of kinetic phenomena in

which hydrogen-bond formation and breaking is a rate-limiting step, including possibly water viscosity and protein folding, and open interesting perspectives for the investigation of intermolecular interactions which influence microscopic friction.

We carried out measurements of parameters describing the dynamics and the photoemission of excited-state dye molecules after photon absorption varying the energy of the photon absorbed by the molecules, i.e. the wavelength of the pumping light. We find no significative dependence within experimental uncertainties of both the initial molecule anisotropy and of the subsequent rotational diffusion dynamics on the photon energy. A small but statistically significant effect of photon energy is instead found in the excited state lifetime of the dye whereas the fluorescence quantum yield shows a considerable enhancement when increasing the wavelength. These results provide a background to discuss the effect of the excess energy on the relaxation processes following absorption. In particular, our results rule out some recent proposals dealing with a photoinduced local heating due to the transfer of the extra energy from the excited molecules to the surrounding and leading to molecular reorientation effects. A simple model of photoinduced local heating and corresponding enhanced rotational diffusion is in accordance with this result.

These measurements also clarify the mechanism leading to the peculiar wavelength dependence of the dye-induced optical nonlinearity observed for an anthraquinone dye. We see that the wavelength dependence of the excited-state molecular parameters involved in the expression for the dye-induced optical nonlinearity, i.e. the fluorescence lifetime, the rotational diffusion constant and the initial degree of anisotropy, cannot justify its wavelength-dependent behavior. Nevertheless, the quantum yield

wavelength dependence shows a good correlation with some measurements of nonlinearity reported in literature. These experimental results suggest a possible explanation of the anomalous wavelength dependence of the Jánossy effect, relying on the fact that an increase of the nonradiative decay rate at higher excitation energies reduces the population of Jánossy-active molecules.

Moreover we performed measurements of the rotational velocity that circularly polarized light can induce on dye-doped liquid crystal droplets. Two laser beams, one of them with wavelength lying in the dye absorption spectrum, are used to trap and spin the droplets. The slower spinning induced by the beam absorbed by the dye molecules inside the droplets can be ascribed only to its power, smaller than the one of the infrared beam. The absorption of polarized light seems not to affect the microscopic rotational motion whereas an orientational effect on molecular scale is expected by the model employed to explain the Jánossy effect. In this model, by considerations on the angular momentum conservation, the angular momentum exchange due to the dye-induced molecular optical torque is expected to take place between internal degrees of freedom of the system. Our results directly show the validity of the latter assumption, that is the angular momentum associated with the dye-induced molecular optical torque is not associated with an enhancement of the total angular momentum exchanged by the dye-liquid crystal system with the external environment.